Laboratoire CRISMAT

CRIstallographie et Sciences des MATériaux

Unité Mixte de Recherche n°6508 CNRS/ENSICAEN

Oxydes de métaux de transition: réseaux carrés et triangulaires pour générer de nouvelles fonctionnalités

Antoine Maignan

Collége de France, Chaire de Physique de la Matière Condensée
Antoine Georges, Cours 6: transition métal-isolant de Mott dans les oxydes de métaux de transition

Why are we interested in oxides ?

plenty of cation combinations (playground for Chemists)
natural abundance
green materials « air prepared » (Pb free etc…)

applications:

microelectronics: dielectrics ($HfSiO_2$) , ferroelectrics ($SrBi_2Ta_2O_9$), QTM quantum computing ($Ca_3Co_2O_6$) ?

energy: (TCOs for PV ITO, Li-batteries Li_xCoO_2, SOFC H_2 $(La,Sr)(Co,Fe)O_{3-d}$, catalysis nanomaterials to replace Pt Rh, superconductivity $YBa_2Cu_3O_7$, thermoelectricity ?)

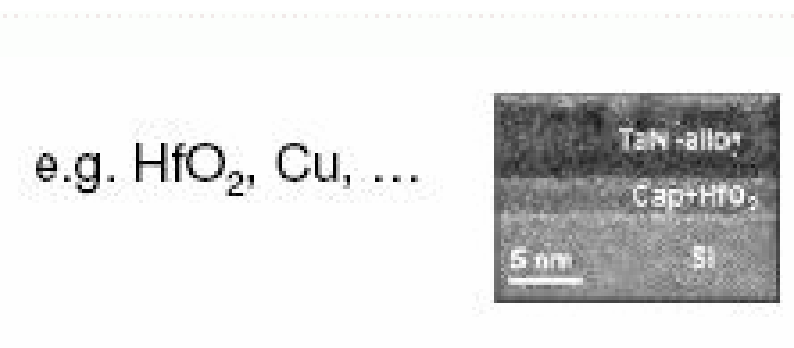

FeRam

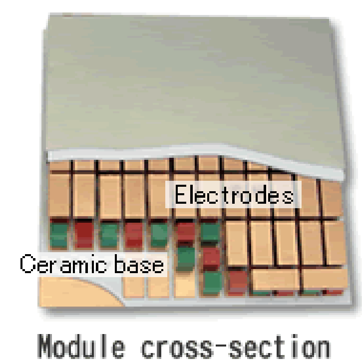

TEG

Plan:

3D magnetic networks:

CMR in perovskite manganites
MIT in cobaltites
Frustrated lattices of the « 114 » type

1D and 2D TM-O-TM networks: hexagonal perovskites and CdI_2 type structures

n-type ***vs*** **p-type** conductivity in oxides

Introduction

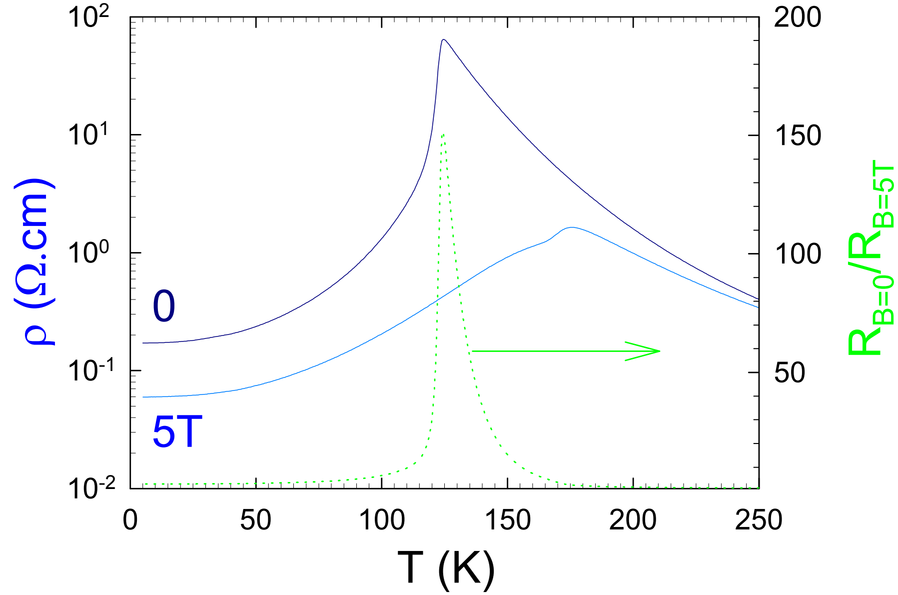

ABO_3

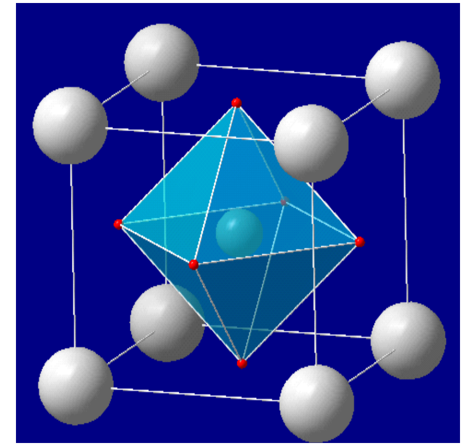

Perovskite: very rich system!
Structures and properties!!

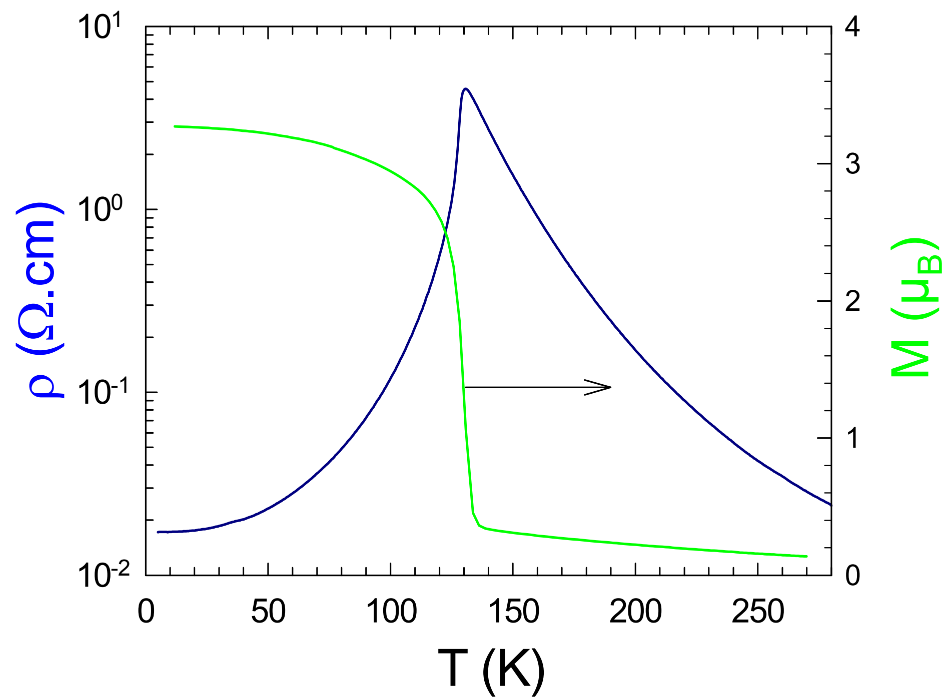

CMR

Strong coupling between structures,transport and magnetism.

Perovskite structure

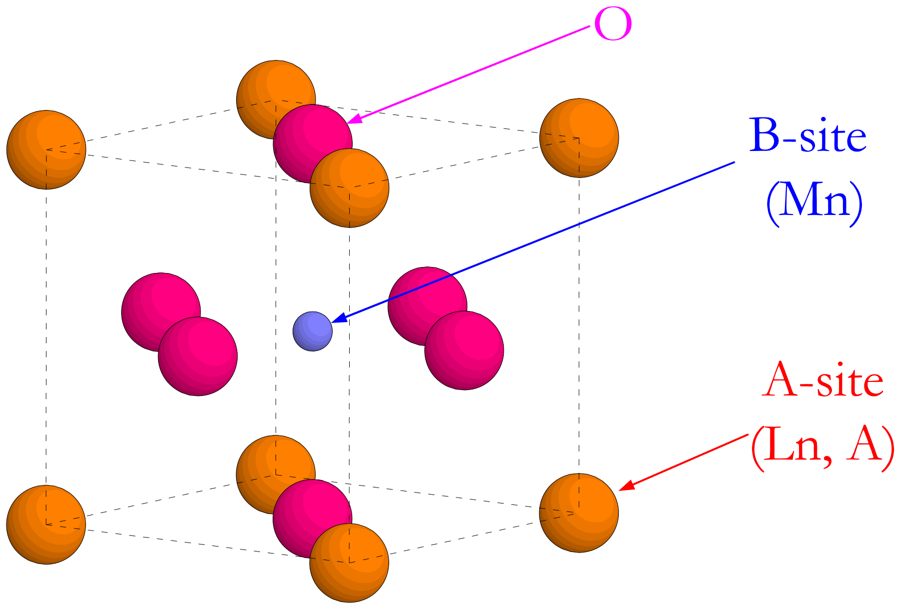

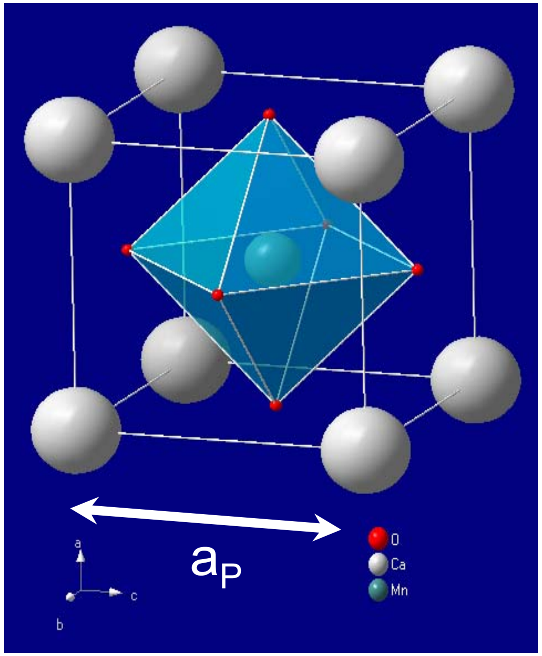

ABO_3

⟹ Flexibility of the structure with regard to cationic and anionic replacements and tolerance to ion defects.

⟹ AO and BO frameworks

Spin-Charge-Orbital coupling

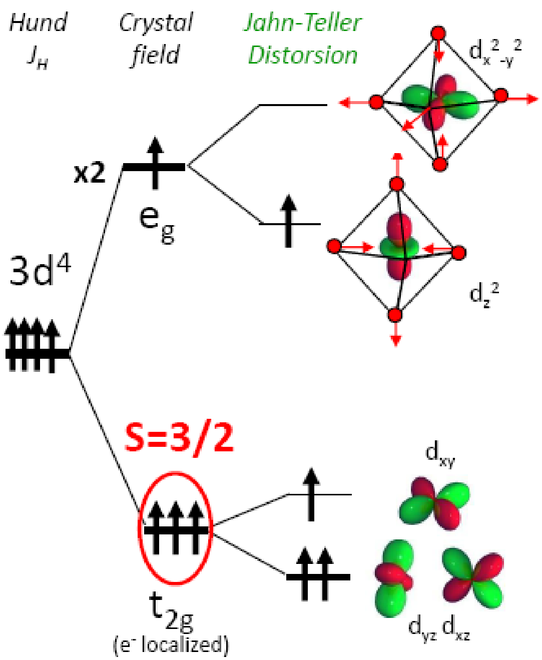

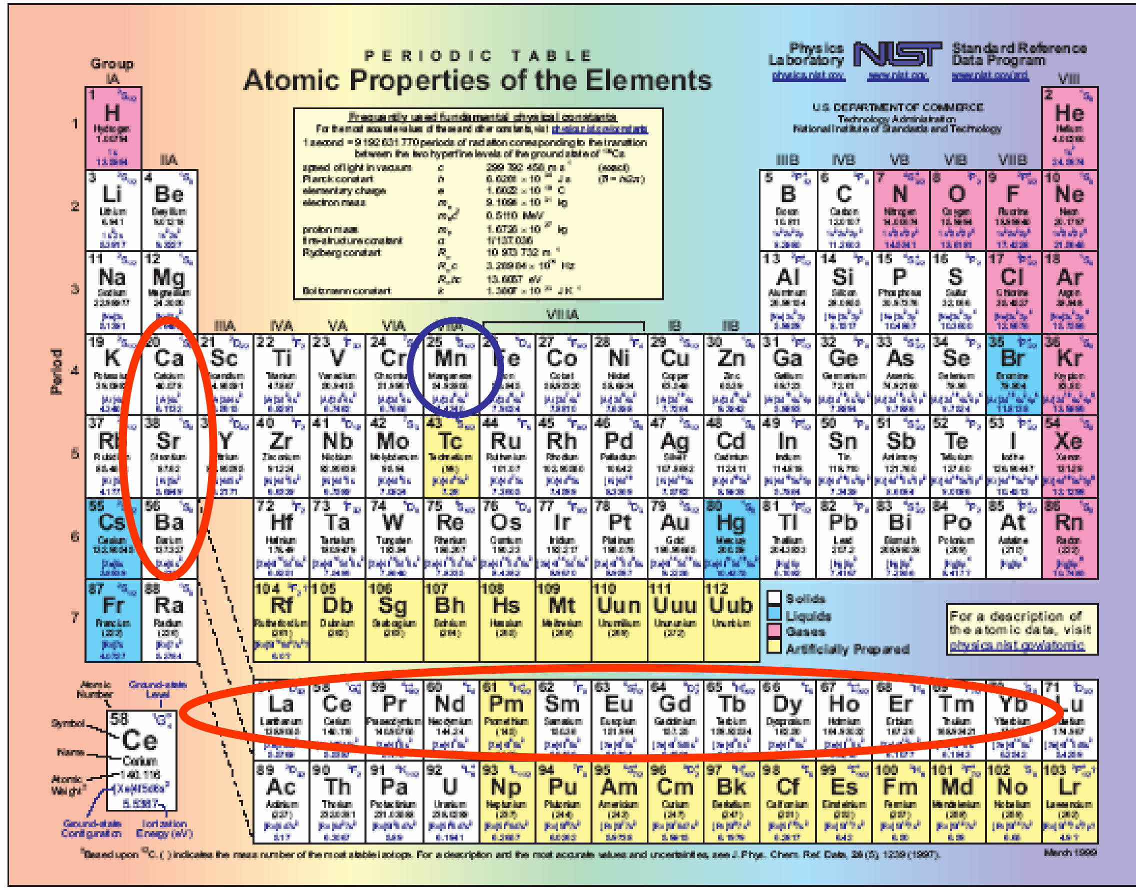

$$Ln^{3+}_{x}\, Ca^{2+}_{1-x}\, Mn^{3+}_{1-x}\, Mn^{4+}_{x}\, O_3$$

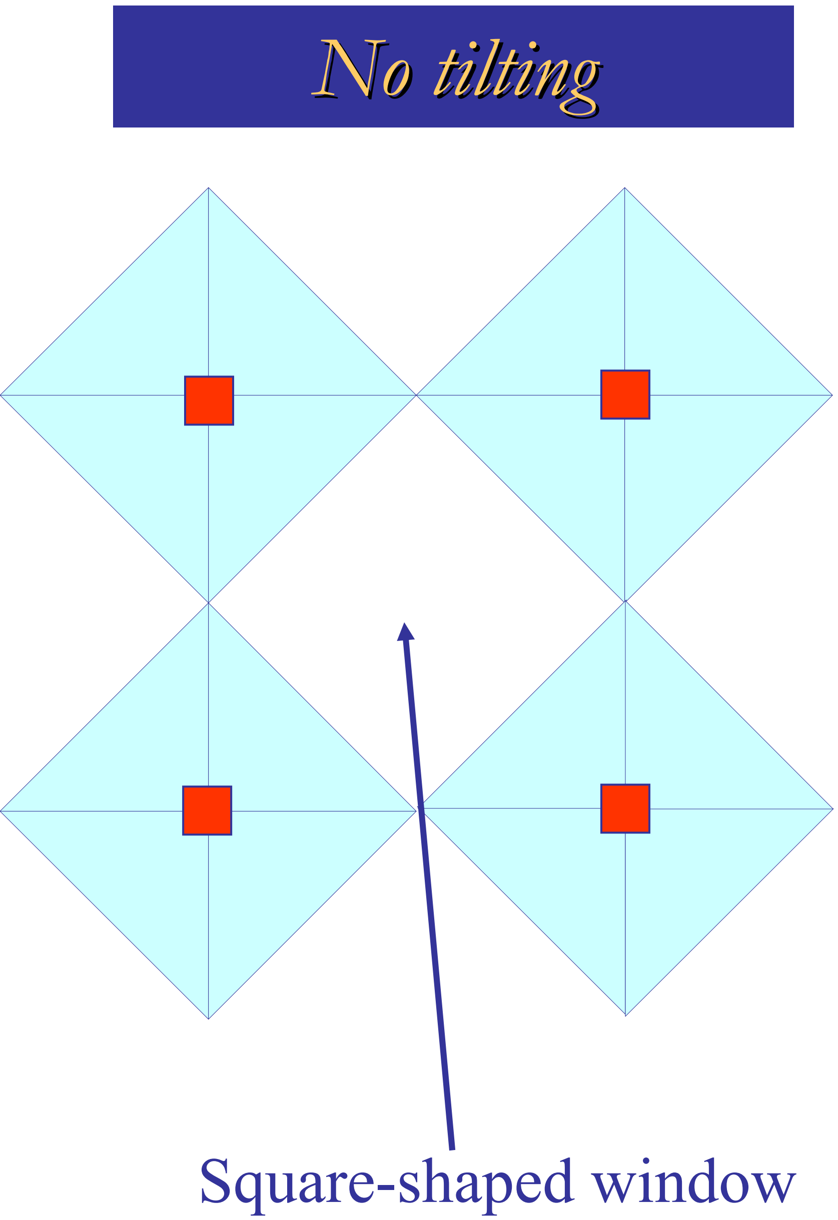
No tilting
Square-shaped window

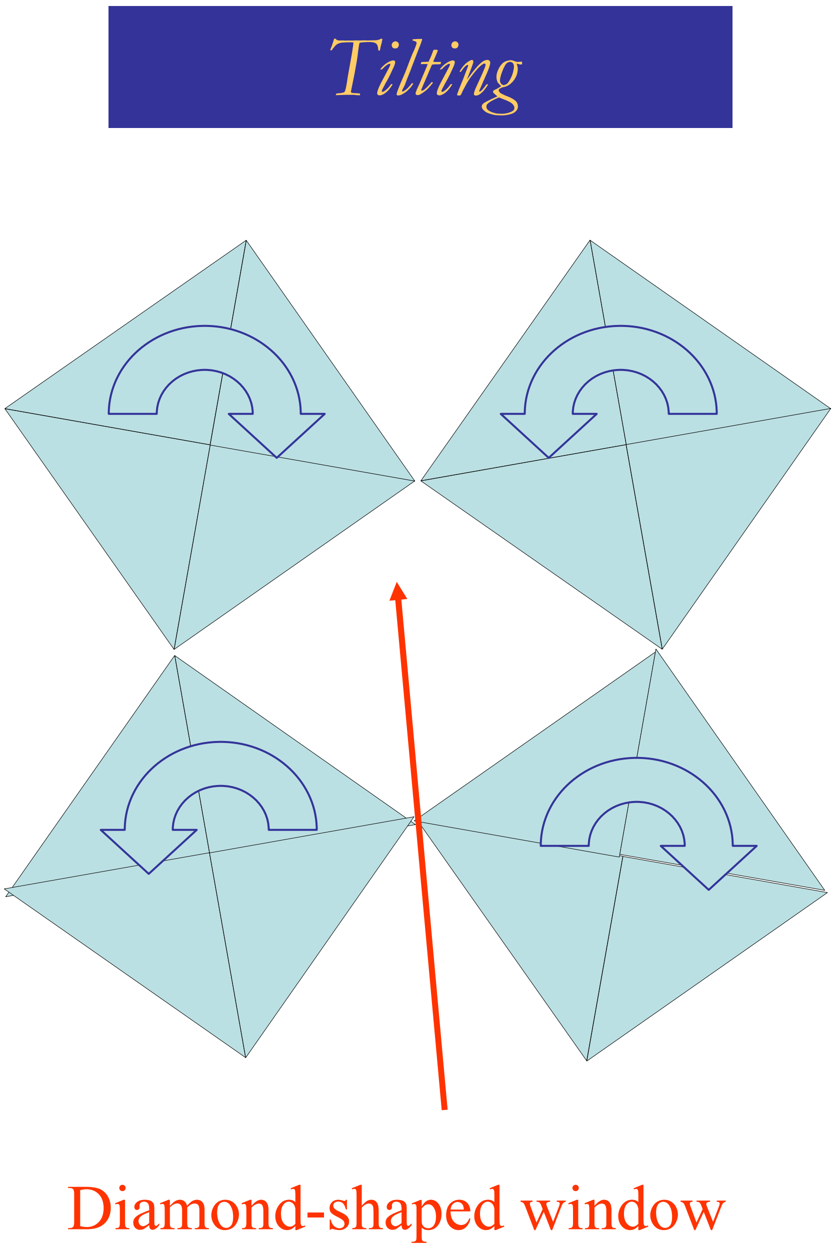
Tilting
Diamond-shaped window

$Ln^{3+}_{x}\,Ca^{2+}_{1-x}\,Mn^{3+}_{1-x}\,Mn^{4+}_{x}\,O_3$

if O3 !!

Tolerance factor — AO / BO frameworks

Goldschmidt factor

$$t = \frac{r_{(Ln,A)} + r_O}{\sqrt{2}(r_{Mn} + r_O)}$$

Distortion

(Ln,A)-O and Mn-O interatomic distances

- manganese valency (Mn^{3+}/Mn^{4+})
- average A-site cationic radius (<r_A>)

$t > 1 \rightarrow$ hexa

$t = 1 \rightarrow$ cubic

$t < 0.96 \rightarrow$ orthorhombic

…

SR+2	4P	6	VI	1.32	1.18
			VII	1.35	1.21
			VIII	1.40	1.26
			IX	1.45	1.31
			X	1.50	1.36
			XII	1.58	1.44 ⟸

CA+2	3P	6	VI	1.14	1.00
			VII	1.20	1.06
			VIII	1.26	1.12
			IX	1.32	1.18
			X	1.37	1.23
			XII	1.48	1.34 ⟸

LA+3	4D10		VI	1.172	1.032
			VII	1.24	1.10
			VIII	1.300	1.160
			IX	1.356	1.216
			X	1.41	1.27
			XII	1.50	1.36 ⟸

Acta Cryst. (1976). A32, 751

Revised Effective Ionic Radii and Systematic Studies of Interatomic in Halides and Chalcogenides

By R. D. Shannon

MN+3	3D	4	V		.72	.58	
			VI	LS	.72	.58	R
				HS	.785	.645	R*
MN+4	3D	3	IV		.53	.39	R
			VI		.670	.530	R*

TABLE I. σ^2 and A contents (x,y,z) for the $Th_{0.35}(Ba_xSr_yCa_z)MnO_3$ series.

x(Ba)	y(Sr)	z(Ca)	$\sigma^2 \times 10^4$ (nm^2)
0.138	0.512	0	1.74
0.16	0.463	0.027	1.84
0.18	0.419	0.051	1.96
0.20	0.374	0.076	2.00
0.22	0.329	0.101	2.12
0.24	0.285	0.125	2.20
0.26	0.24	0.15	2.30
0.30	0.15	0.20	2.47
0.3675	0	0.2825	2.80

properties

$Th_{0.35}(Ba_xSr_yCa_z)MnO_3$

A-site disorder

$$\sigma^2 = \Sigma y_i r_i^2 - \langle r_A \rangle^2$$

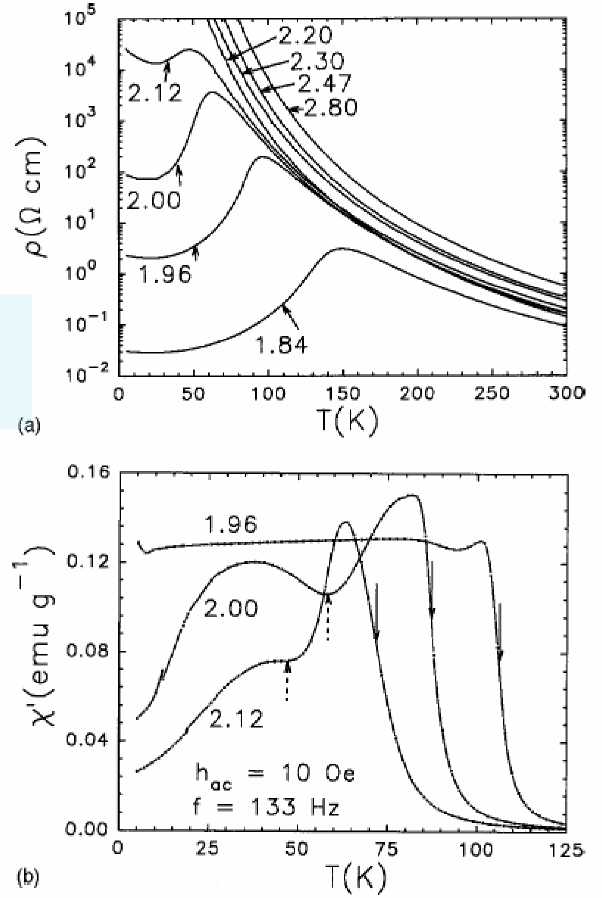

FIG. 2. (a) T-dependent resistivity (ρ) of the $Th_{0.35}A_{0.65}MnO_3$ samples registered in the absence of magnetic field. $\sigma^2 \times 10^4$ (nm^2) values are labeled on the graph. (b) T-dependent real part of the ac susceptibility (χ') for the $Th_{0.35}A_{0.65}MnO_3$ samples (10 Oe and f = 133 Hz). The solid vertical arrows indicate the inflection points determining T_C. Dashed vertical arrows indicate the χ' minimum temperature, which correspond to the ρ maximum on (a).

Fixed Mn valence

$Ln_{0.7}A_{0.3}MnO_3$

Fixed $\langle r_A \rangle$ = 1.255 Å

#$Nd_{0.7}Ba_{0.3}MnO_3$

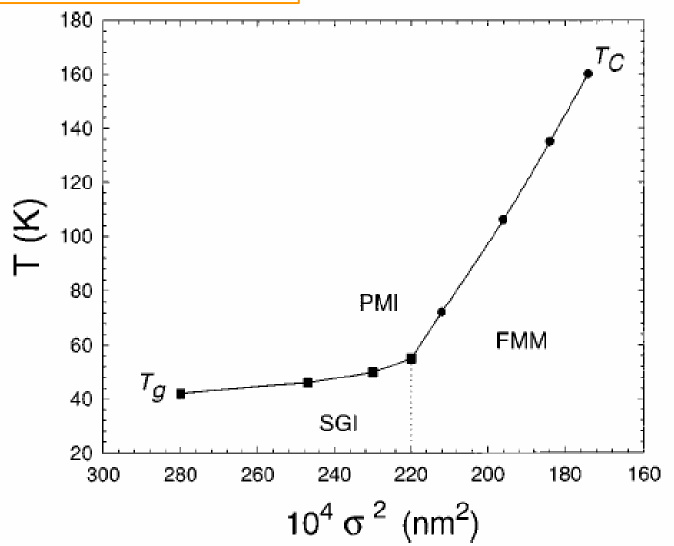

FIG. 8. Electronic and magnetic diagram established for the $Th_{0.35}A_{0.65}MnO_3$ series: T_C (●) and T_g (○) as a function of the variance σ^2. The boundary between the SGI and FMM regions is symbolized by the dotted line.

PHYSICAL REVIEW B VOLUME 60, NUMBER 22 1 DECEMBER 1999-II

Size mismatch: A crucial factor for generating a spin-glass insulator in manganites

Manganites : Complex magnetic and electronic phase diagram

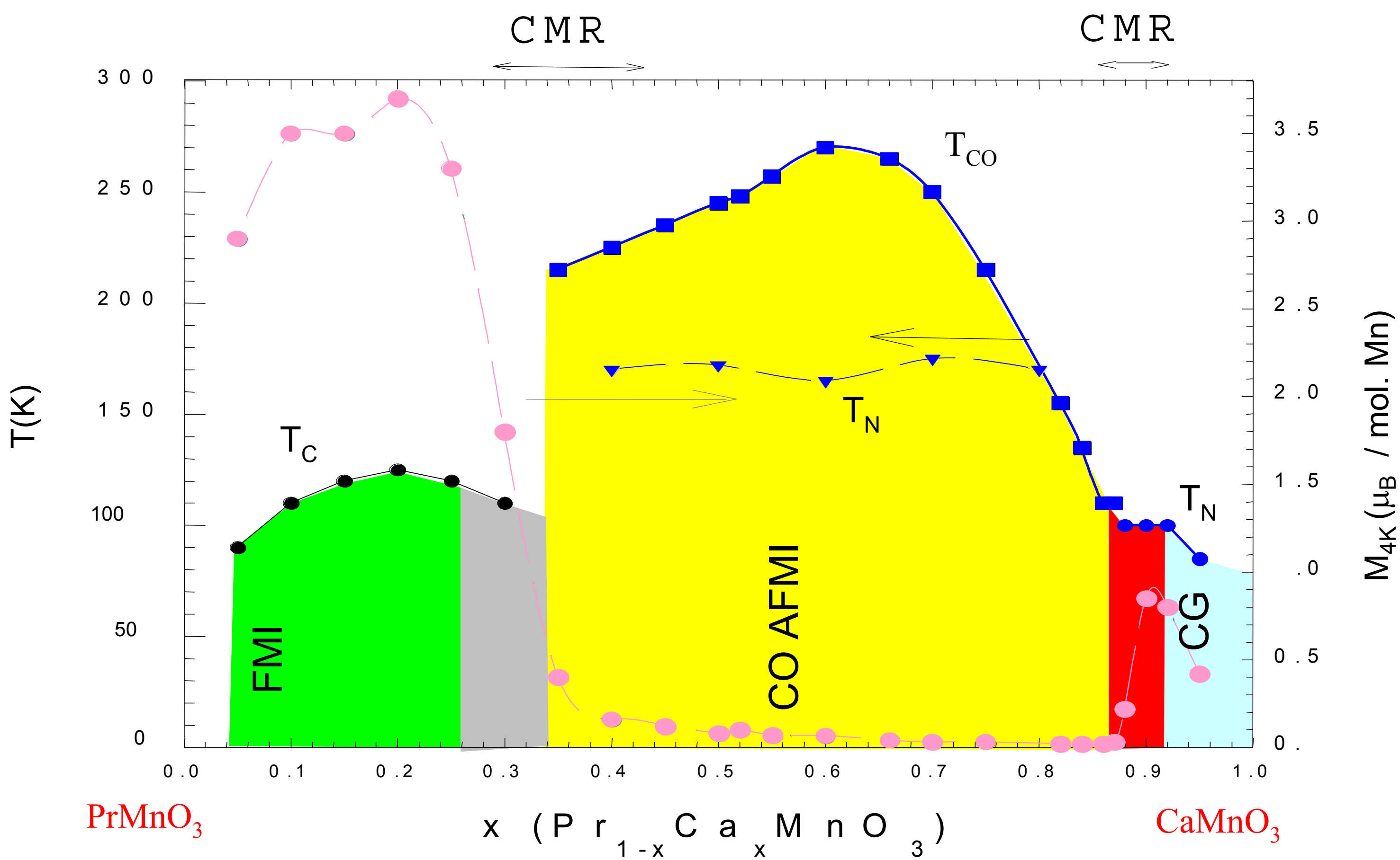

Magnetic properties : magnetization, susceptibility….

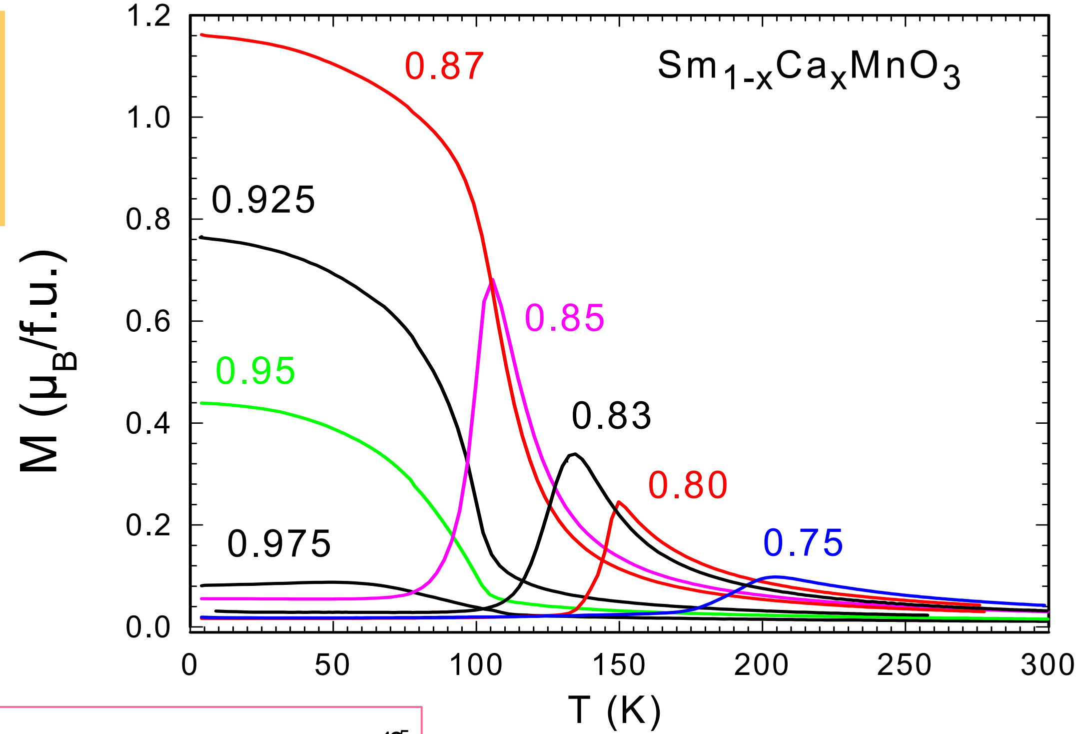

… Correlated with transport properties

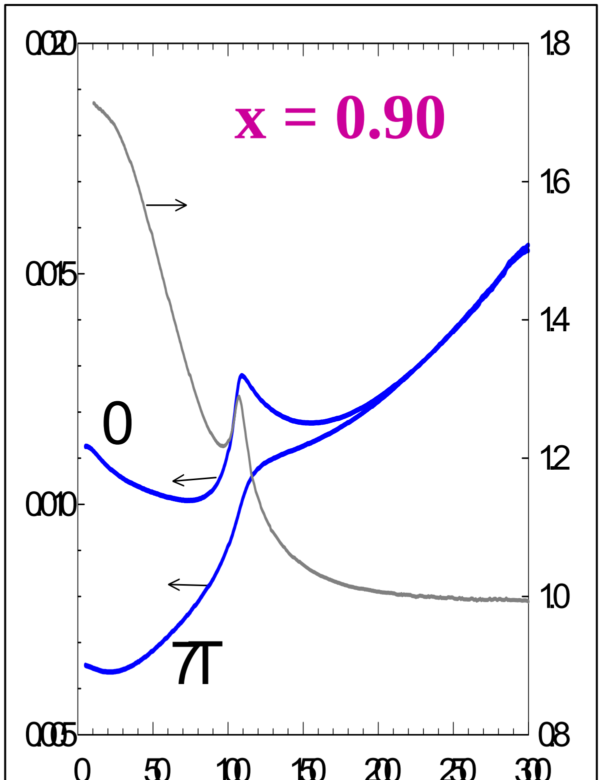

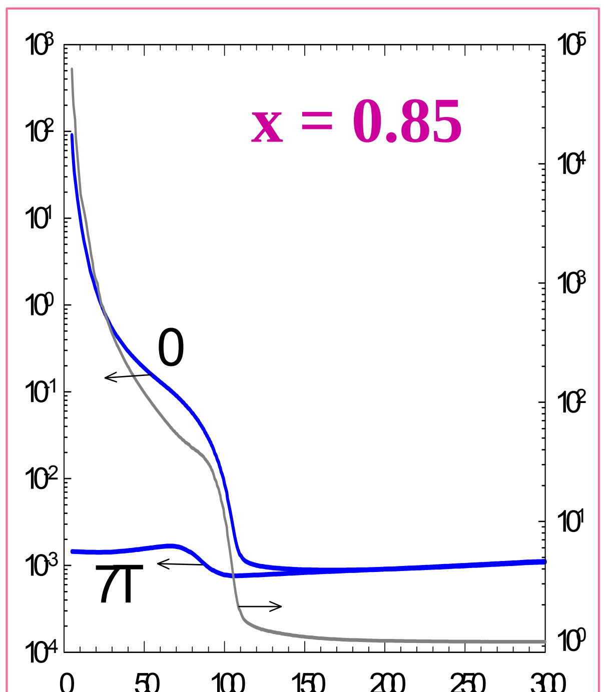

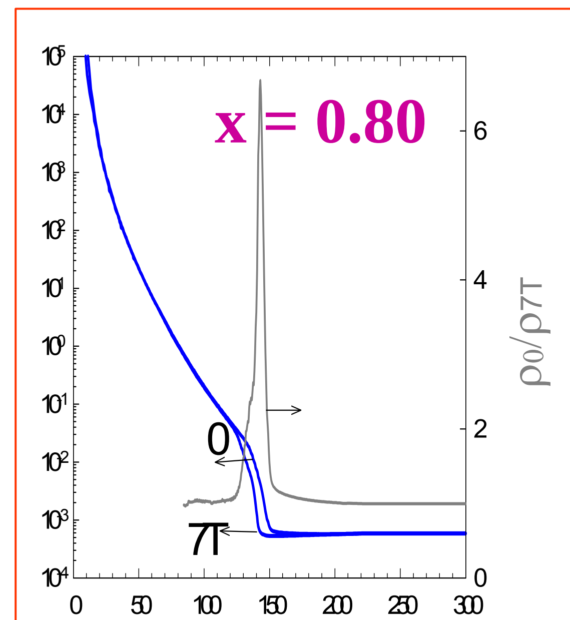

J. Solid State Chem. 134, 1, 198 (1997)

Phys. Rev. B 60, 14057 (1999)

Impurity induced CO

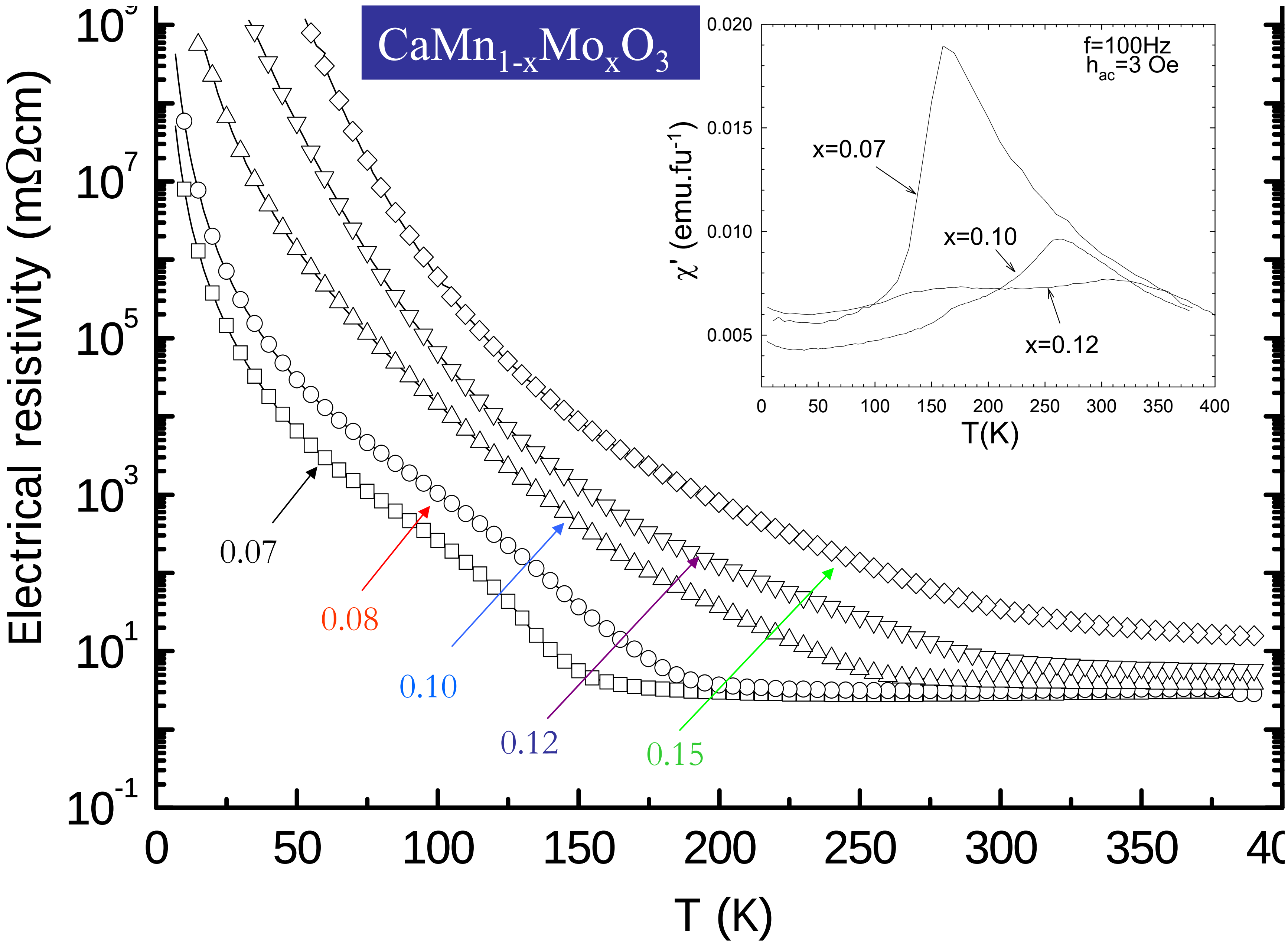

Ex1

ND-LLB-G4 1 *f (T)*

$CaMn_{0.9}Mo_{0.1}O_3$

magnetism [T_N]and structure [T_{OO}] *vs.* T

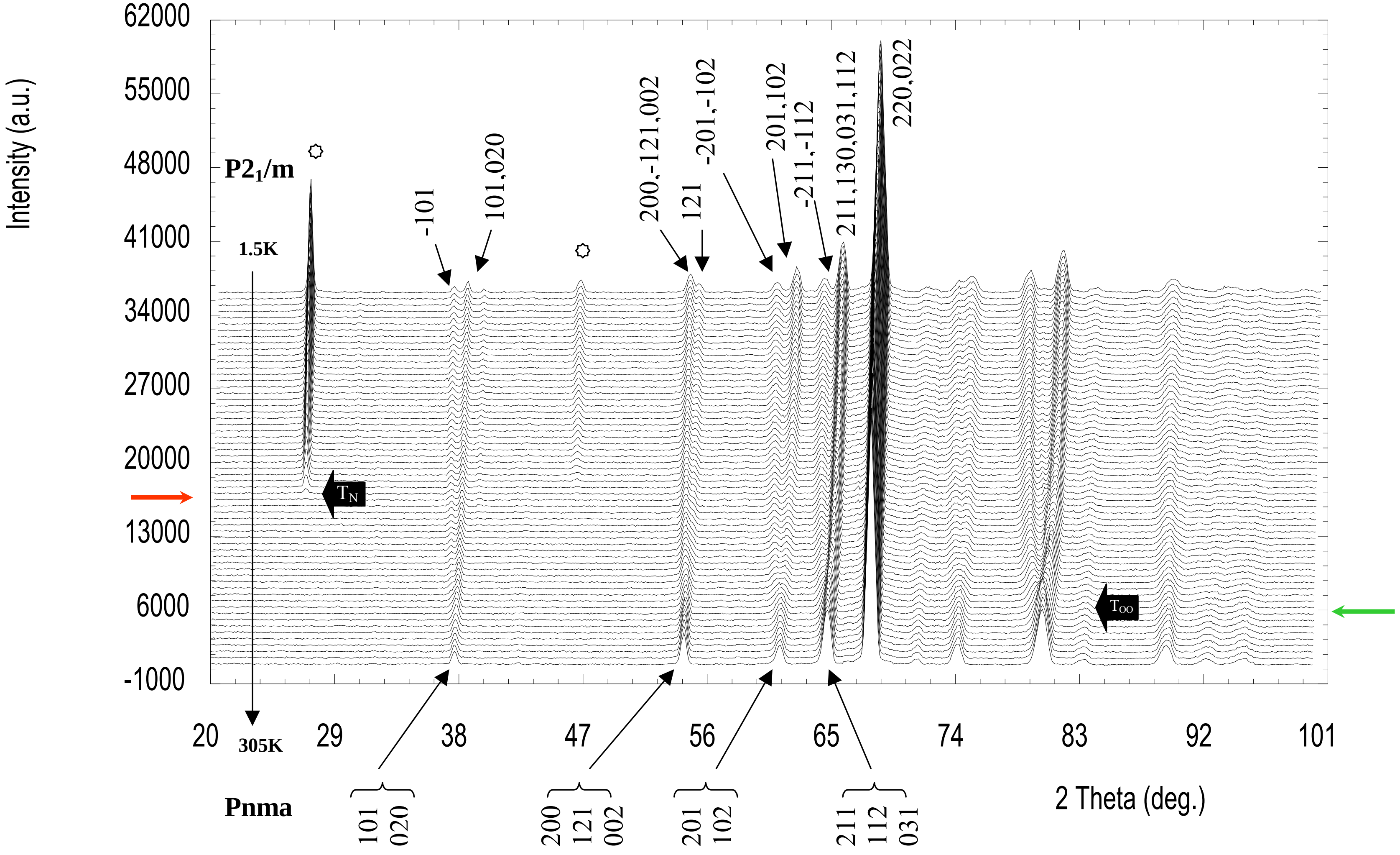

Ex1

ME *f(T)*

$CaMn_{0.9}Mo_{0.1}O_3$

DE 300K 90K → image

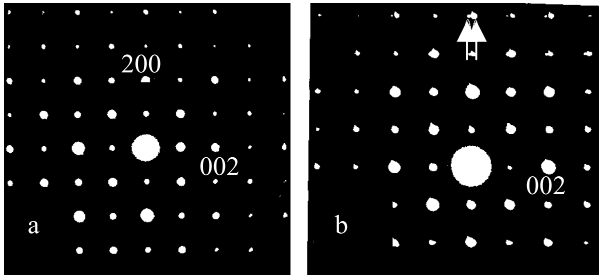

Pnma $P2_1/m$

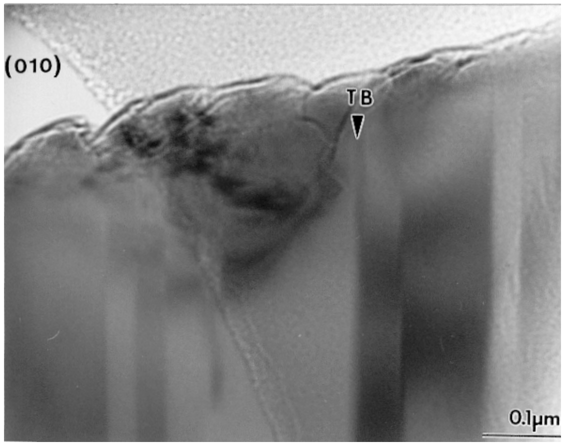

Propriétés physiques *f(T)*

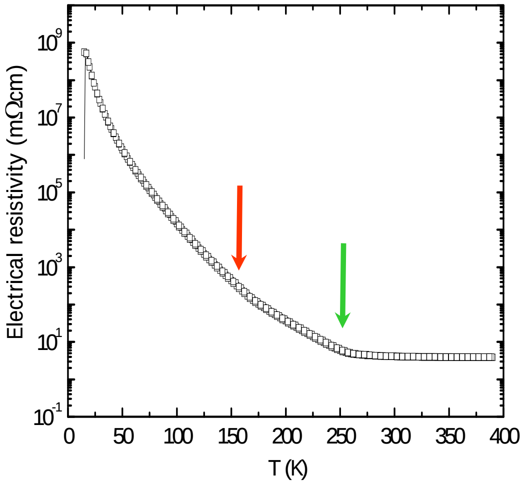

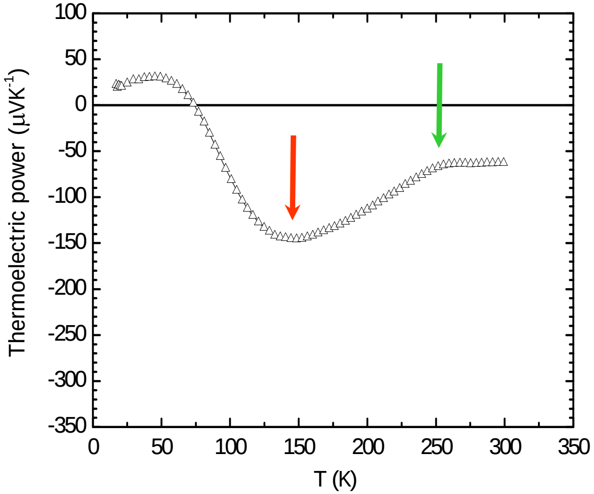

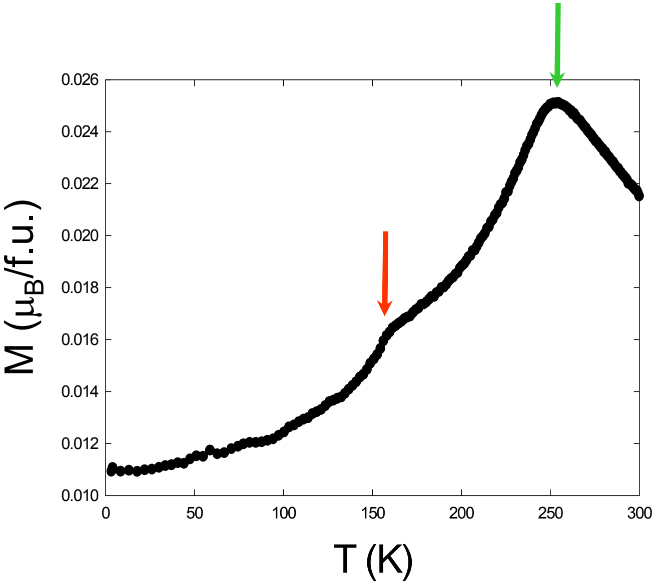

Ex1

$CaMn_{1-x}Mo_xO_3$

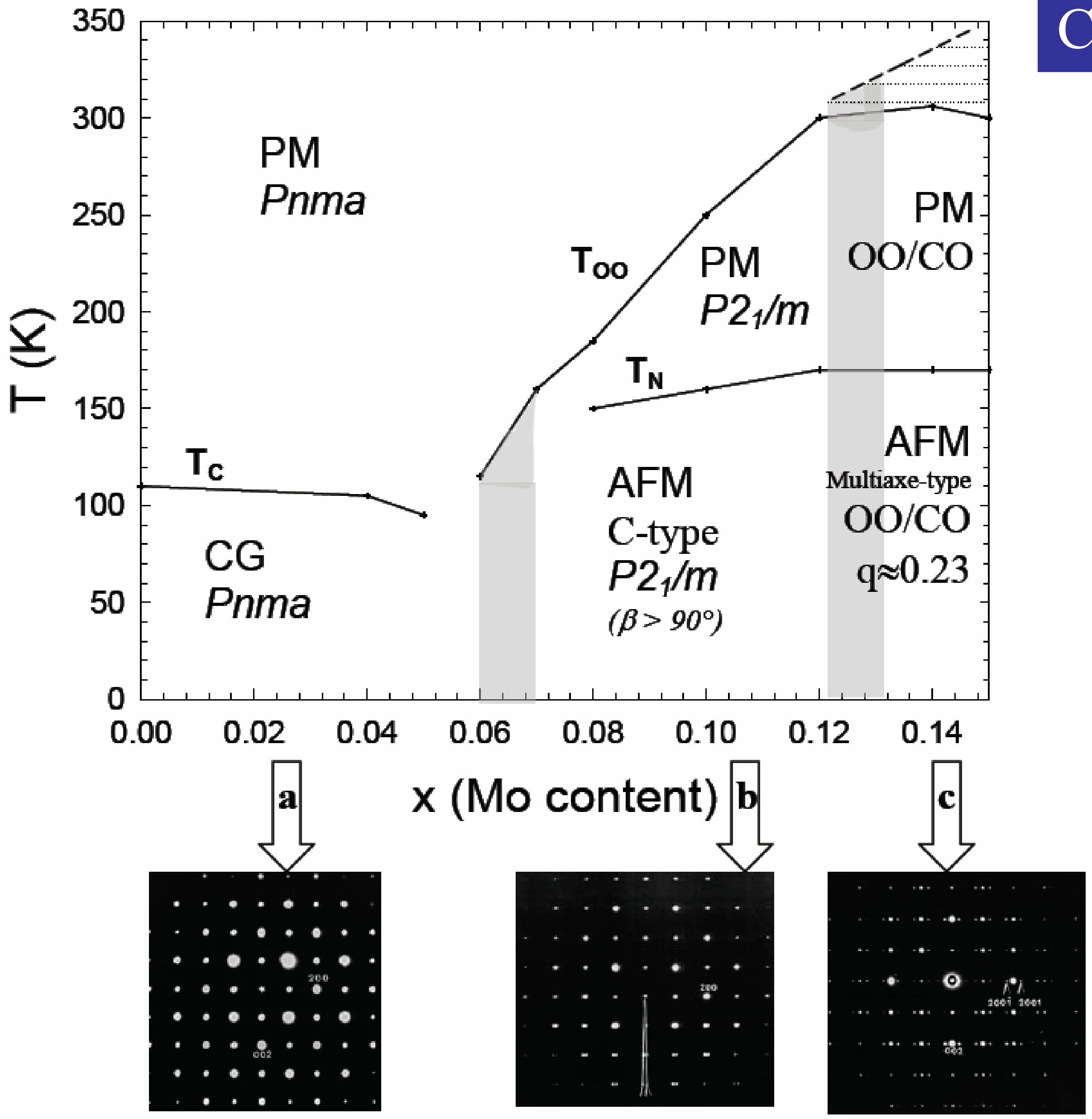

Charge and orbital Ordering

e.g. $Pr_{0.5}Ca_{0.5}MnO_3$

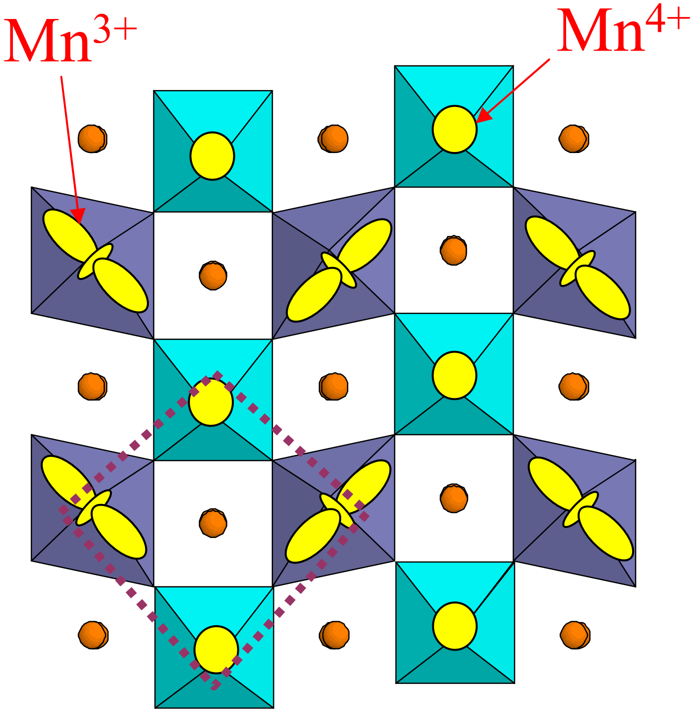

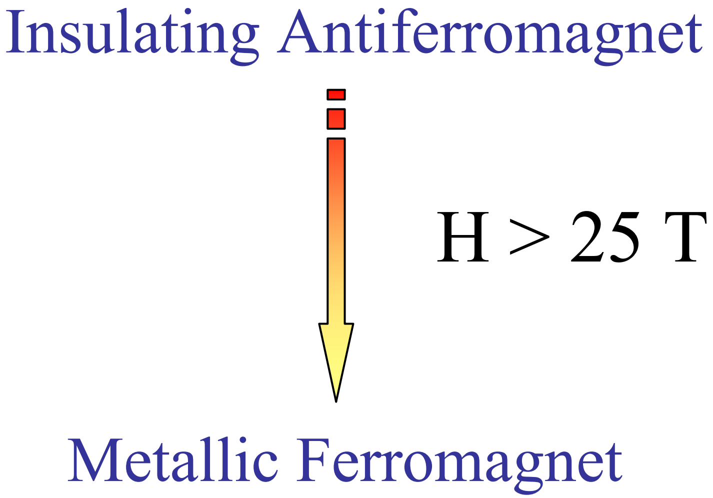

Manganites : successive M(H) at 2.5 K, T= 300K

The ferromagnetic fraction decreases with the number of thermal cycling : history effect

$Pr_{0.5}Ca_{0.47}Ba_{0.03}MnO_3$

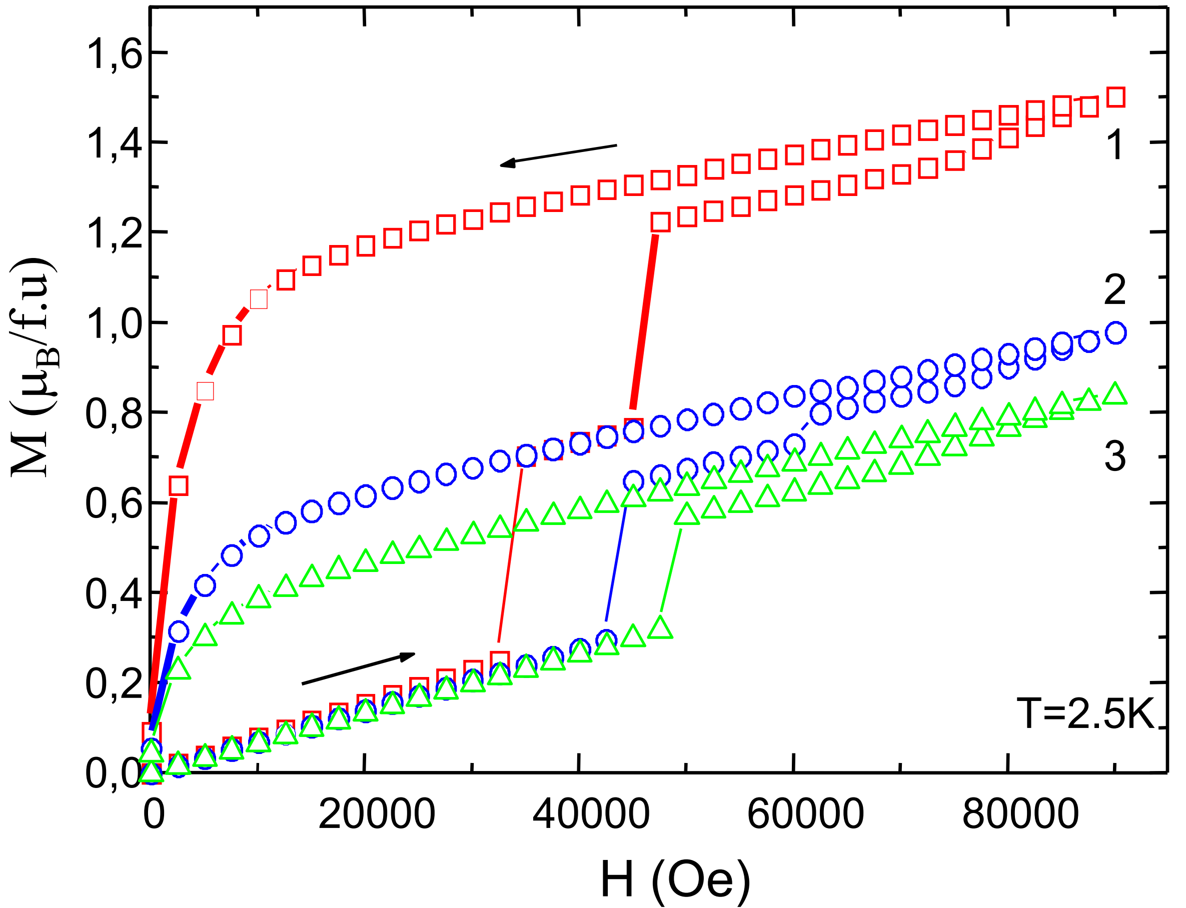

Characteristic H of the steps : irreproducibility

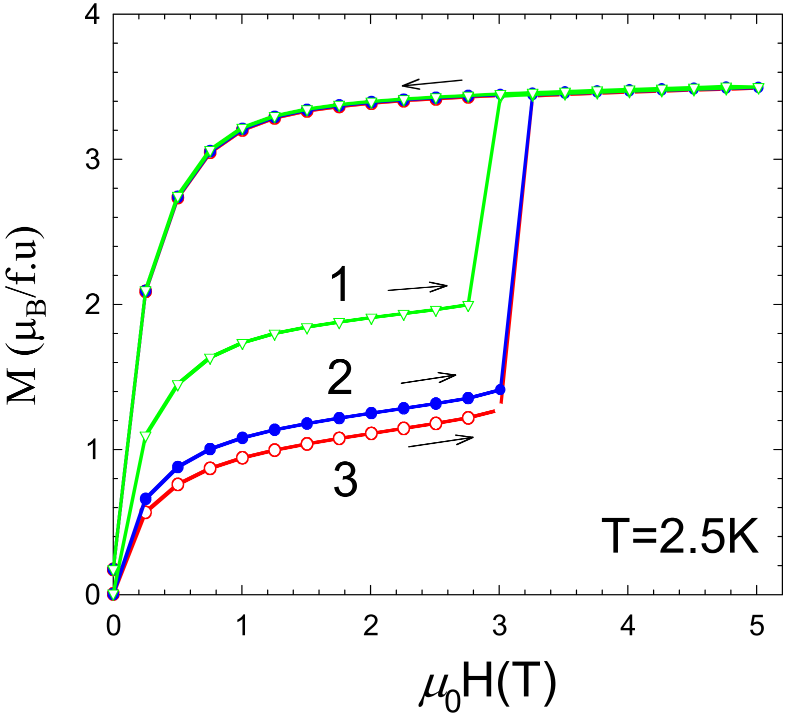

$Pr_{0.6}Ca_{0.4}Mn_{0.99}Cr_{0.01}O_3$

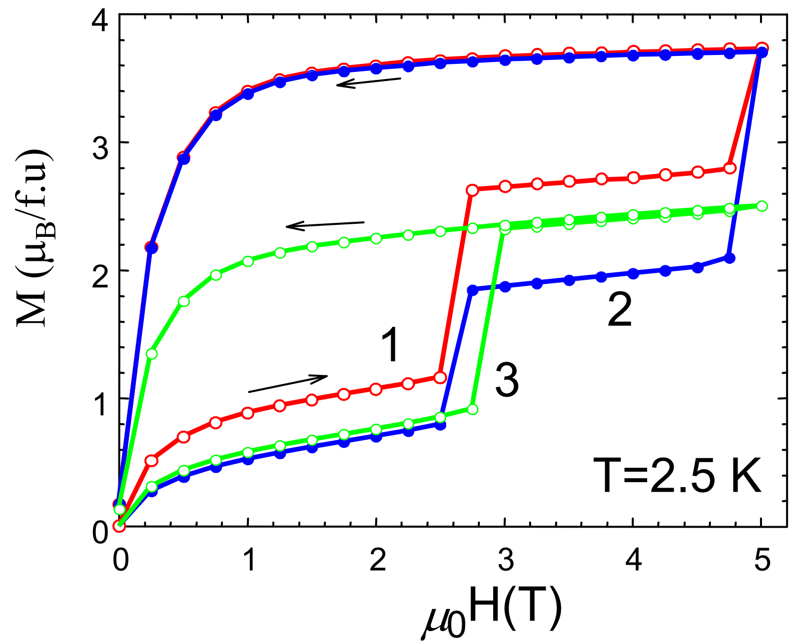

$Pr_{0.6}Ca_{0.4}Mn_{0.98}Ga_{0.02}O_3$

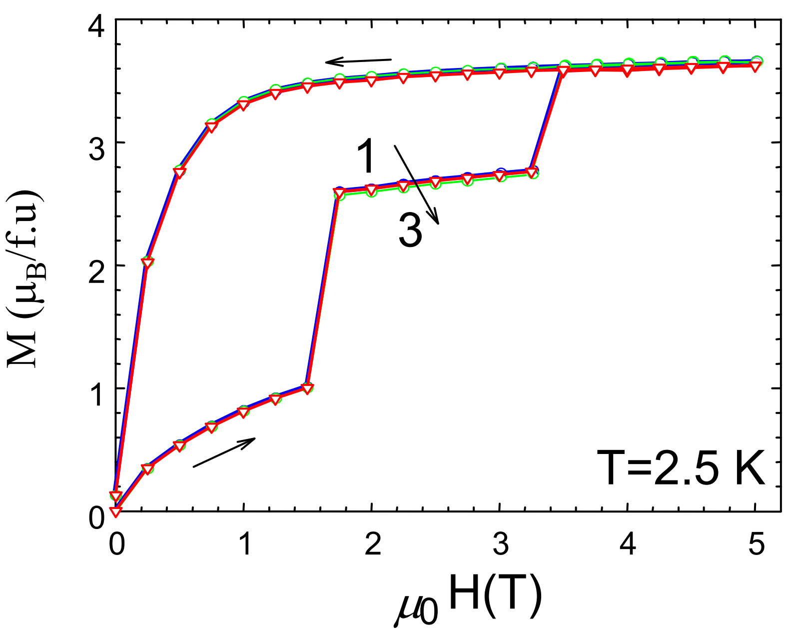

$Pr_{0.6}Ca_{0.4}Mn_{0.96}Ga_{0.04}O_3$

Influence of the temperature

Avalanches

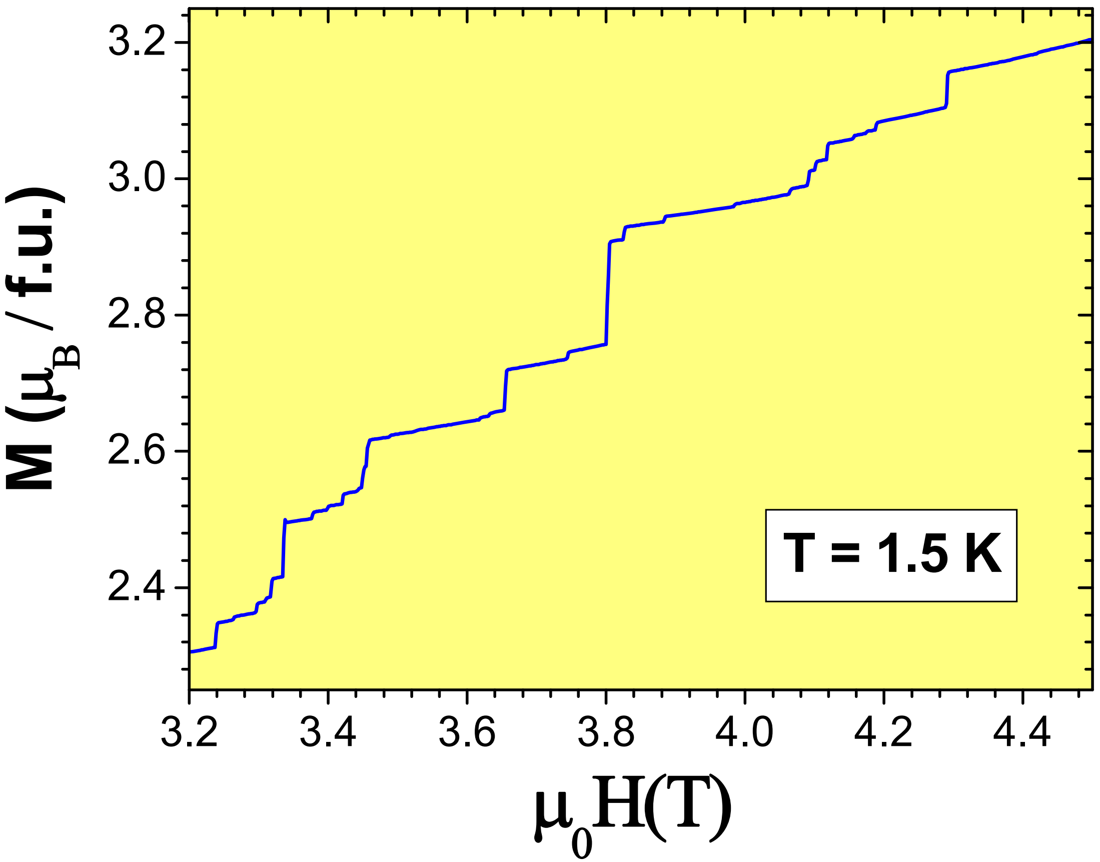

At even lower T, additional steps : no characteristic scales as expected in MT like transition

Magnetization Steps

No “critical fields” strictly speaking
No specific magnetization values associated with the plateaus

Stepwise growth of the FM phase at the expense of the AFCOO phase ?

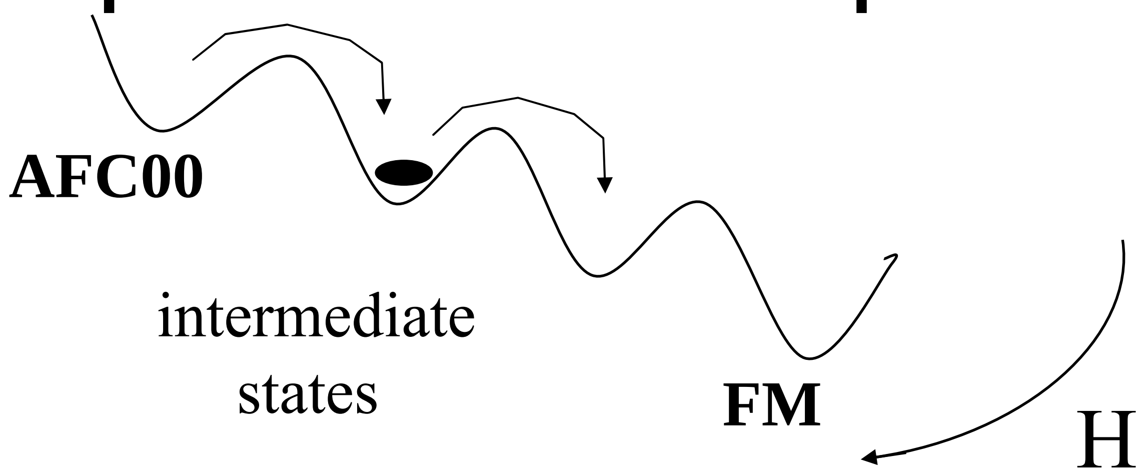

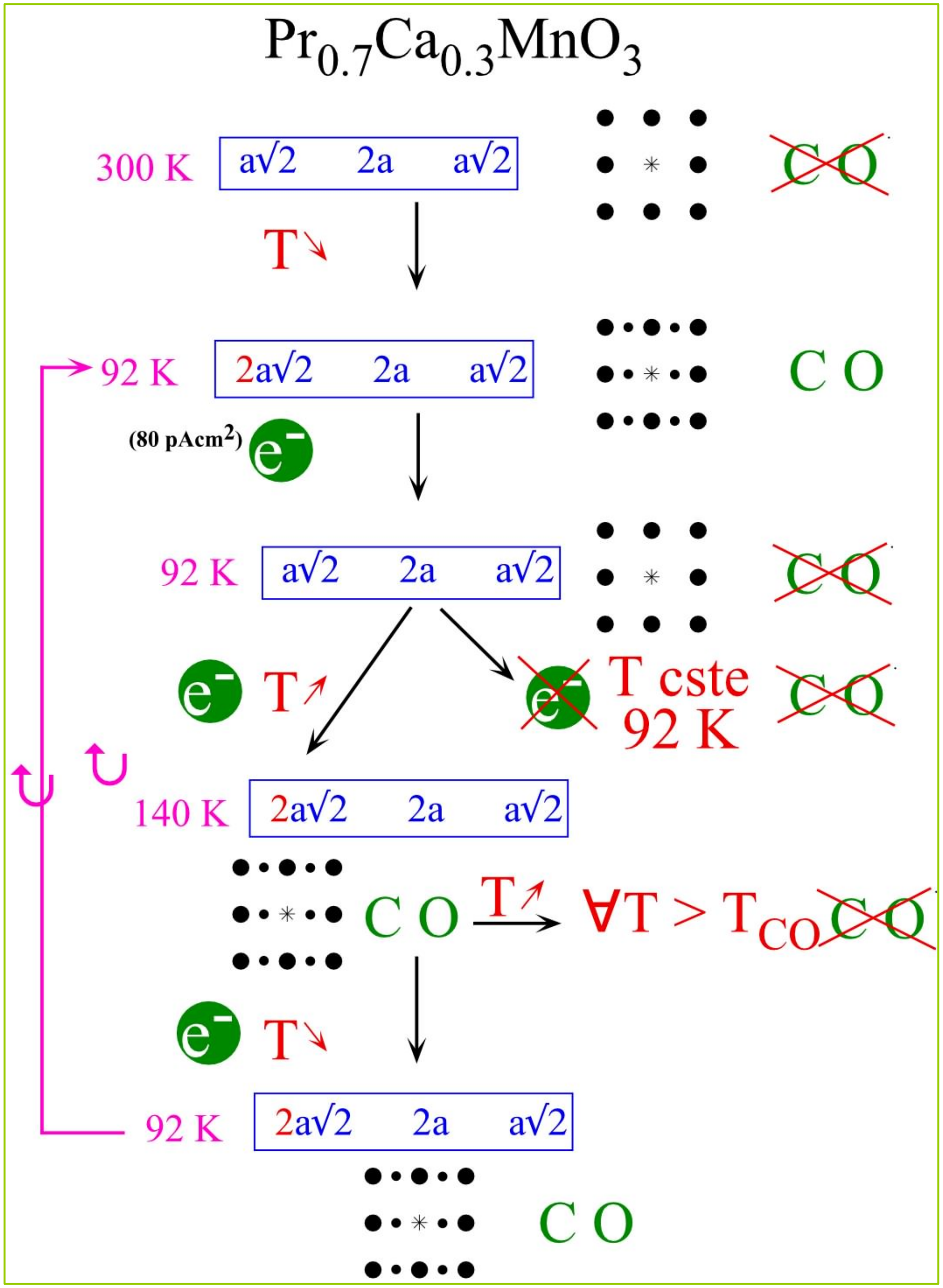

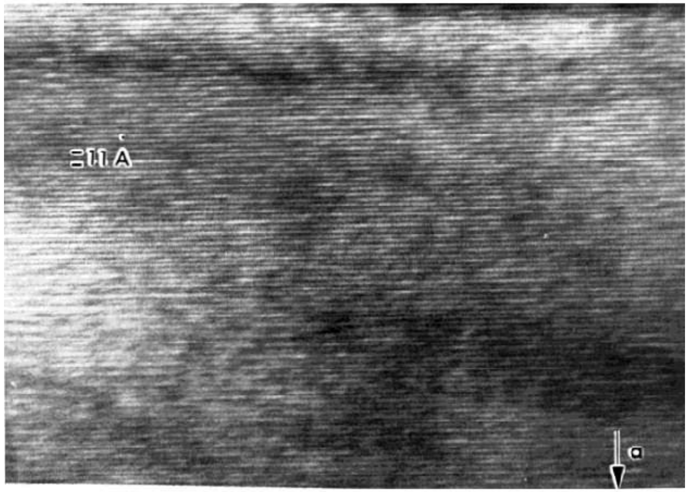

92 K : Lattice image of CO structure

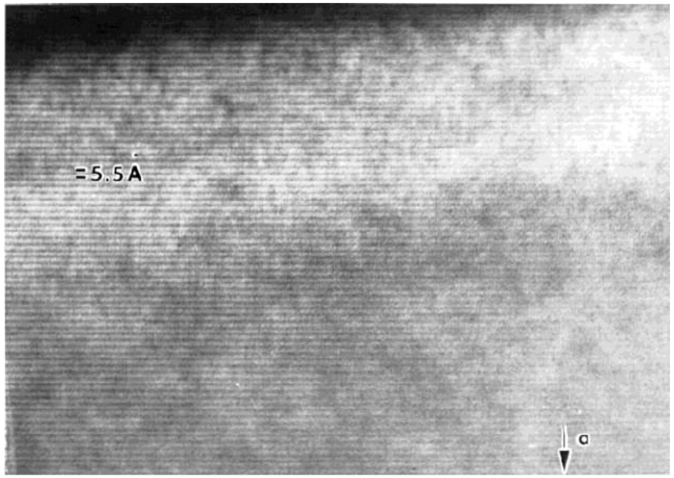

92 K : Same area after e⁻ irradiation

CO

Plan:

3D magnetic networks:

CMR in perovskite manganites

MIT in cobaltites

Frustrated lattices of the « 114 » type

1D and 2D TM-O-TM networks: hexagonal perovskites
and CdI_2 type structures

n-type ***vs*** **p-type** conductivity in oxides

Oxygen and cation ordering: ordered perovskite

YBa_2Cu_3O
7

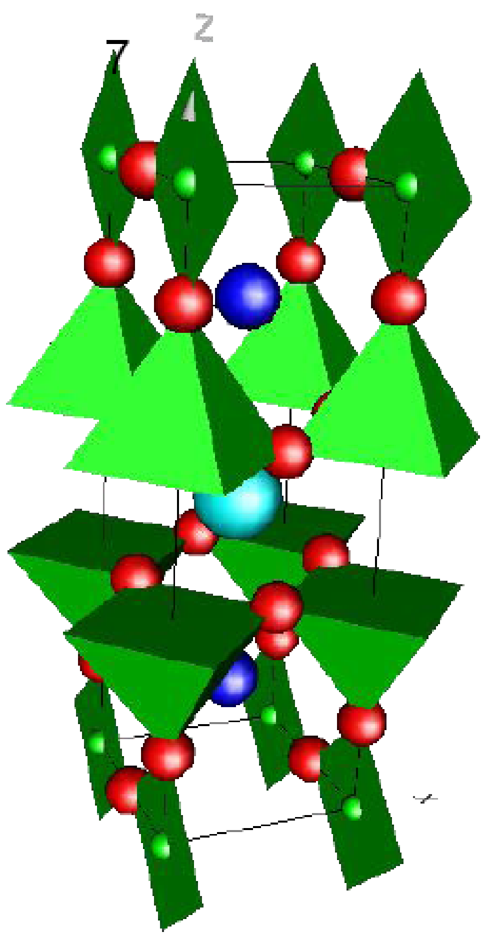

123

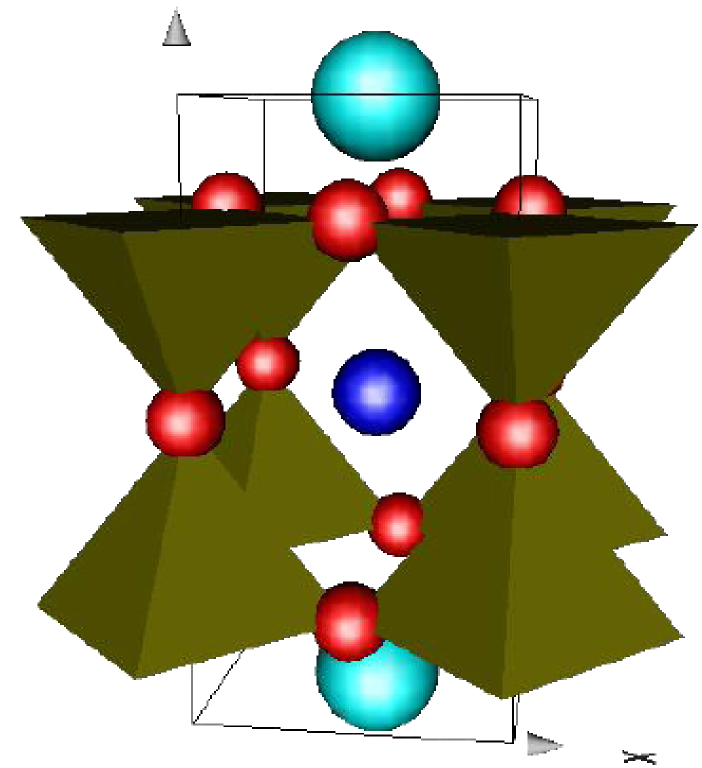

$LBaCo_2O_{5.5}$ 112

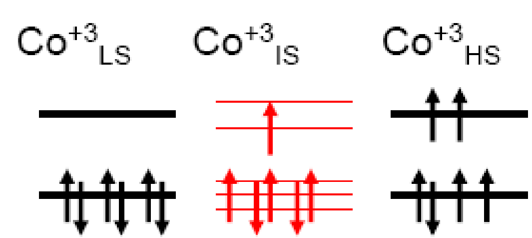

Hole *vs* Electron asymmetry

$LnBaCo_2O_{5+x}$: x=0.5, pure trivalent cobalt, $T_{MI}=f(r_A)$
trivalent Ho and Y same ionic radius (0.1072 and 0.1075nm)

T_{MI}=300K

$HoBaCo_2O_{5.5}$

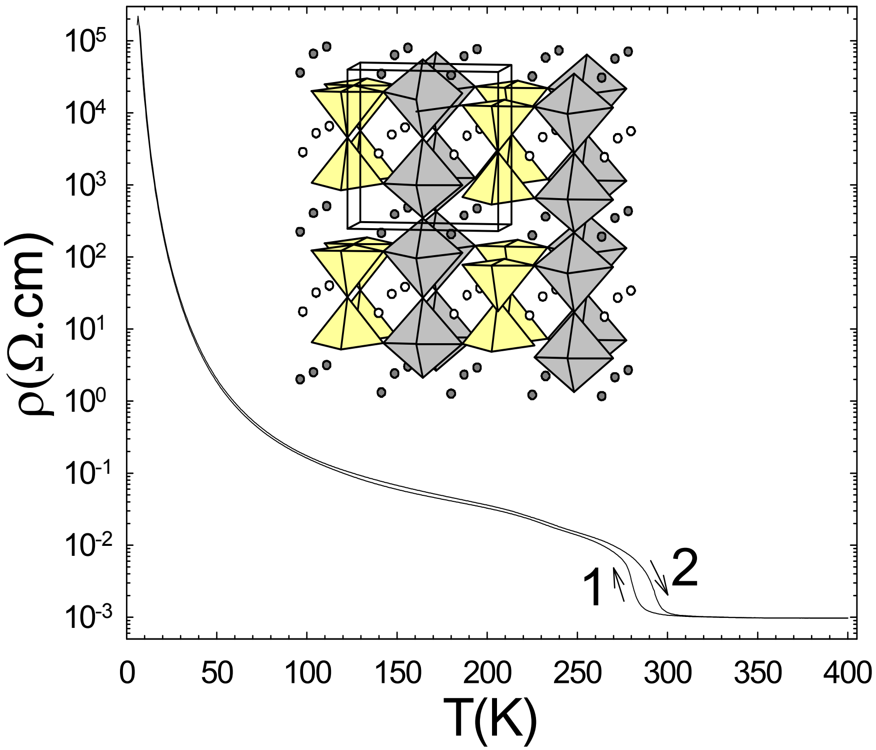

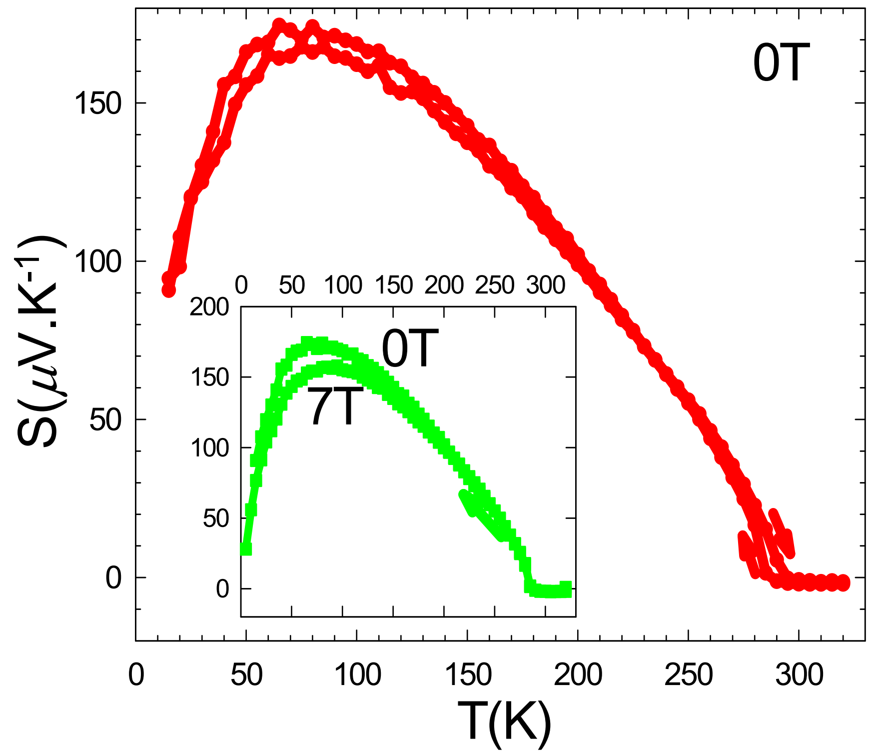

TEP sign change at T_{MI} from
metal S = -2 μV.K^{-1} *(e^-)* to insulator S>>0 *(h^+)*

« Co^{3+} » - 112 cobaltites

Possible spin blockade in 112

High T : an e_g electron Co^{2+} can move in a background of IS/HS Co^{3+}
Broad e_g band , S<0 and small abs. value

Low T : an e_g electron Co^{2+} cannot move in a background of LS Co^{3+} , requires to flip other spins, wrong spin-states LS Co^{2+} and IS Co^{3+} instead of LS

Low T : a t_g hole Co^{4+} can hop in a background of LS Co^{3+} ,
Localization of heavy holes as T decreases, S>>0

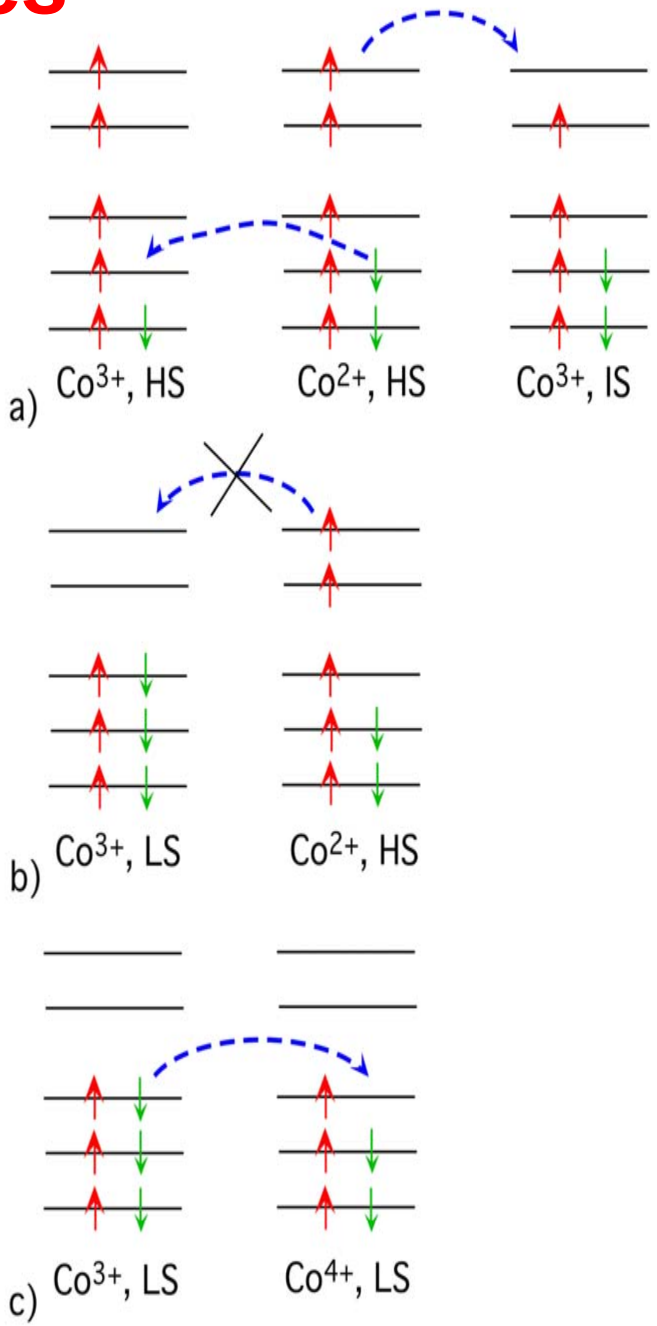

A. Maignan et al, Phys. Rev. Lett. 93, 026401 (2004)

CuO tenorite oxide

spiral induced electric polarization in the 213K-230K range
where an incommensurate antiferromagnetic structure is observed

C2/c monoclinic structure (distorted NaCl struct.)

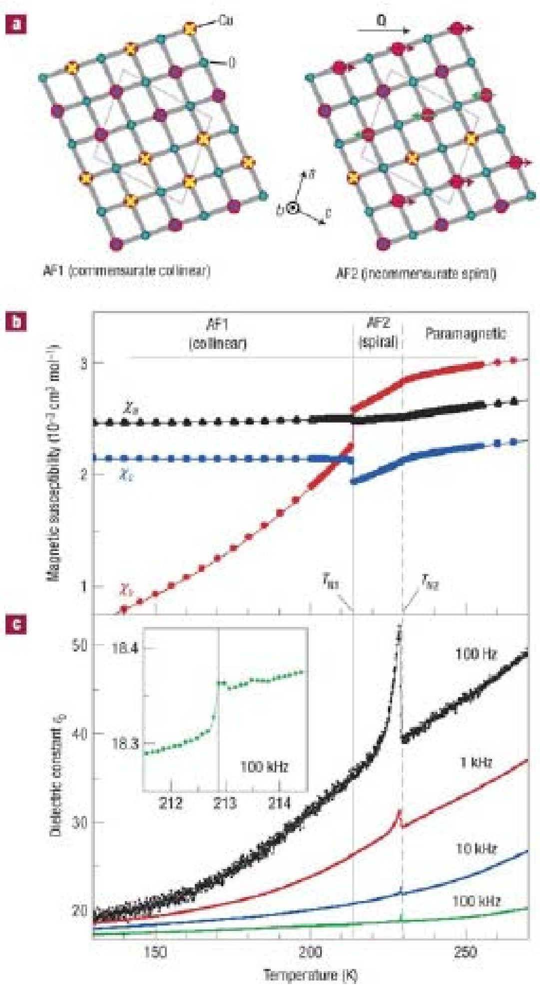

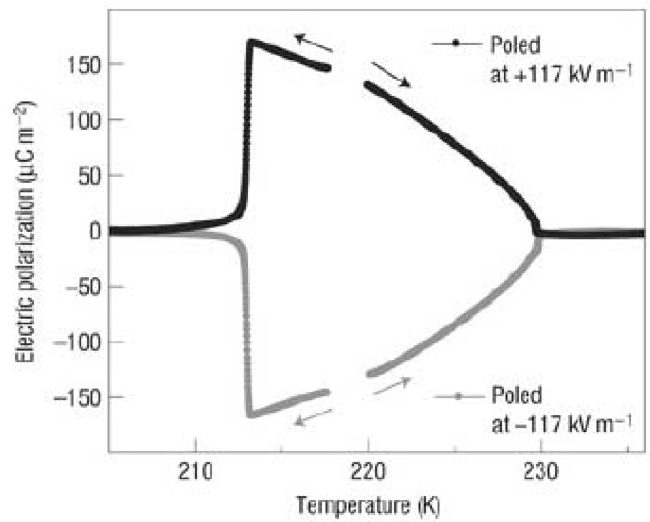

Kimura, Nature Materials 7, 291 - 294 (2008)

112- $YBaCuFeO_5$ ordered perovskite (Y/BaO), isostructural to $YBaCo_2O_5$

Do Fe and Cu order ?

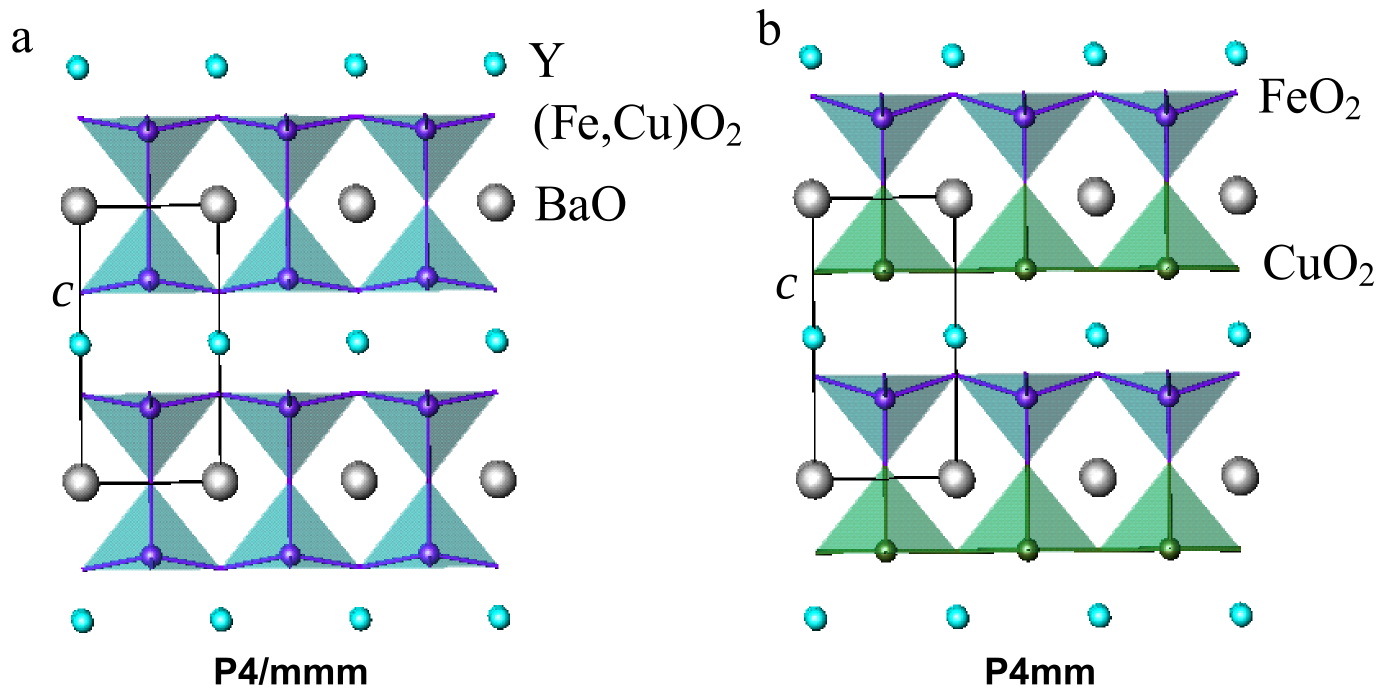

FIG. 1. (Color online) (a) Schematic drawing of the $LBaM_2O_5$ structure for $L=Y^{3+}$ and $M=Cu^{2+}$, Fe^{3+}. (b) In the $P4mm$ acentric structure, the different positions of Fe and Cu in the pyramids might be favorable to electric polarization along the c-axis.

Kundys B et al., APPLIED PHYSICS LETTERS 94 , 072506 2009

$YBaCuFeO_5$

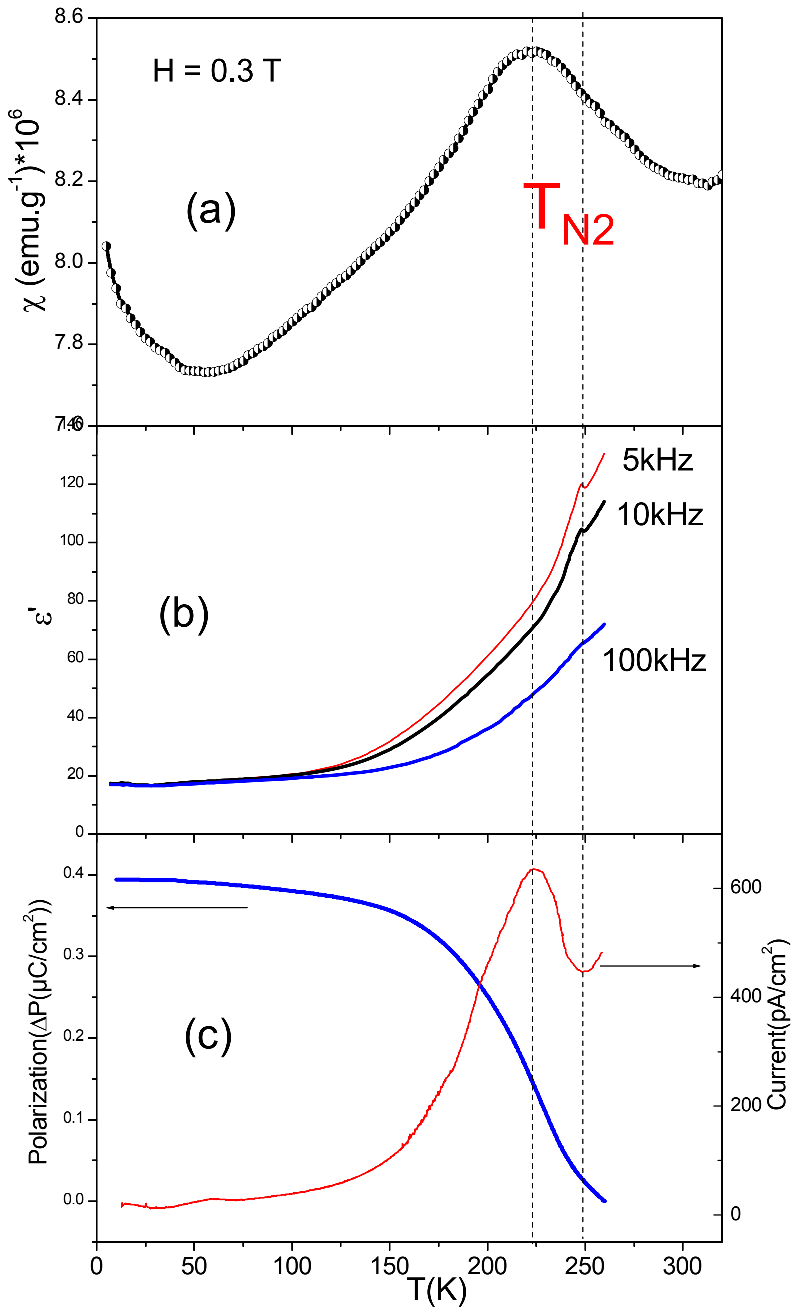

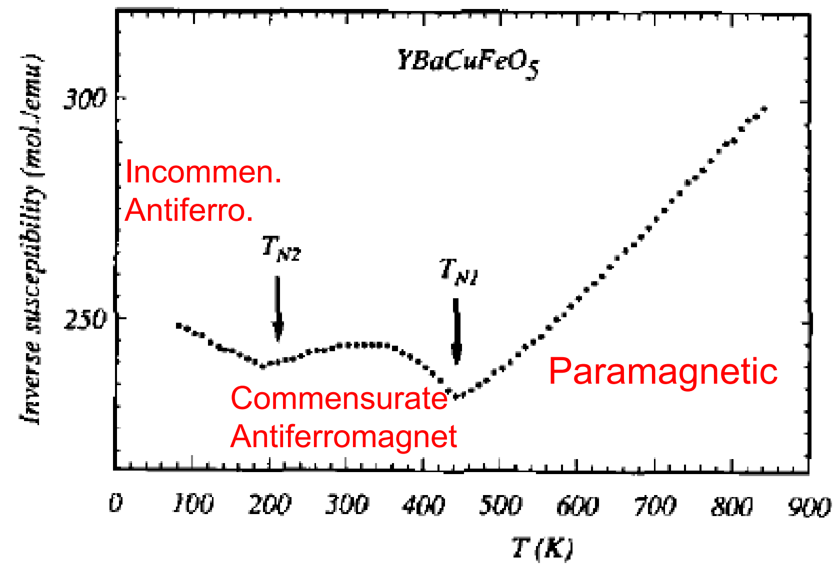

Complex Incommensurate AF structure

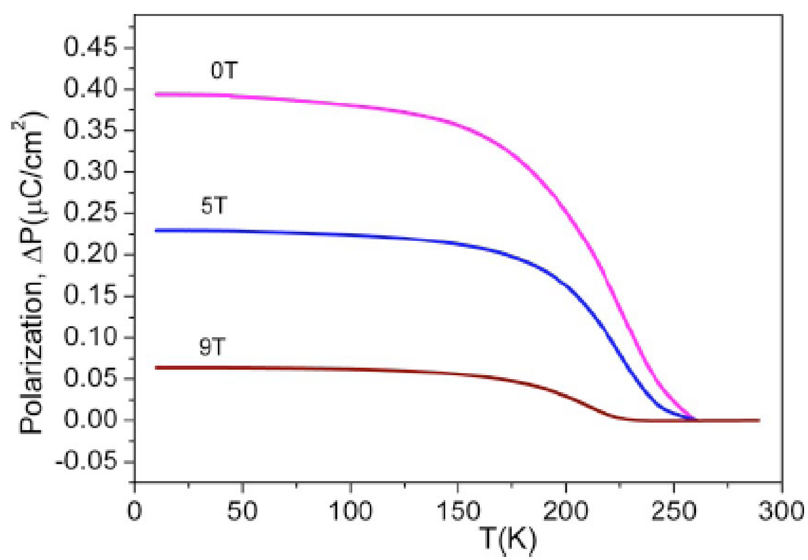

Magnetoelectric coupling

Plan:

3D magnetic networks:

CMR in perovskite manganites

MIT in cobaltites

Frustrated lattices of the « 114 » type

1D and 2D TM-O-TM networks: hexagonal perovskites and CdI_2 type structures

n-type ***vs*** **p-type** conductivity in oxides

$LnBaCo_4O_7$

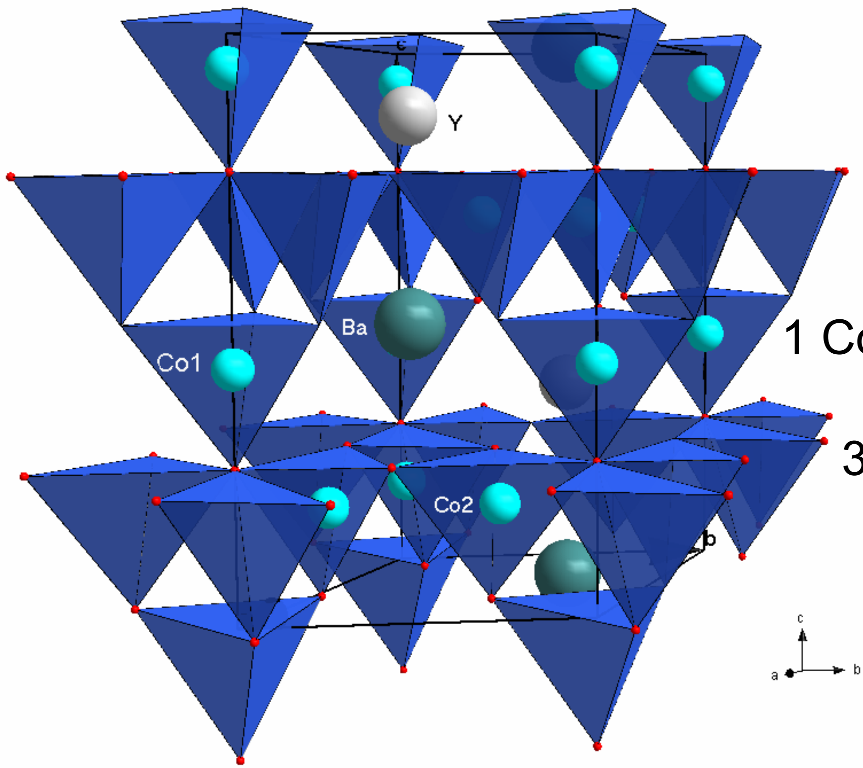

Network of CoO_4 tetrahedra

1 Co(1) : triangular

3 Co(2) : kagomé

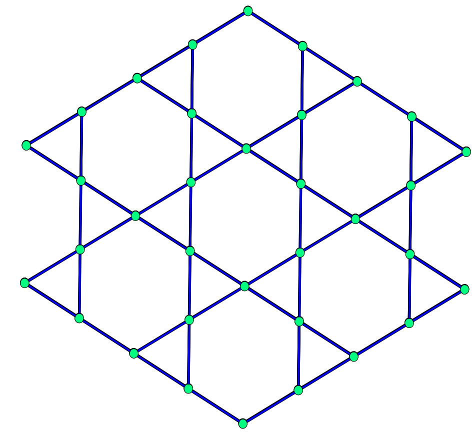

kagome

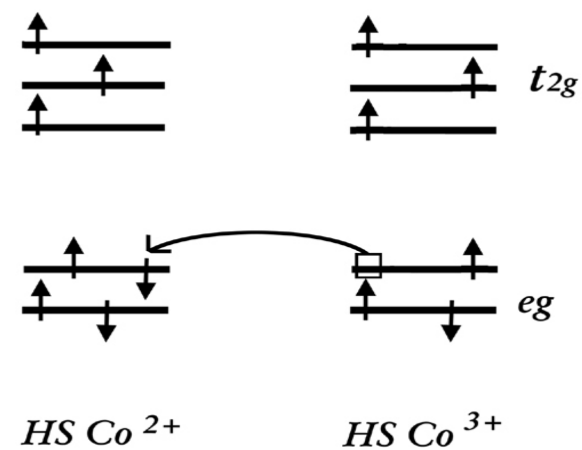

$v_{Co} = 2.25$ $3Co^{2+} : 1Co^{3+}$

Charge ordering ?

Co cations: 2 frustrated magnetic networks

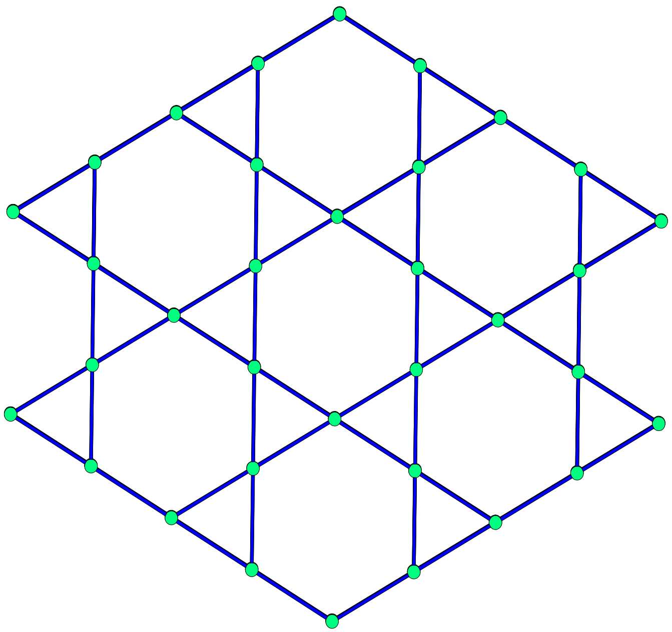

kagome

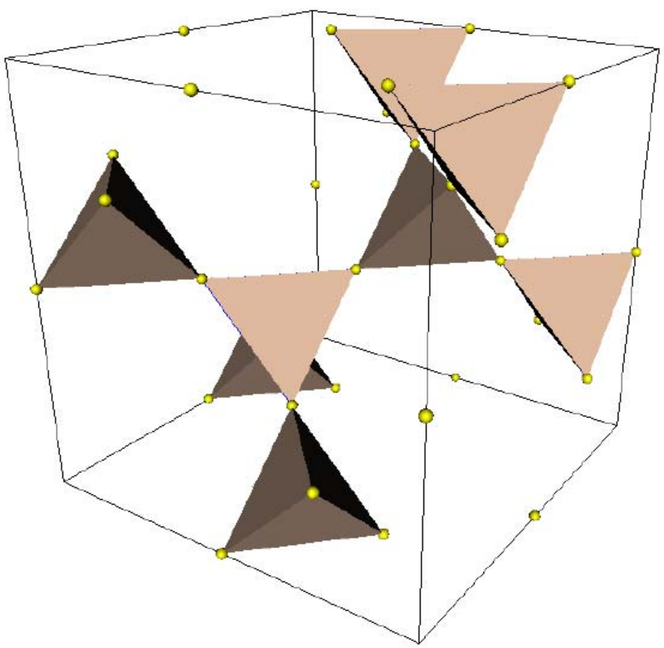

pyrochlore

$YbBaCo_4O_7$ and $YbBaCo_4O_8$

$LBaCo_4O_7$: ionic radius of L^{3+} controls T_S

Space group $P6_3mc$,
a ≈ 0.63 nm, c ≈ 1.03 nm

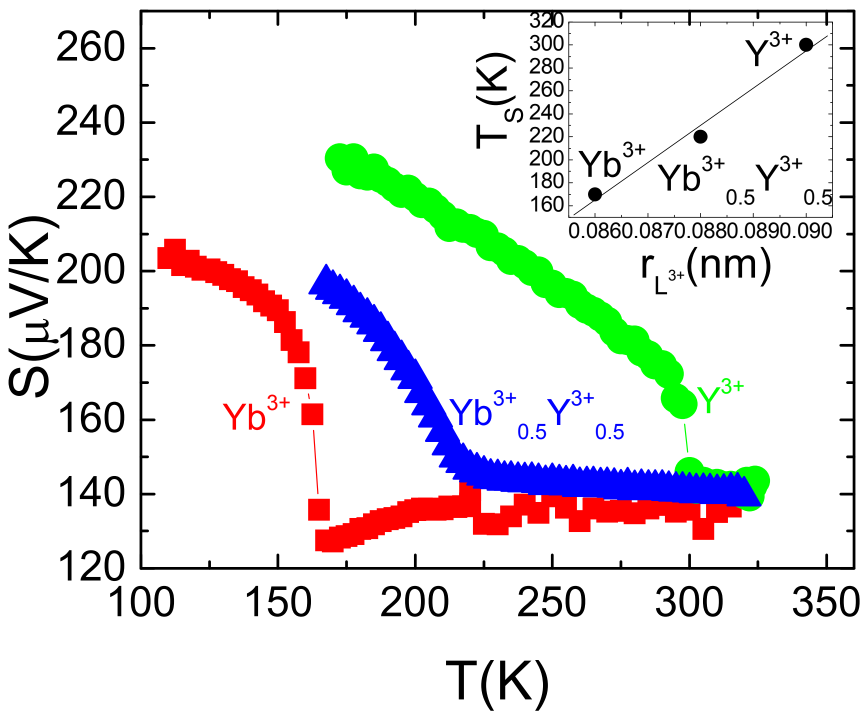

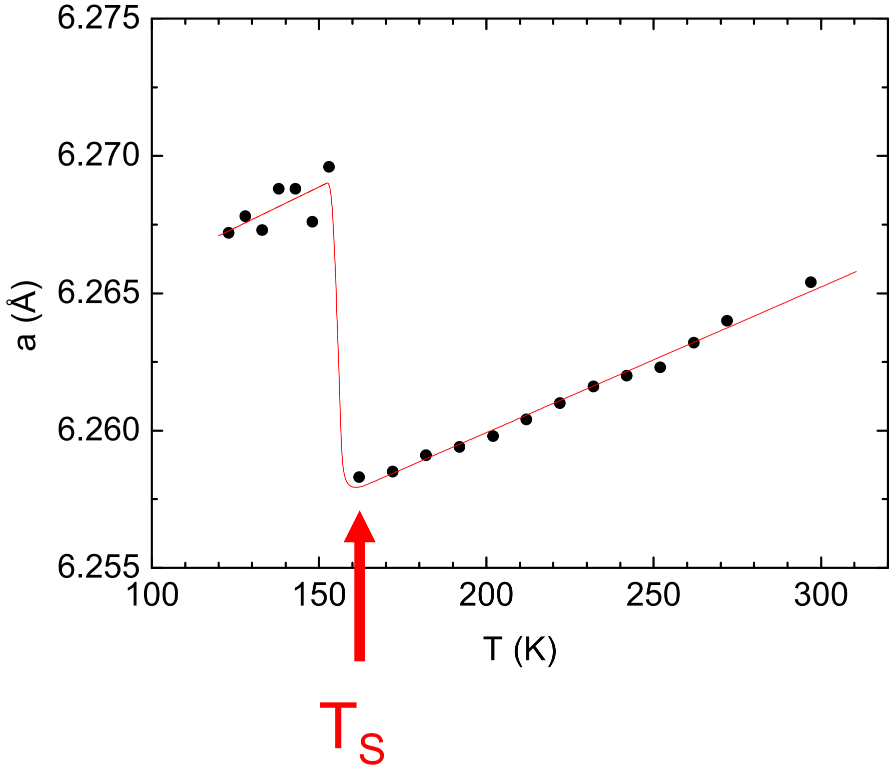

$YbBaCo_4O_7$:
from geometric frustation to long–range AF

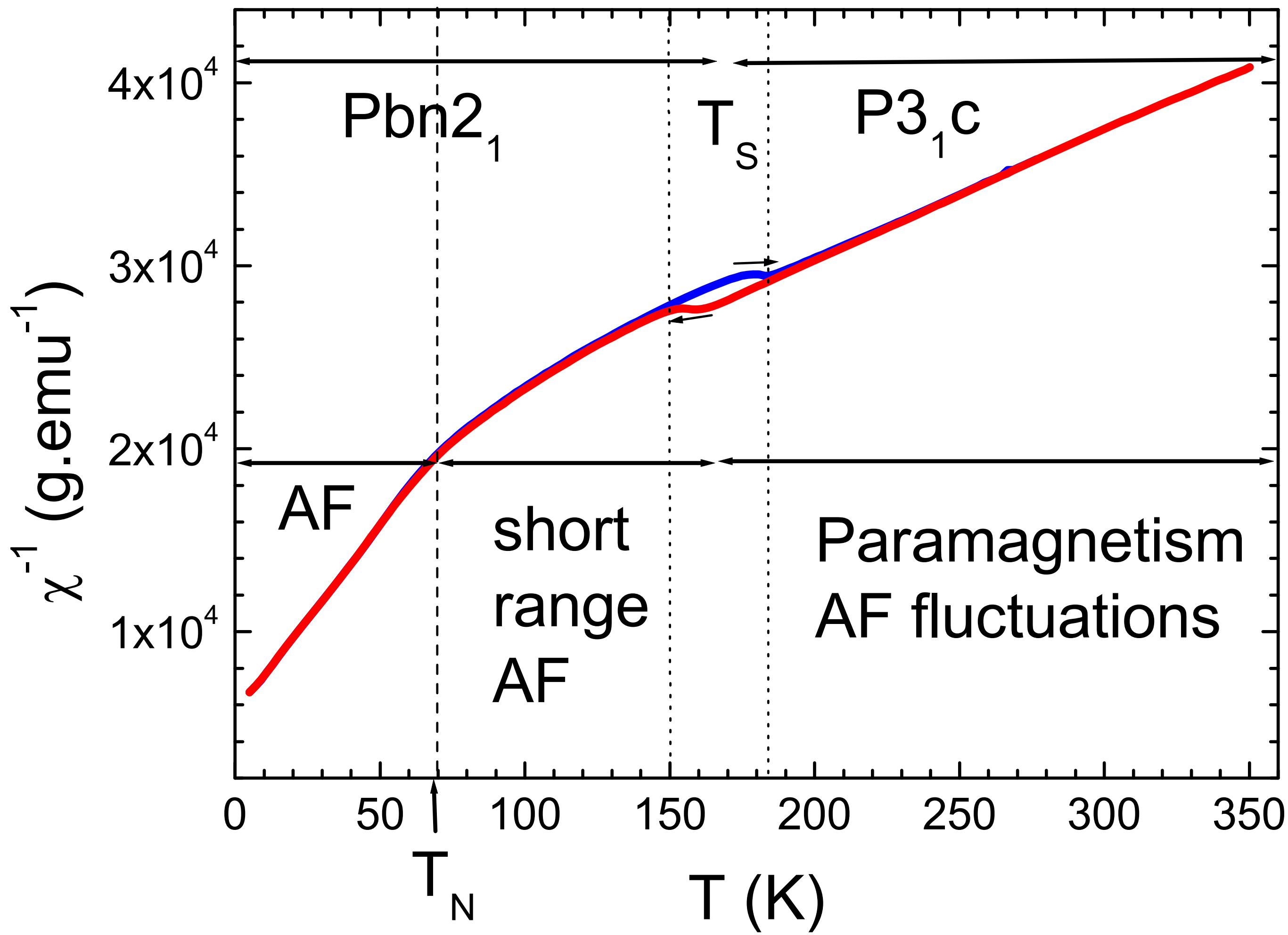

Geometric frustration lift by a first-order structural transition

$CaBaCo_4O_7$

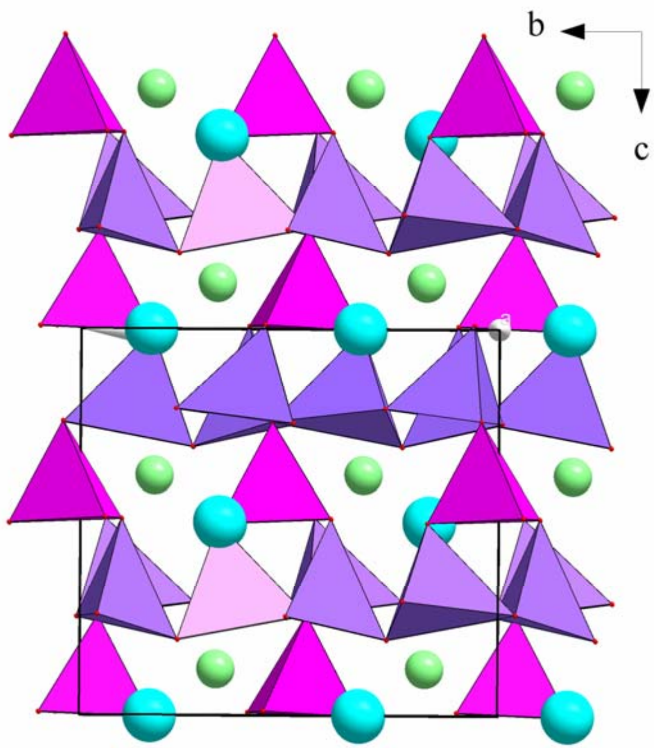

Formula sum	*$CaBaCo_4O_7$*
Formula weight	525.134 g/mol
Crystal system	orthorhombic
Space group	P b n 21 (33)
Cell parameters	a=6.2872(2) Å b=11.0043(3) Å c=10.1913(2) Å
Cell volume	705.10(3) Å^3
Calc. density	1.23664 g/cm^3

Distortion

Atom	*x*	*y*	*z*	
Ca	1/2	1/2	1/2	4b
Ba	1/4	3/4	3/4	4c
Co1	0	0.1209	0.1209	16e
O1	0	0	3/4	24f
O2	1/4	1/4	3/4	4d

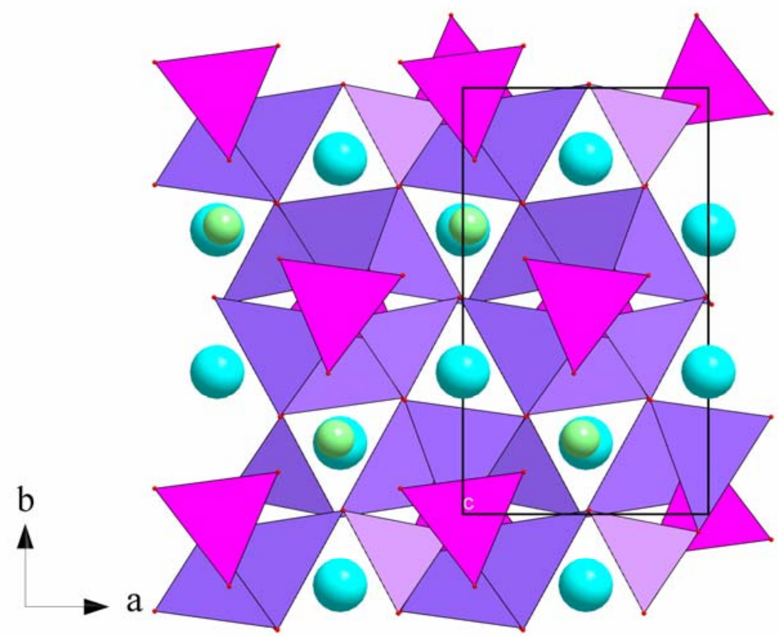

$CaBaCo_4O_7$

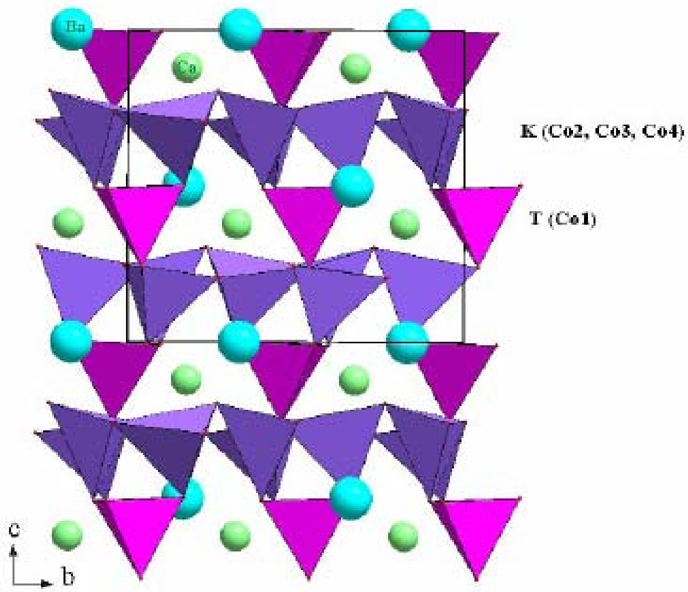

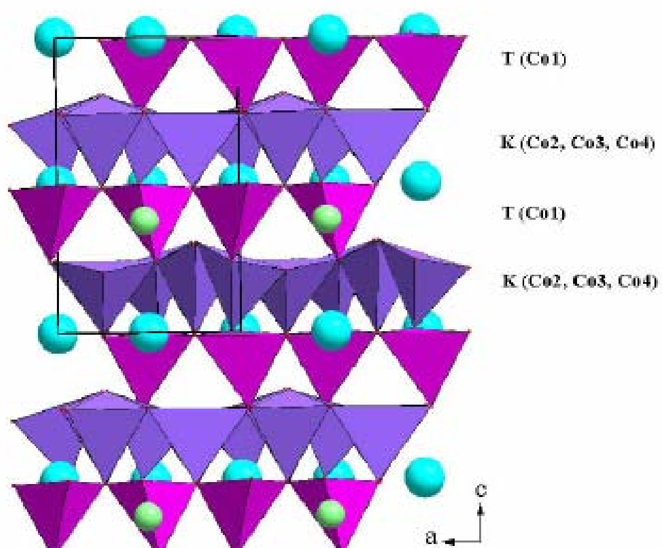

Ferrimagnetic

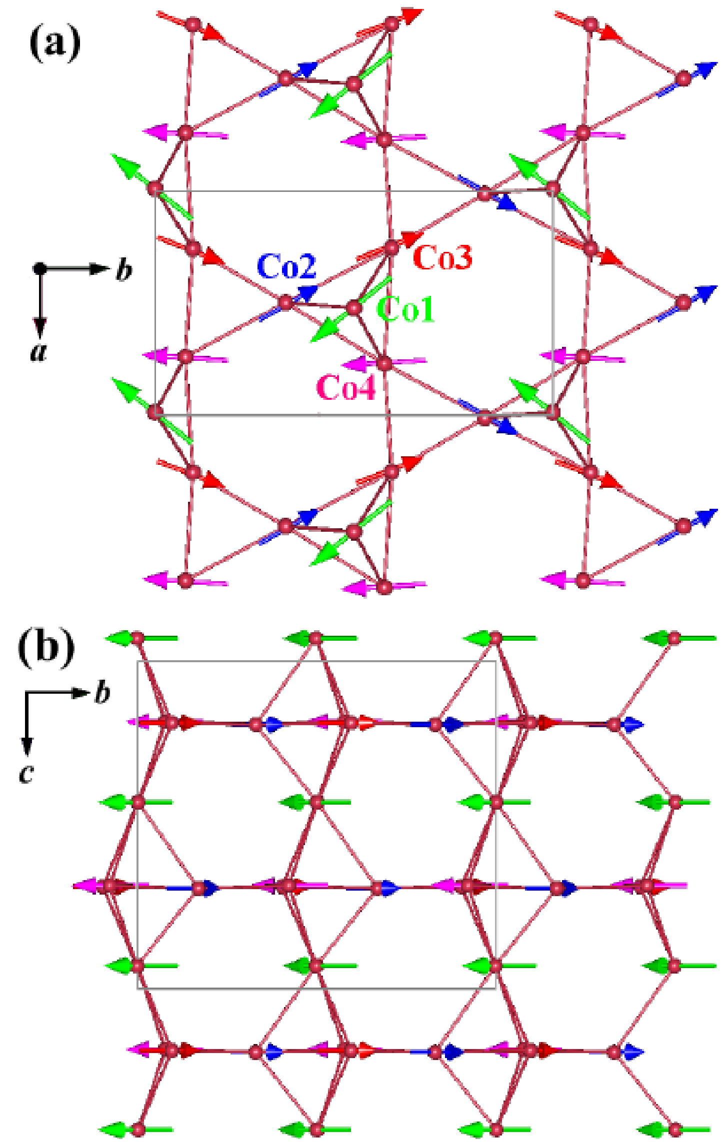

Ferrimagnetic 114

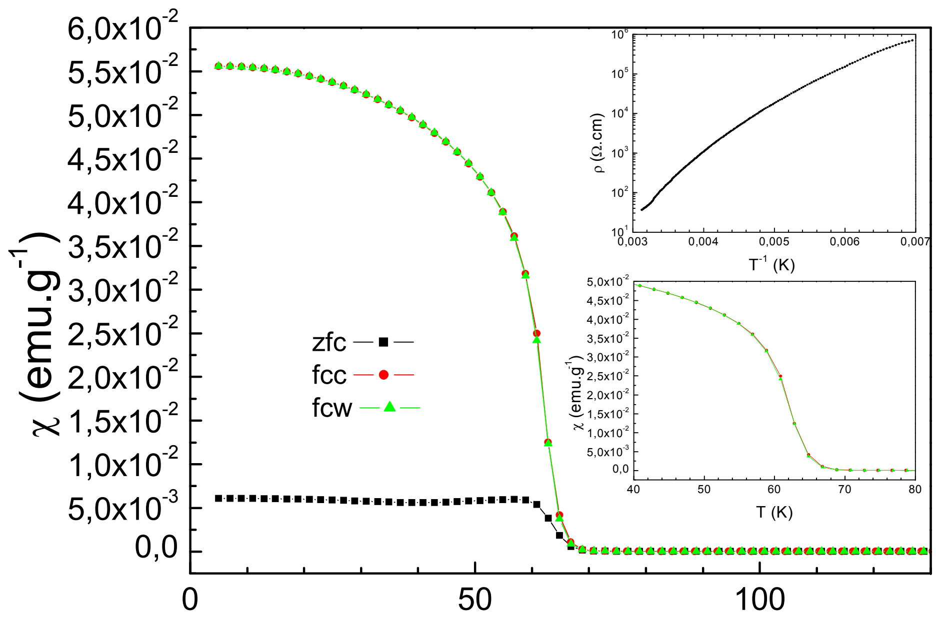

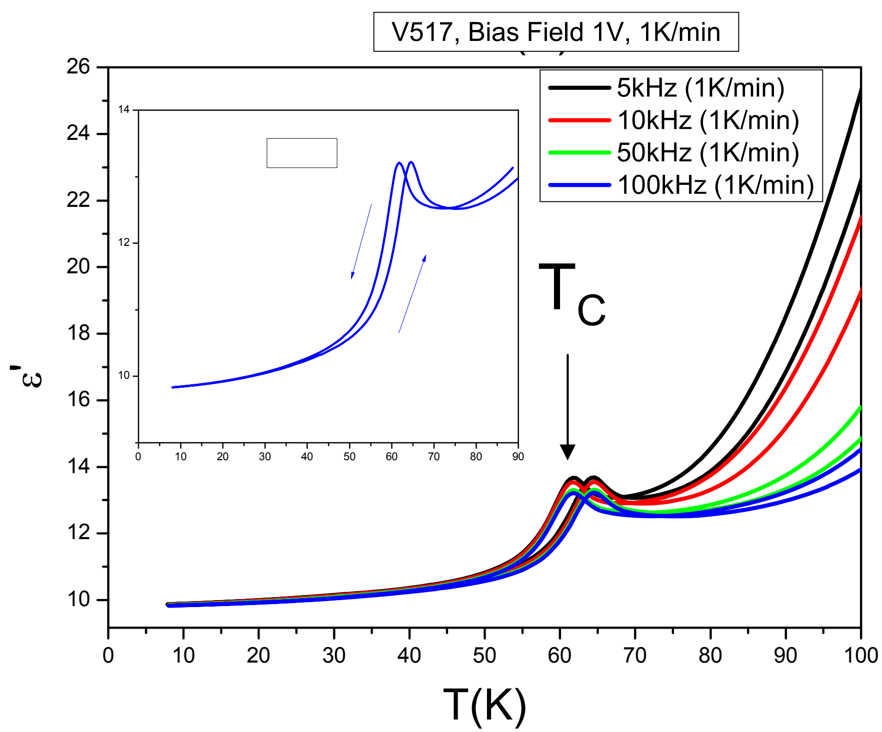

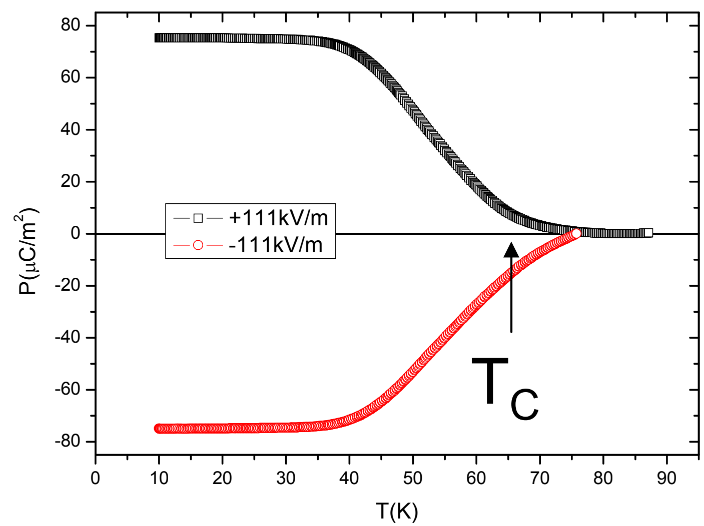

Spin induced ferroelectric

Plan:

3D magnetic networks:

CMR in perovskite manganites

MIT in cobaltites

Frustrated lattices of the « 114 » type

1D and 2D TM-O-TM networks: hexagonal perovskites

and CdI_2 type structures

n-type ***vs*** **p-type** conductivity in oxides

ABO_3 hexagonal perovskite

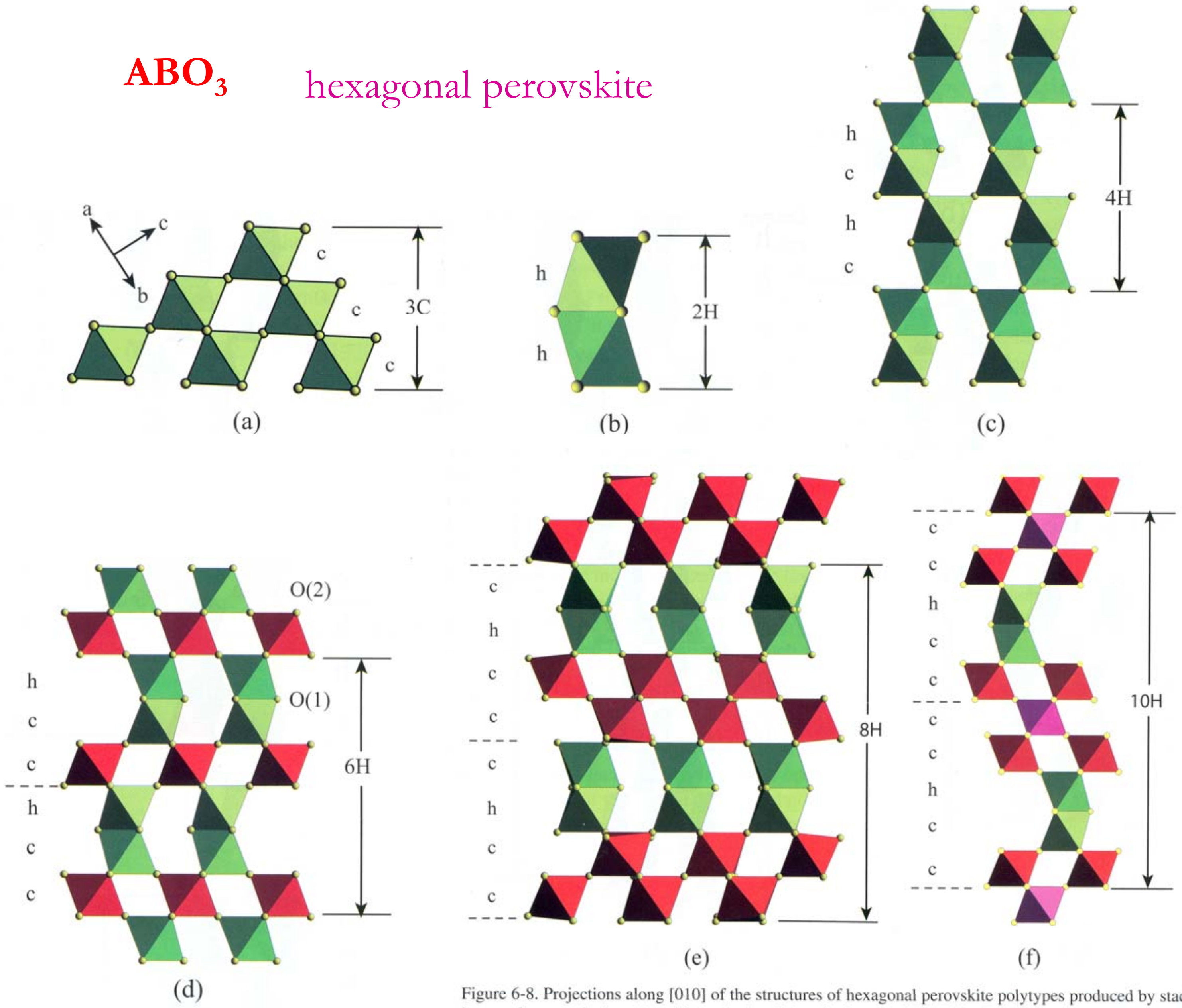

Figure 6-8. Projections along [010] of the structures of hexagonal perovskite polytypes produced by stacking layers of corner-sharing (c) and face-sharing (h) octahedra. (A) 3C $SrTiO_3$; (B) 2H BaNiO3; (C) 4H $BaRuO_3$; (D) 6H $BaTiO_3$; (E) 8H $Ba_8Ta_4Ti_3O_{24}$; (F) 10H $Ba_{10}Ta_{7.04}Ti_{1.2}O_{30}$.

Hexagonal Perovskites
2H-$BaCo^{4+}O_3$: a 1D compound with edge-shared CoO_6 octahedra

Hexagonal close packed stacking of the AO_3 layers
Every AO_3 unit, one octahedron is created, occupied by Co^{4+}

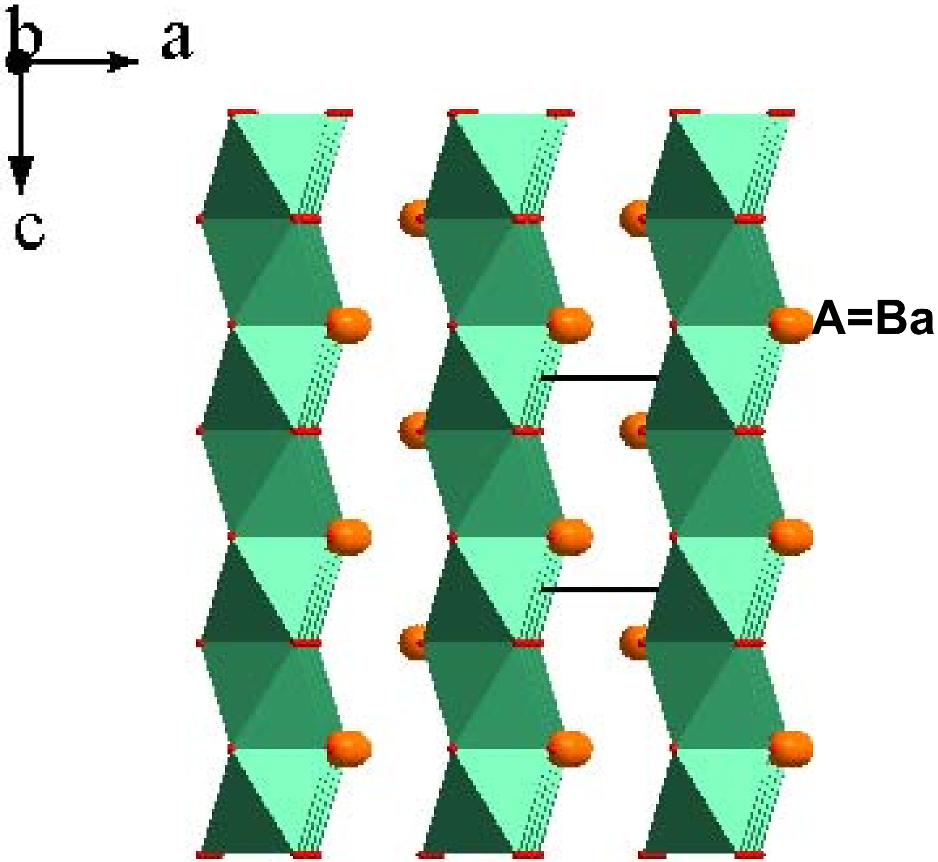

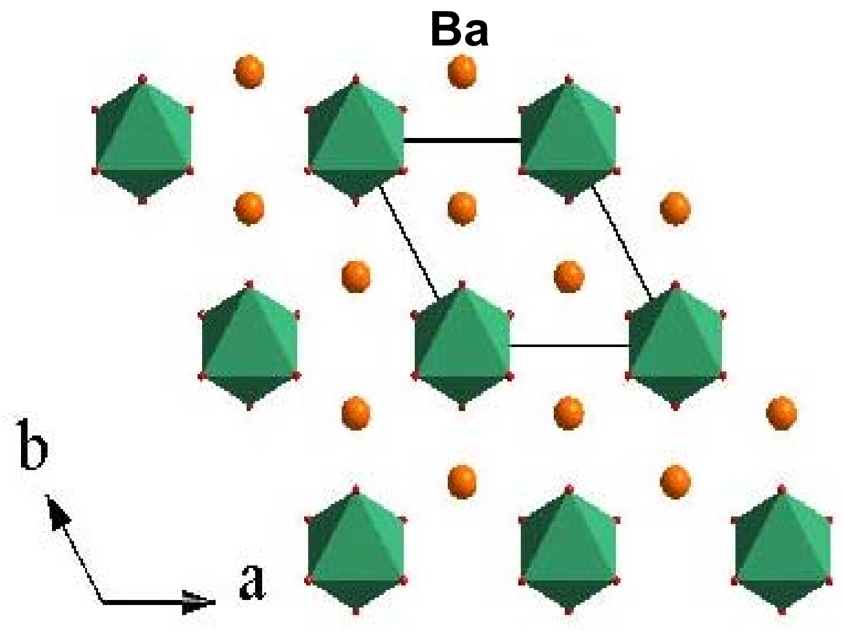

The chains of CoO_6 octahedra form a triangular array

M. Parraset al, J. Solid State Chem. 120 , 327 (1995)

12H-$Ba_{0.9}Co^{+3.2}O_{2.6}$: units of edge-shared CoO_6 octahedra bridged by CoO_4 tetrahedra

Alternating hexagonal *(h)* and cubic *(c)* stacking of the $AO_{3-\delta}$ layers *(hhhccc)* yields the 12-H

Creation of CoO_4 tetrahedra

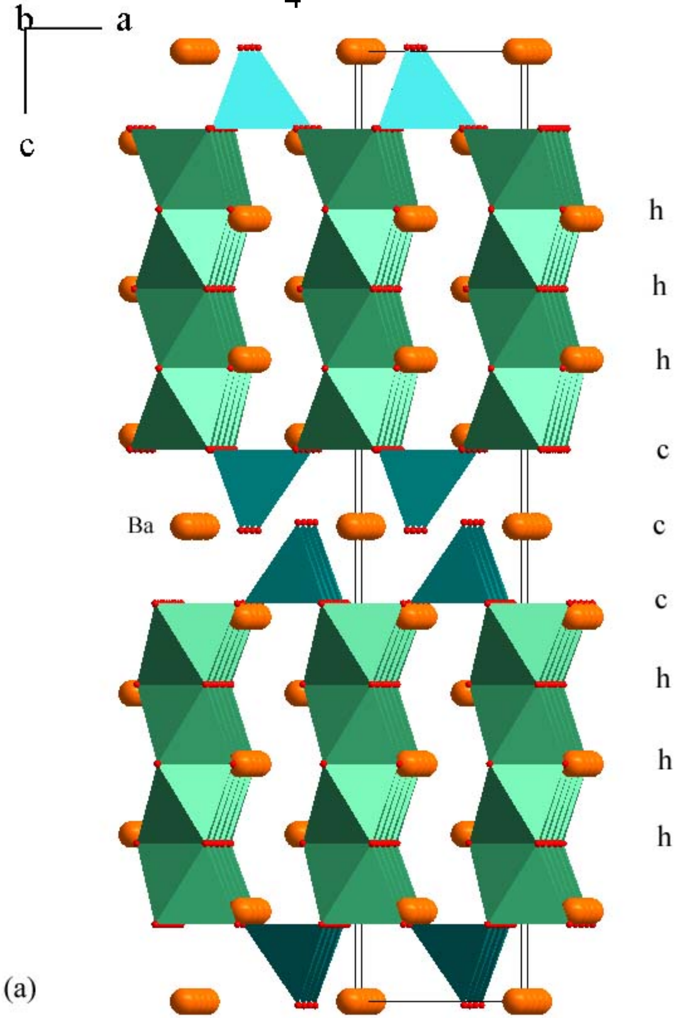

(a)

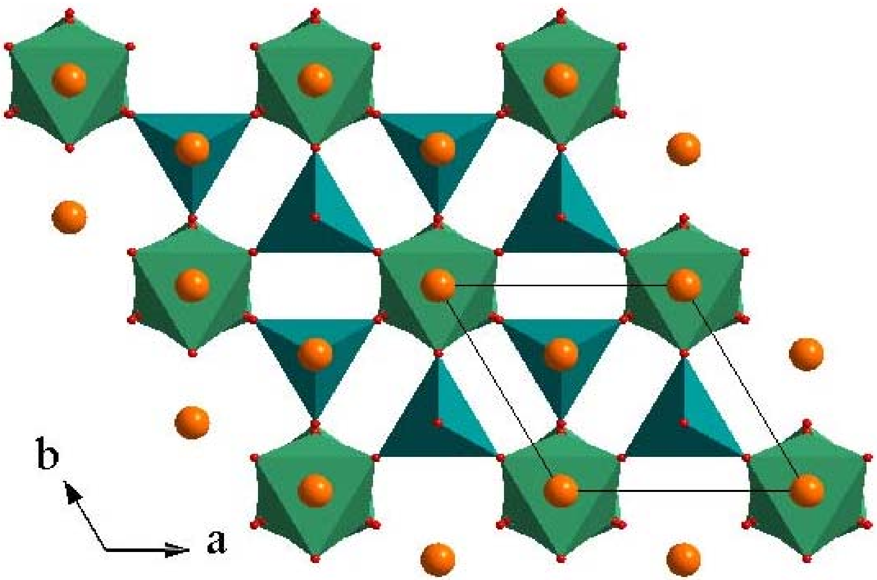

3D array of CoO_n polyhedra

A.J. Jacobson et J.L. Hutchison, J. Solid State Chem. 35, 334 (1980)
K. Boulahya et al , Phys. Rev. B 71, 144402 (1999)

12H-$Ba_{0.9}Co^{+3.2}O_{2.6}$: structure

Transmission electron microscopy : hhhccc

EDS coupled to ED : Ba/Co = 0.9 ratio

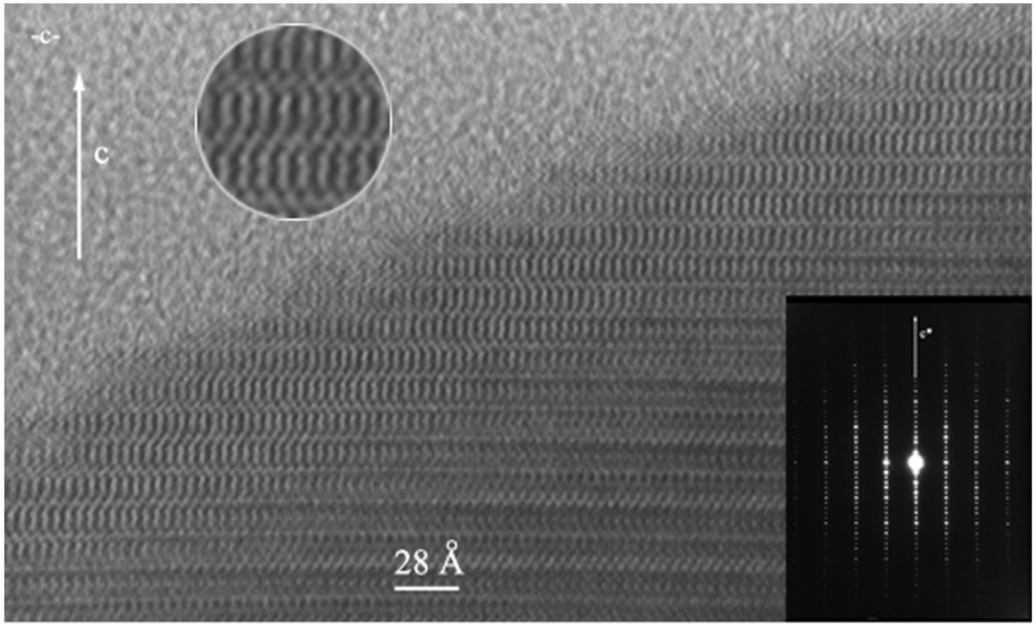

X-ray diffraction :
12H, *P63/mmc*
a=0.56612 (1) nm
c=2.84627 (8) nm

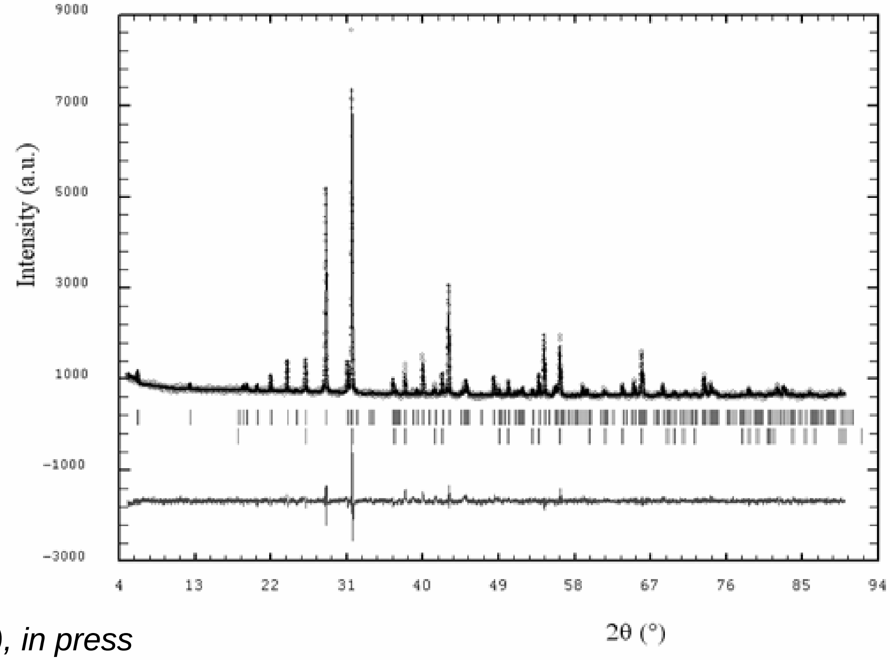

A. Maignan et al , J. of Solid State Chem. 179 (2006), in press

$A_{3n+3m}A'_nB_{3m+n}O_{9m+6n}$:
intergrowth of $n[A_3O_9]$ and $m[A_3A'O_6]$ triple layers
Creates B octahedral sites and trigonal prism sites (A')
For A'=B=Co and n=1, m=0 $Ca_3Co_2O_6$

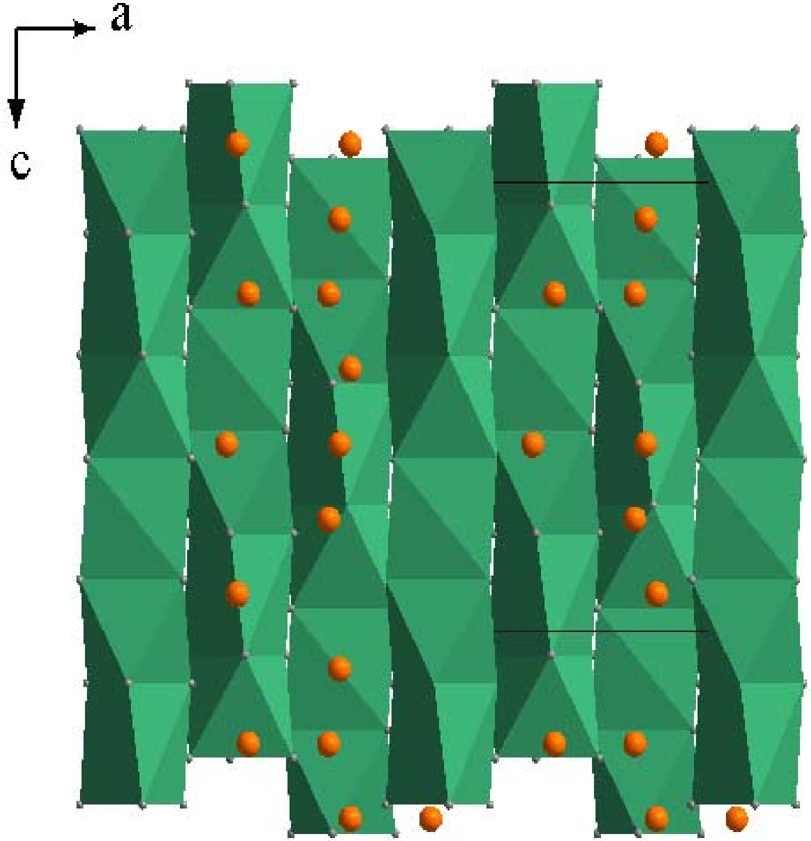

1:1 CoO_6 trigonal prism and octahedron

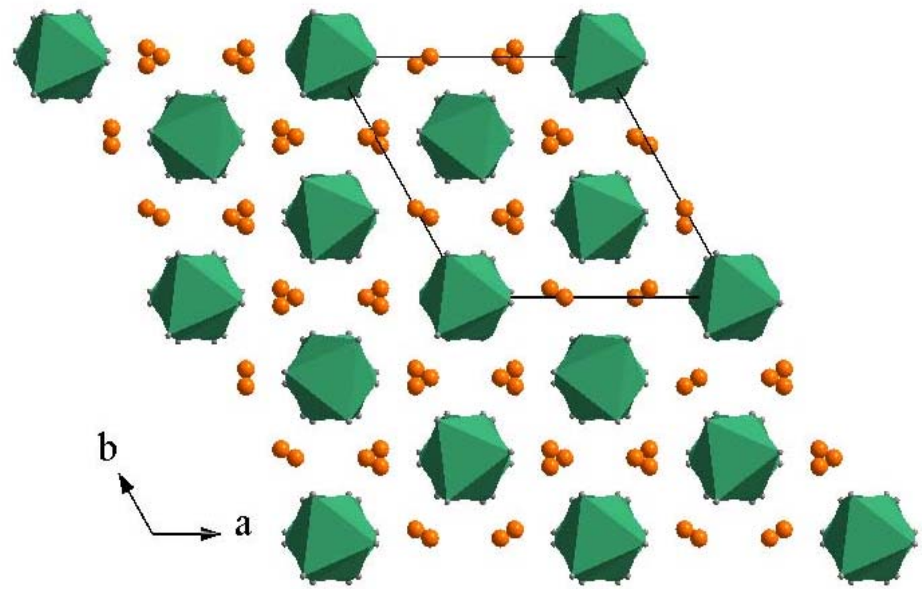

Geometric frustration : hexagonal

a = b = 9.13 Å c = 10.58 Å
interchain distance : 5.24 Å
intrachain distance : 2.6 Å
space group R3 c

K.E. Stitzer et al, Curr. Opin. Solid State Mater. Sci. 5, 535 (2001)

H. Fjellvag et al , J. Solid State Chem. 124, 10 (1996)

$SrCoO_3$: edge-shared $Co^{4+}O_6$ octahedra in the *Pm3m* cubic perovskite

(a=0.3836 nm)

Ferromagnet with TC = 280 K , Co^{4+}-O-Co^{4+} 180° exchange

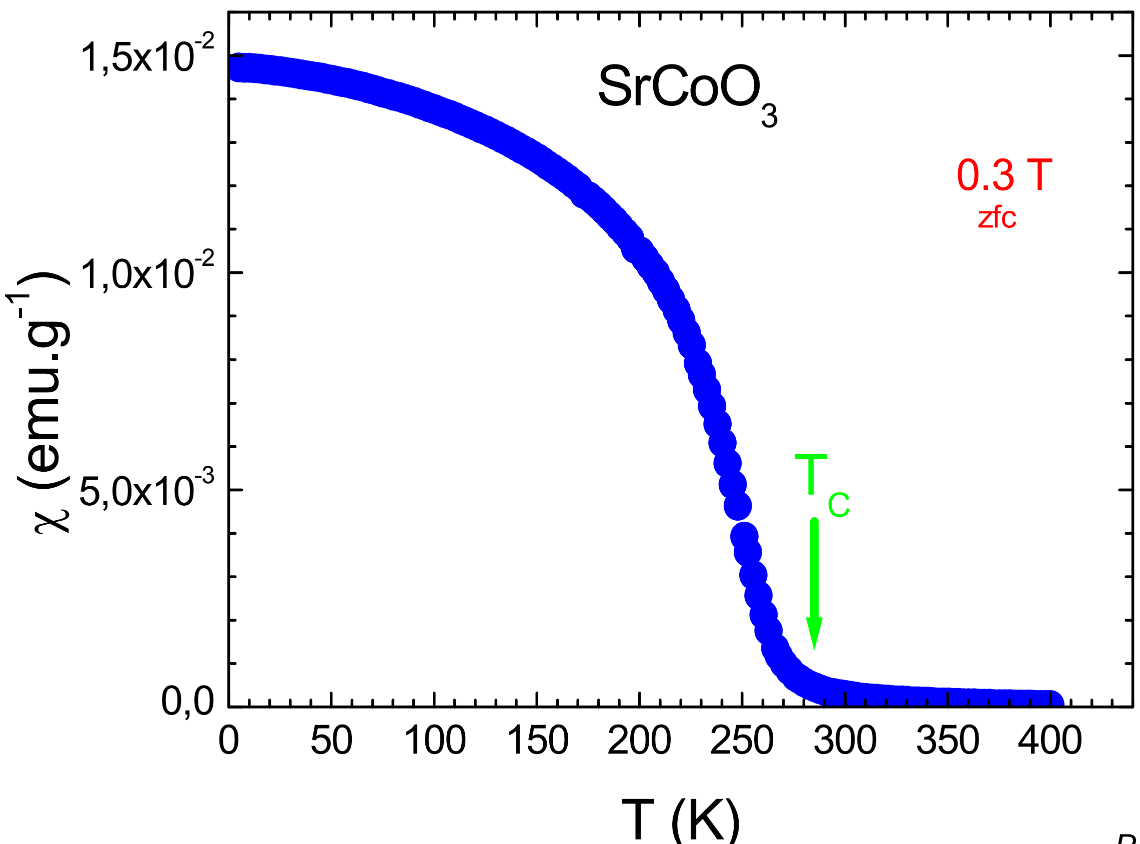

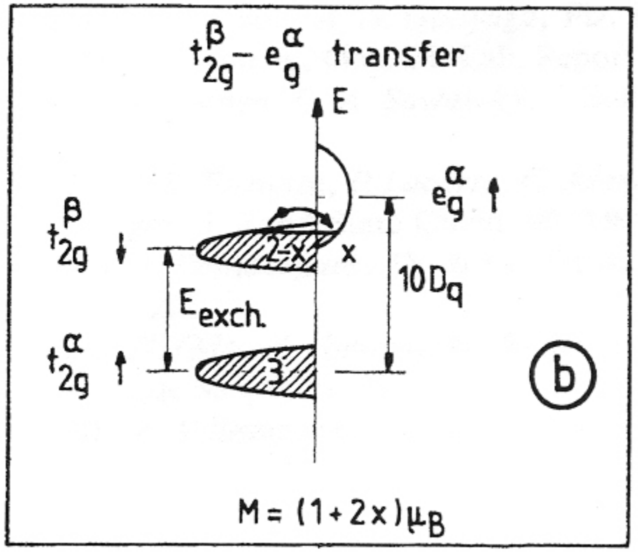

P. Bezdicka et al, Z. Anorg. Allg. Chem. 619, 7 (1993)

SrCoO$_3$: edge-shared Co^{4+}O$_6$ octahedra in the *Pm3m* cubic perovskite

Conventional ferromagnet

M_S = 1.75 μ_B/Co

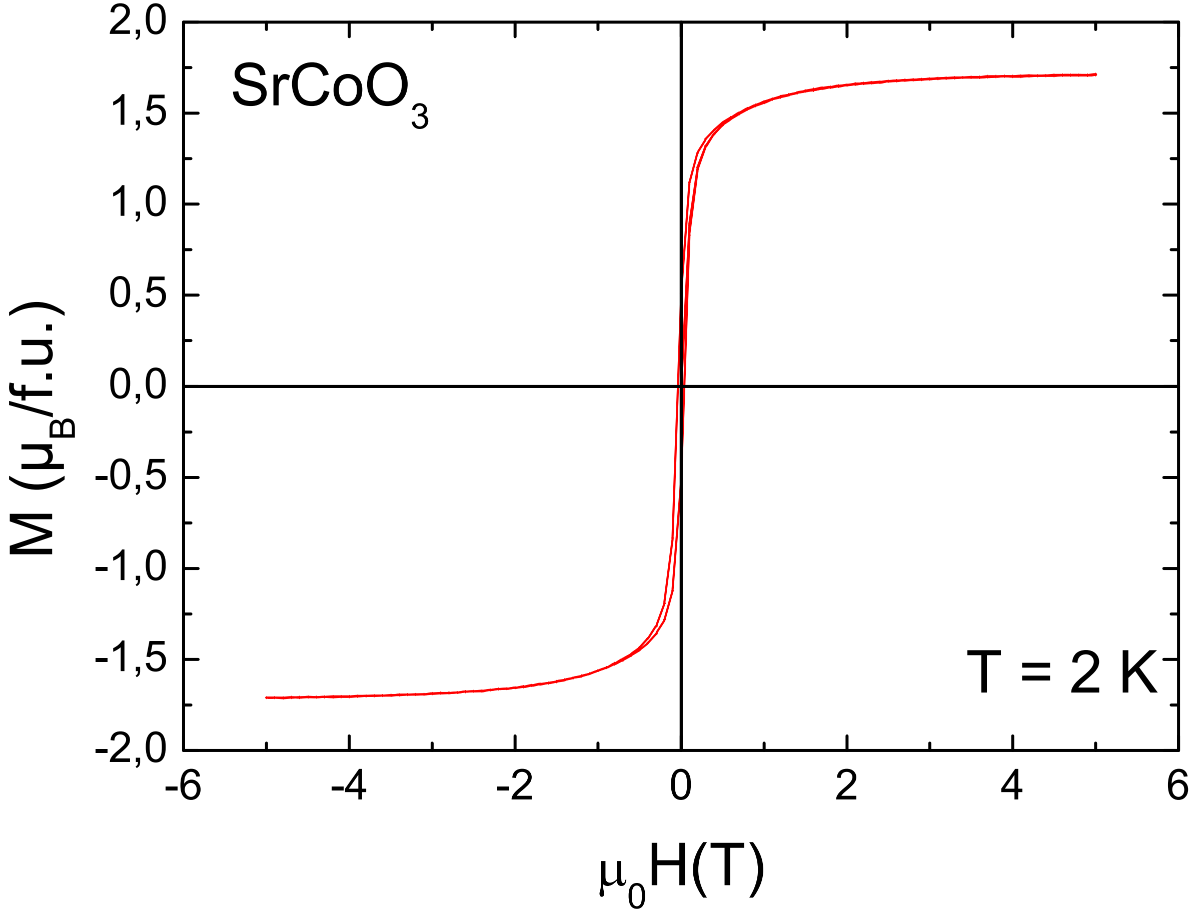

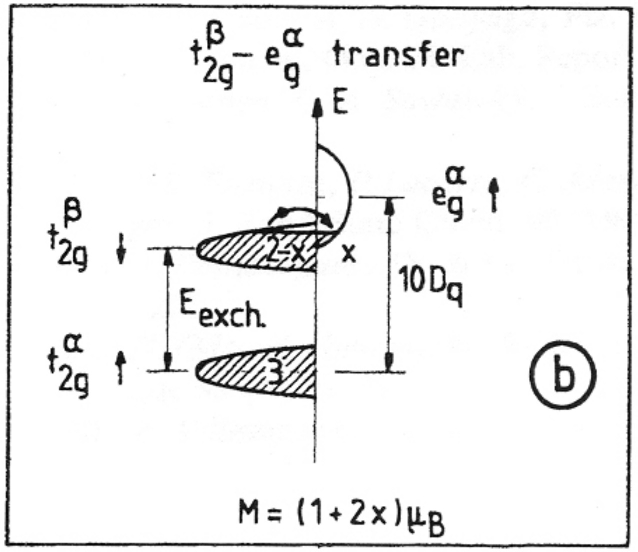

Co^{4+} is neither 100% LS or HS

2H-$BaCo^{+4}O_3$: weak ferromagnetism below T_C = 50 K ?
effect of the 1D character of the Co-O array

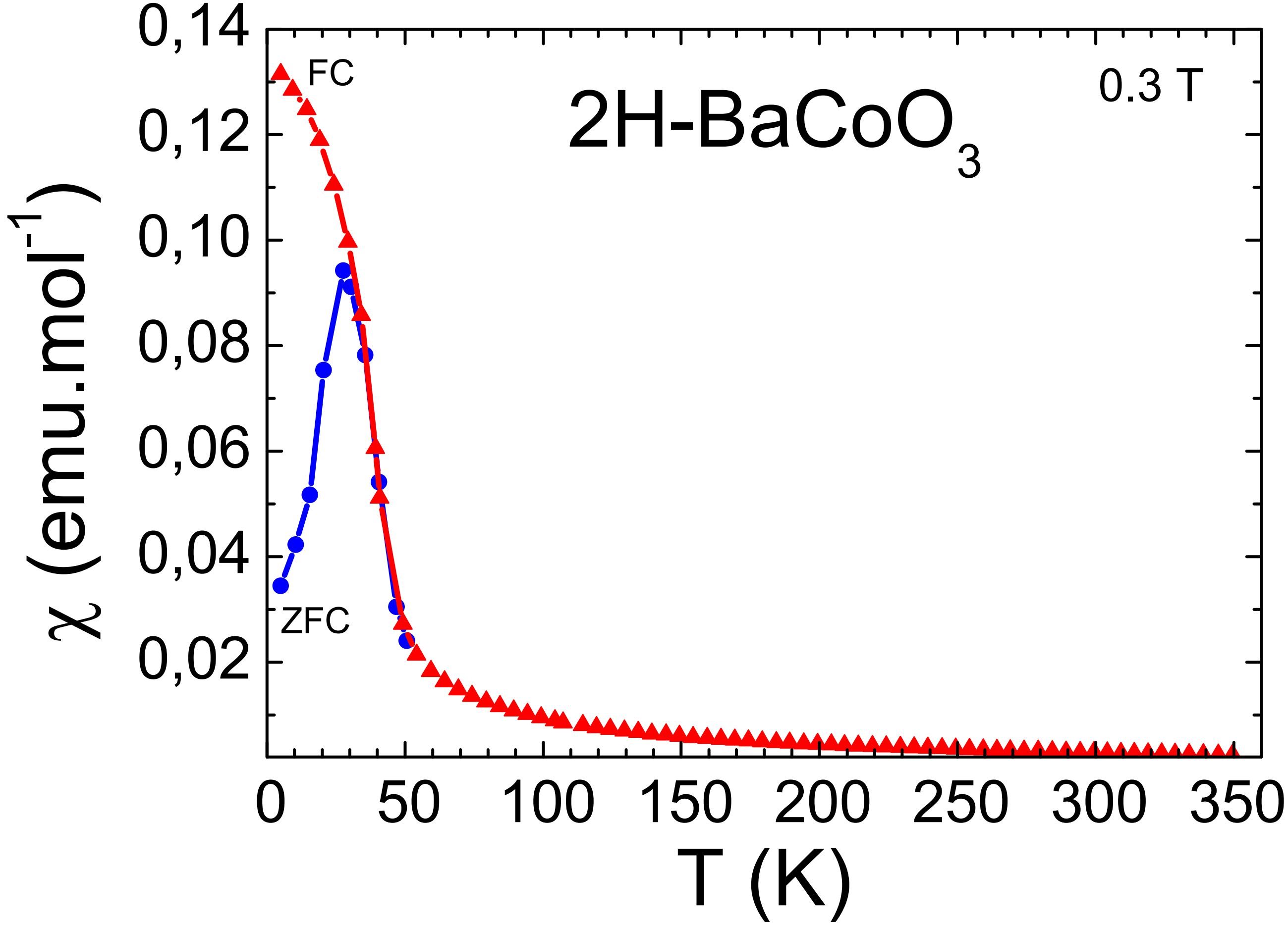

$12H\text{-}Ba_{0.9}Co^{+3.2}O_{2.6}$: ferromagnetism below T_C = 50 K

Magnetic susceptibility values 10 times larger than in the 2H

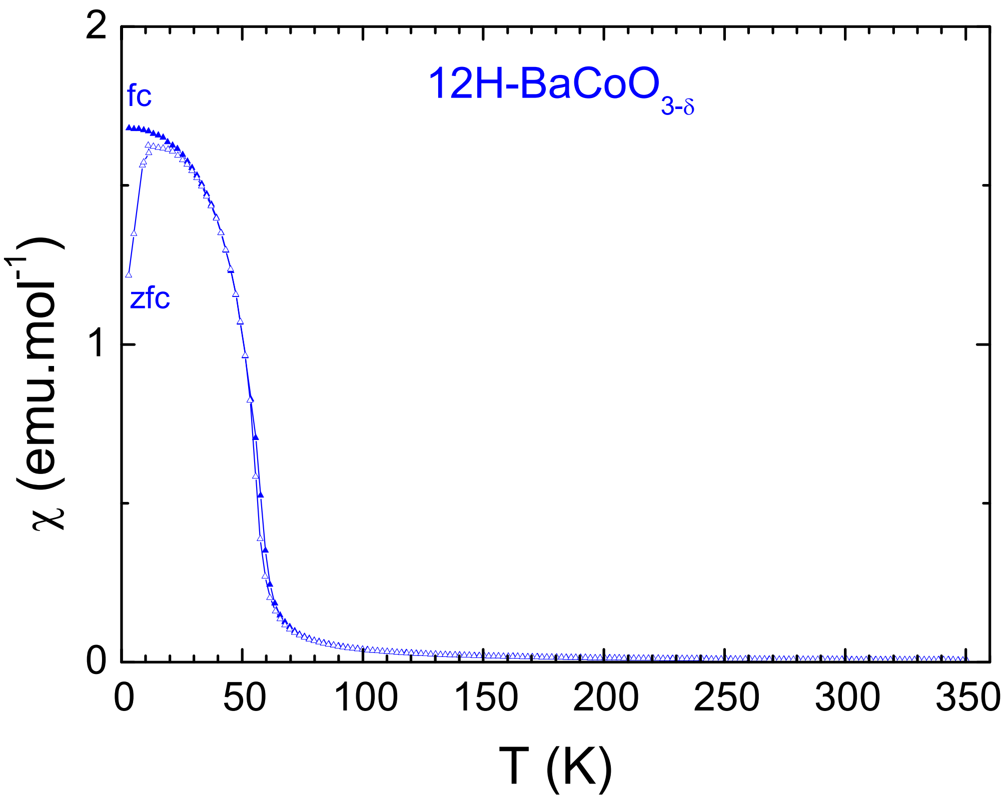

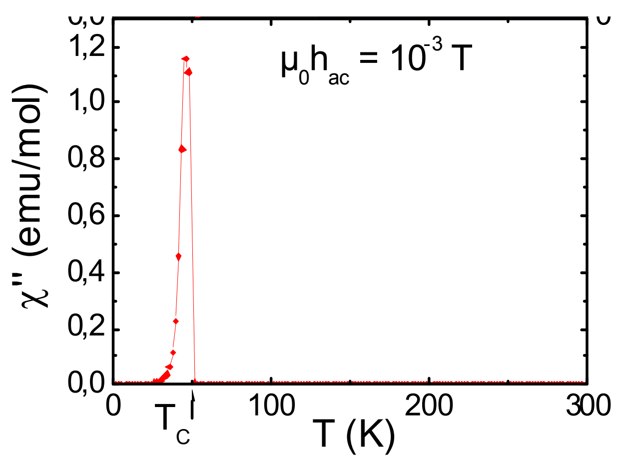

12H-$Ba_{0.9}Co^{+3.2}O_{2.6}$: negative magnetoresistance at T_C = 50 K

spin/charge interplay

Bump in the ρ(T) curve at T_C

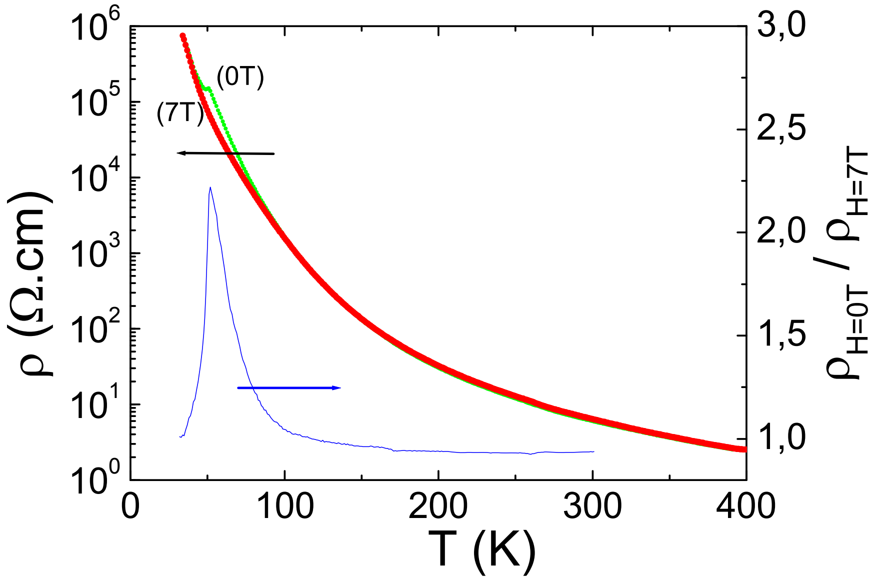

-60% at 50K in 7 T

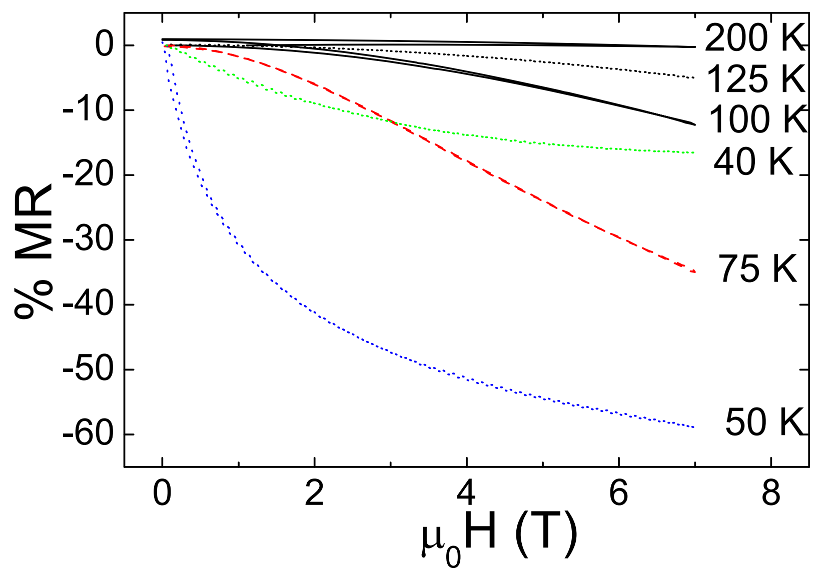

Large H dependence at T_C

No MR measured in the 2H : related to the ferromagnetism of the 12H

2H-$BaCo^{+4}O_3$: weak ferromagnetism below T_C = 50 K ?

M^{5T} = 0.15 m_B/Co at 2.5 K
$\mu_o H_c$ ~ 0.8T at 2.5 K

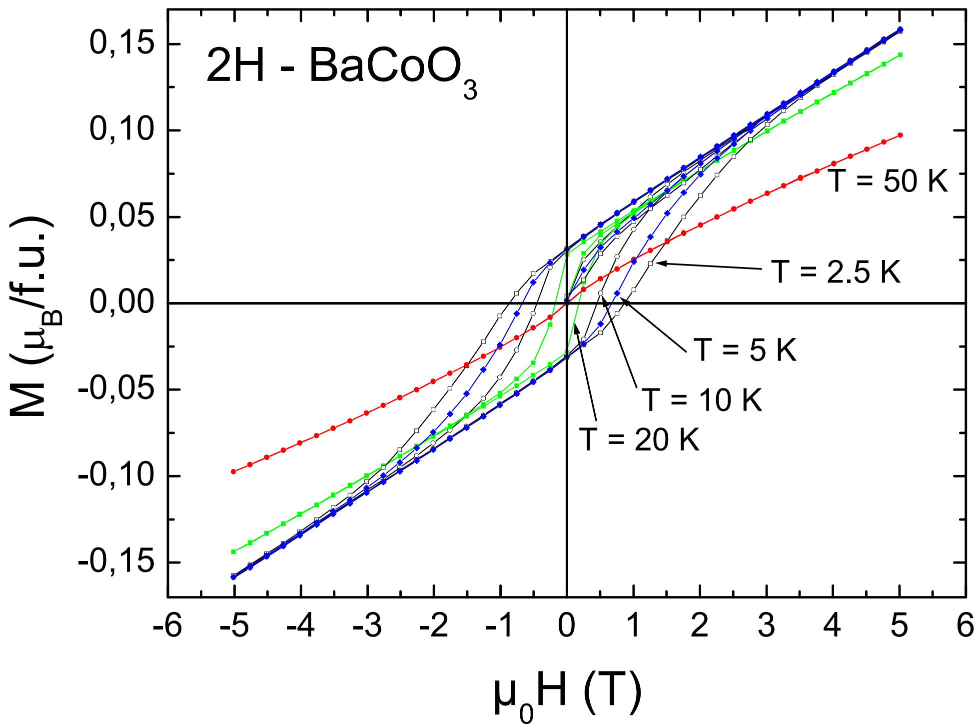

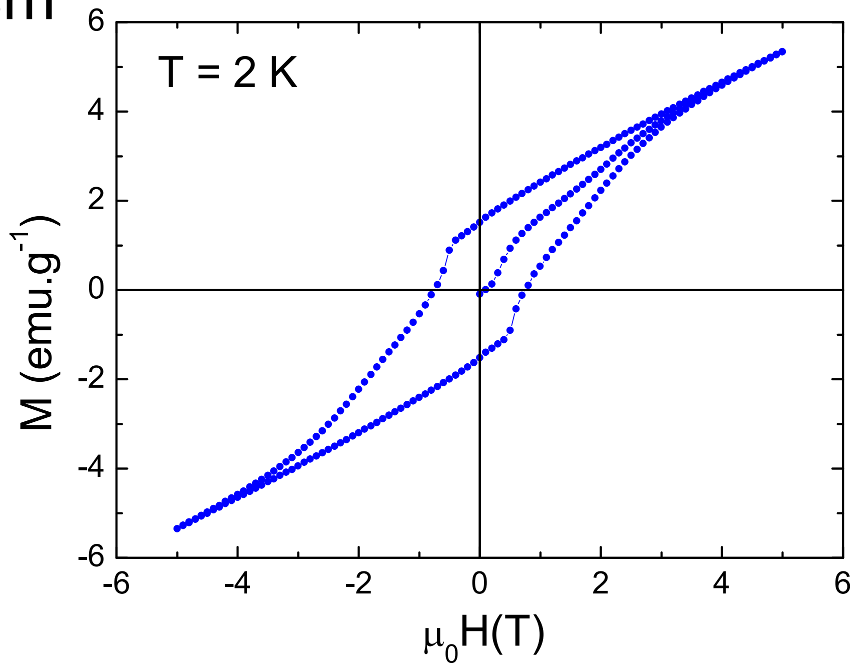

At 2K no special change

12H-$Ba_{0.9}Co^{+3.2}O_{2.6}$: ferromagnetism below T_C = 50 K

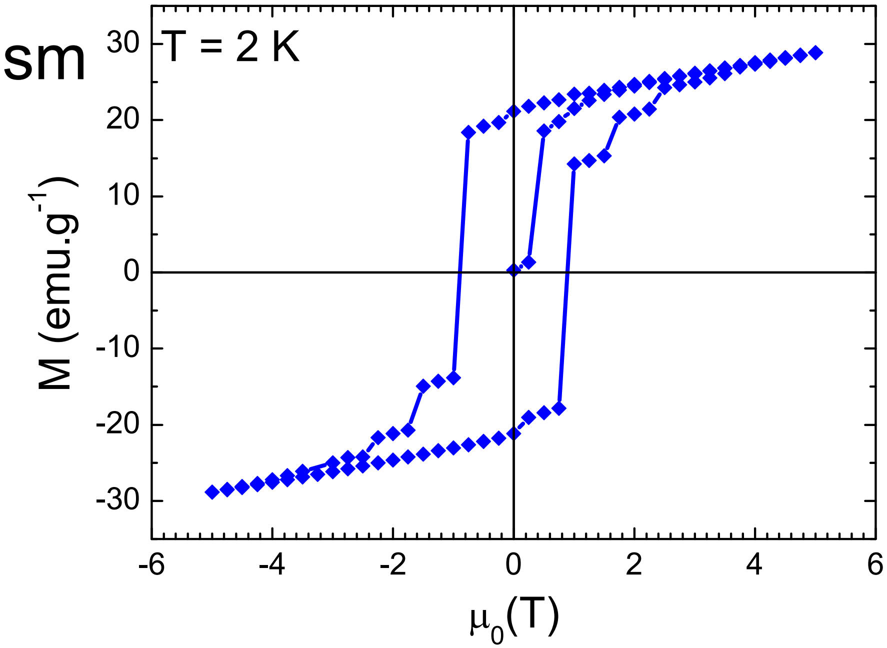

M^{5T} = 1.2 μ_B/Co and $\mu_0 H_c$ ~ 1T at 2.5 K

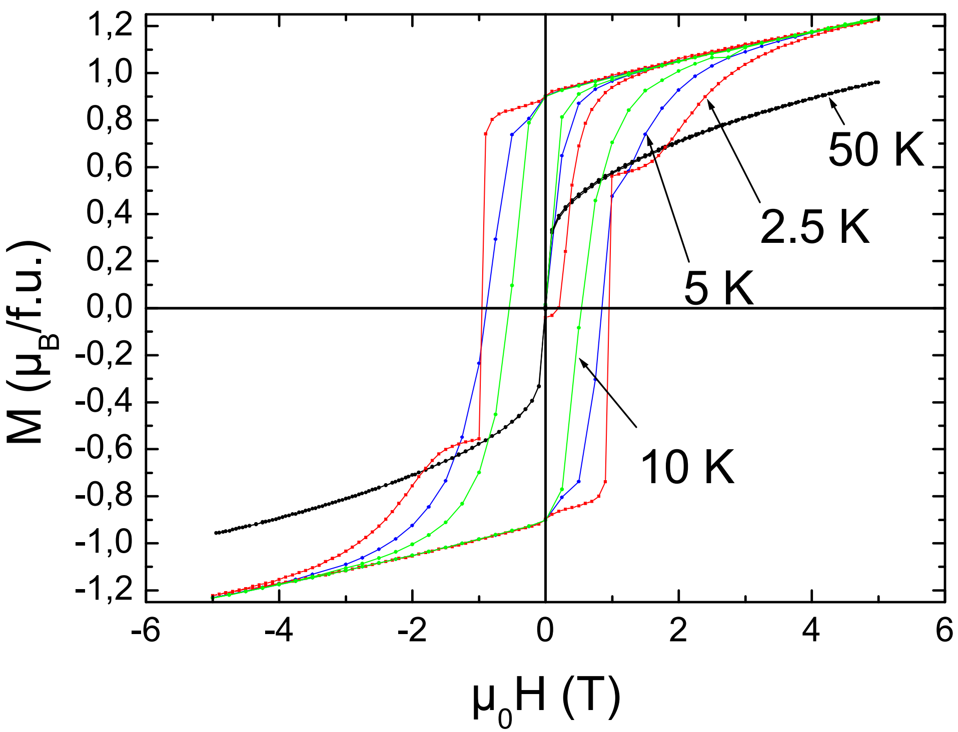

At 2K, additional M jumps

Similar to the 5H

12H-$Ba_{0.9}Co^{+3.2}O_{2.6}$: M jumps at 2 K

Varying the H sweep rate or the waiting time does not suppress the steps

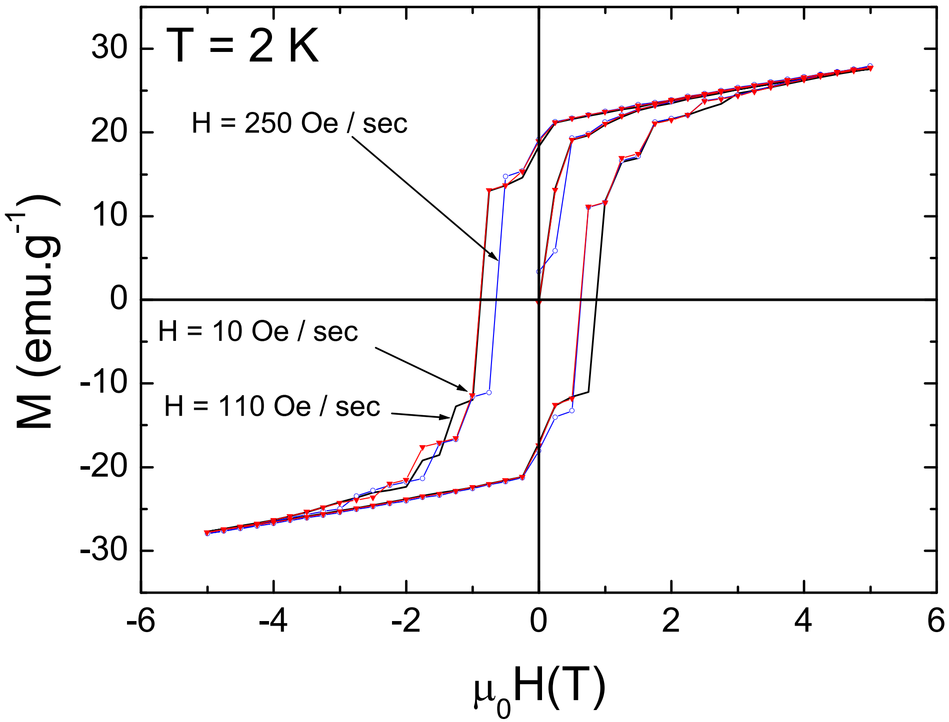

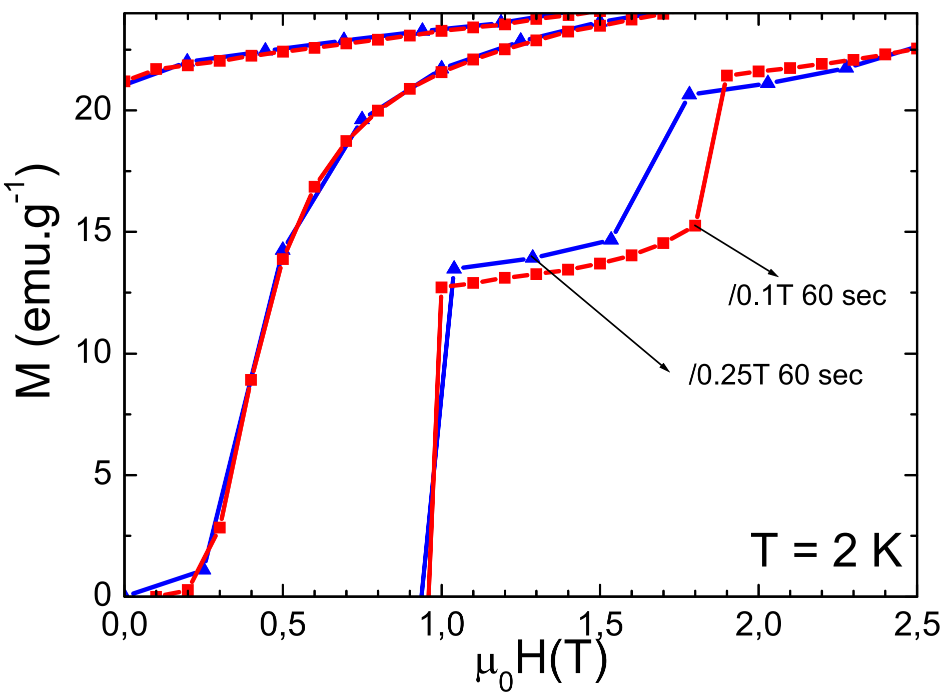

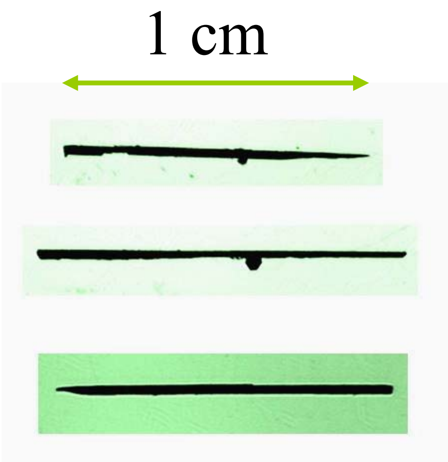

$Ca_3Co_2O_6$ single crystals

$A_{3n+3m}A'_nB_{3m+n}O_{9m+6n}$:

A'=B=Co and n=1, m=0 $Ca_3Co_2O_6$

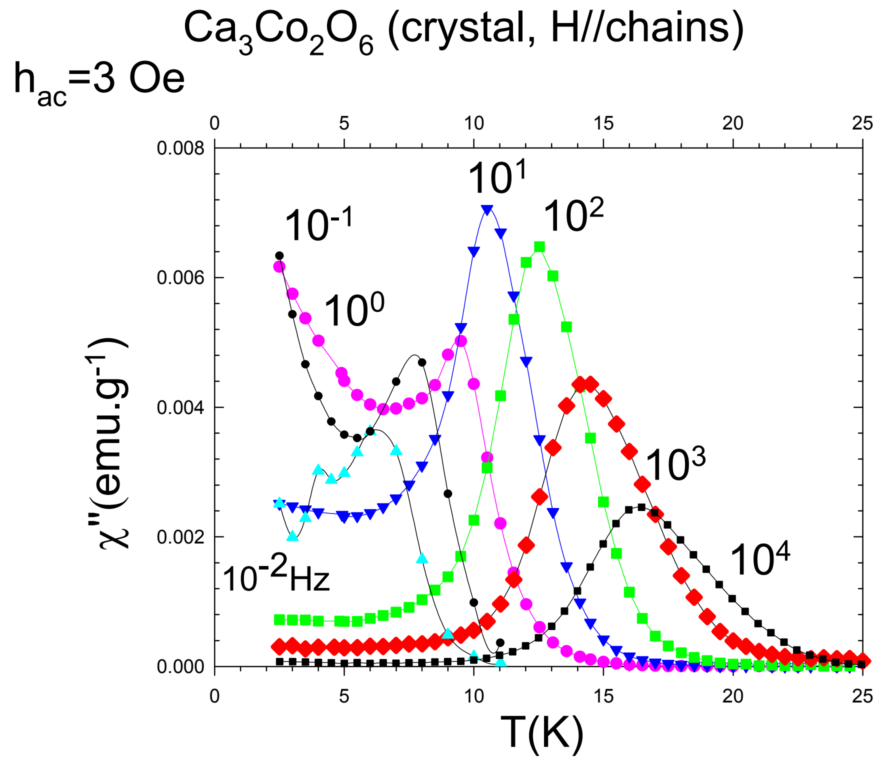

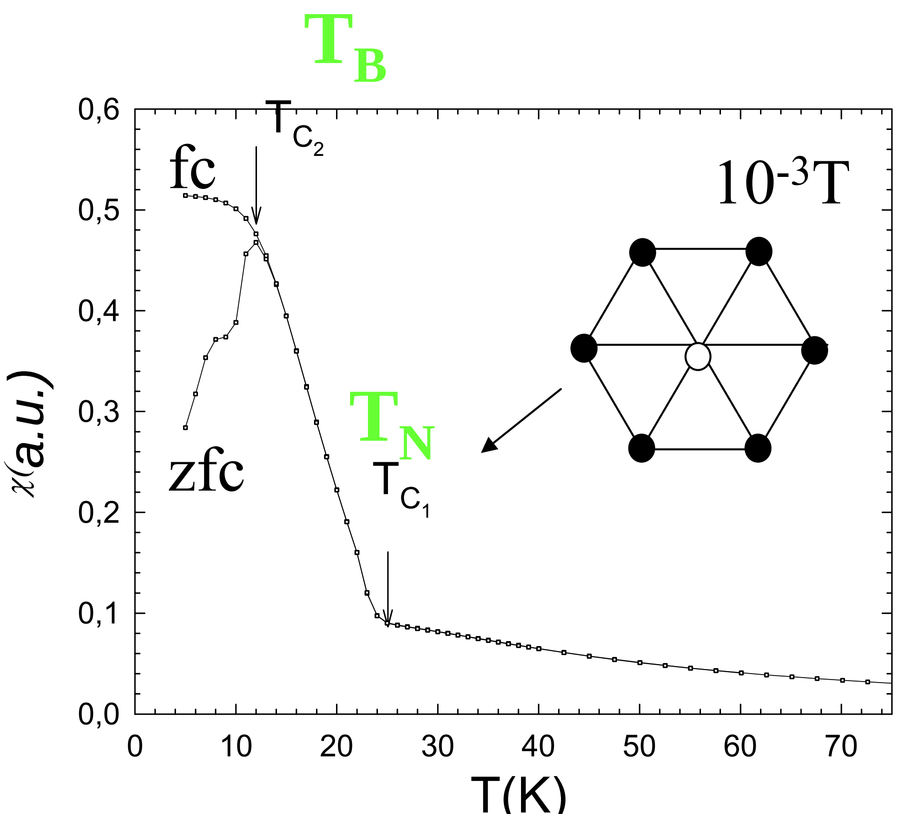

For f>1 Hz, T(χ''$_{max}$) increases as in a superparamagnet

But f <1Hz, fixed T(χ''$_{max}$)

A. Maignan et al., EPJB 15, 657 (2000)

$Ca_3Co_2O_6$

Magnetism

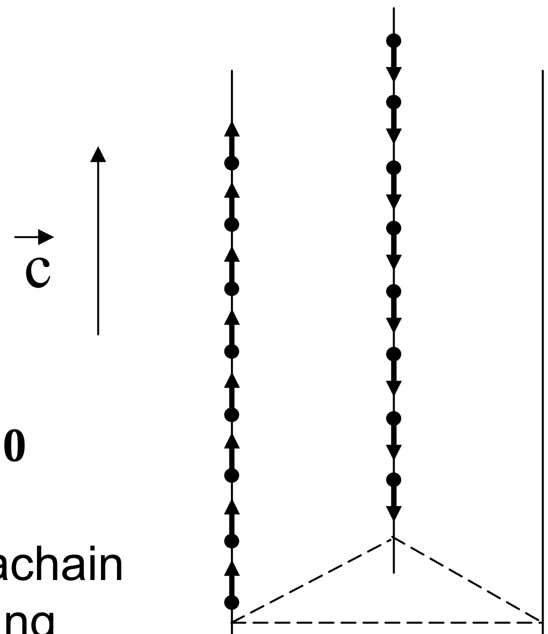

$J > 0$

Ferro Intrachain Coupling

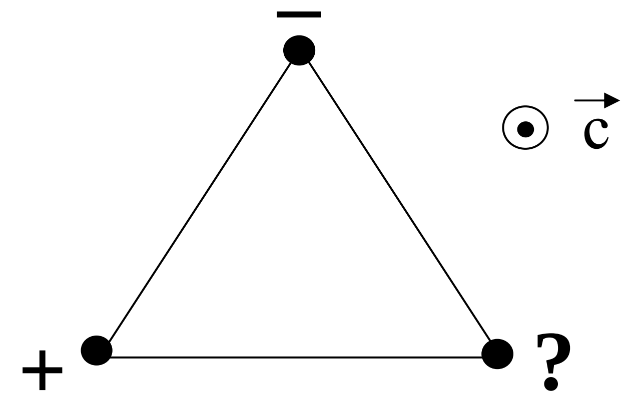

$J' < 0$

AntiFerro Interchain Coupling

Strong local anisotropy (TP)

" 1 D + Frustration "

S = 0 → Octahedron
S = 2 → Trigonal Prism } **Co^{3+}**

intrachain : ferro (F)
interchain : antiferro (AF)

T_N = 25K

Decrease of the AF peak intensity below ~ 15K !
Loss of the magnetic coherence along the chain ?
→ isolated finite spin units ?

S. Aasland et al, Solid State Comm. 1997, 101, 197.

XMCD on crystals : TP S=2, Oct. S=0
large orbital moment 1.7 μB

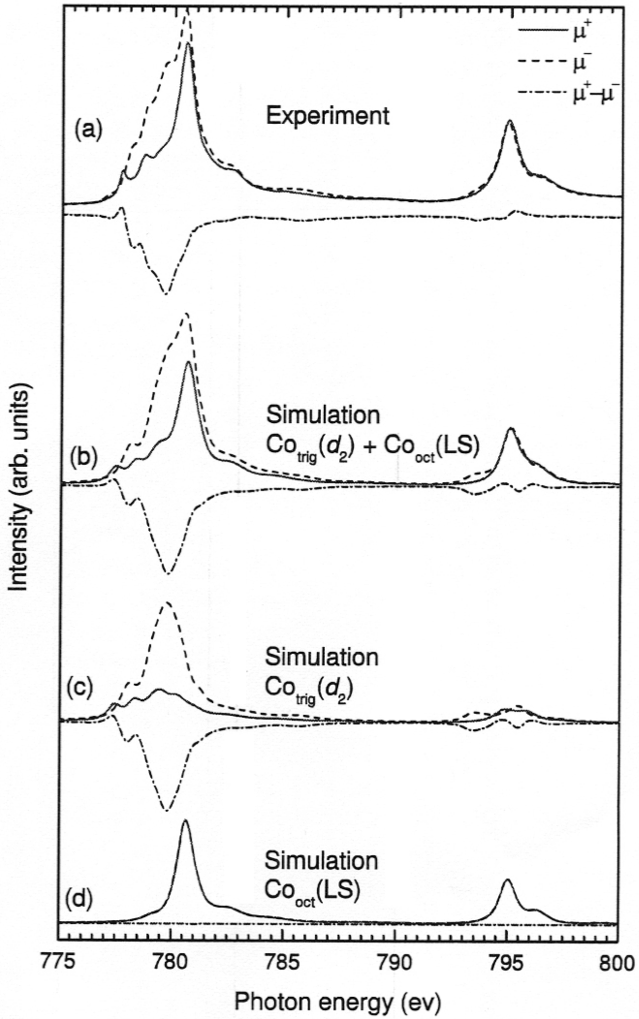

FIG. 2: (Color online) (a) Measured soft-x-ray absorption spectra with parallel (μ^+, red solid line) and antiparallel (μ^-, black dashed line) alignment between photon spin and magnetic field, together with the difference spectrum ($\mu^+ - \mu^-$, blue dash-dotted); (b) Simulated sum spectra assuming a doubly occupied d_2 orbital for the Co_{trig} and low-spin (LS) Co_{oct} ions; (c) and (d) Contribution of the Co_{trig} and Co_{oct} ions to the simulated sum spectra.

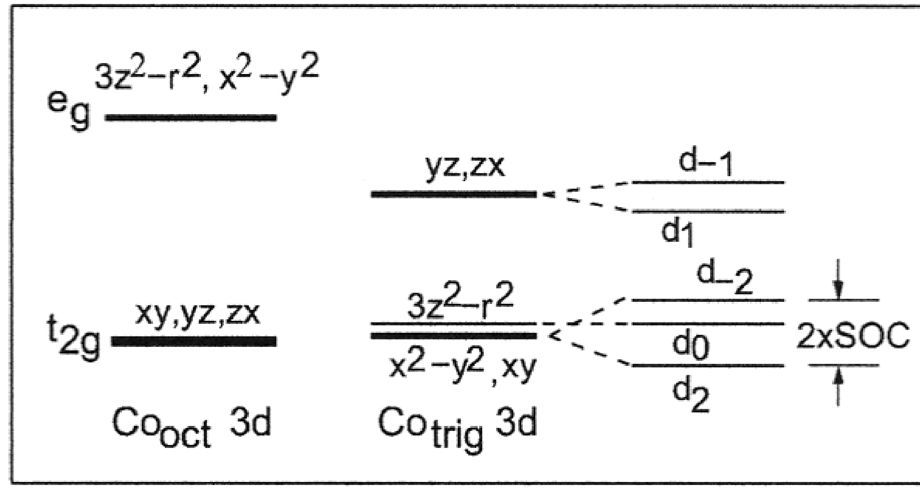

FIG. 2: Local crystal field energy diagram for: (left) Co_{oct} and (right) Co_{trig} without and with spin-orbit coupling.

Consistent with the special crystal field splitting in the Trig. Prism : orbital d_2

Predicts large orbital moment :
exp. Ms (10K) > 4 μ_B

Responsible for the strong magnetic anisotropy

L. H. Tjeng et al, Köln University

$Ca_3Co_2O_6$

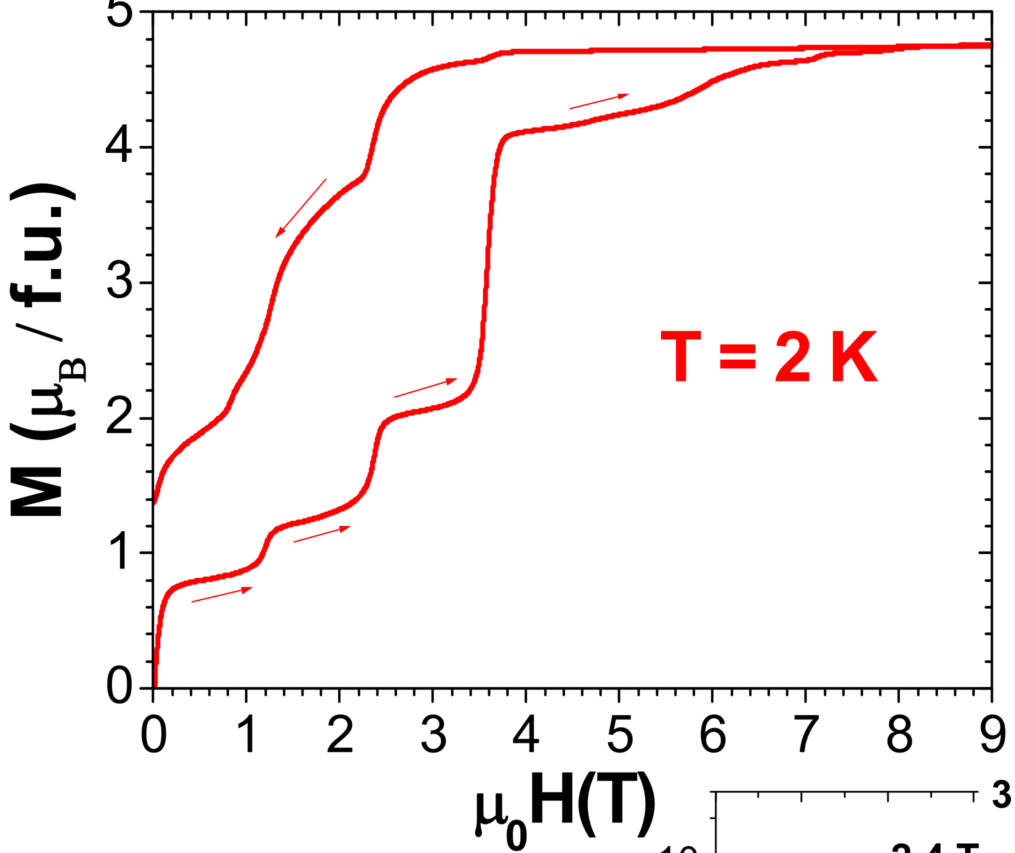

n=1, m=0

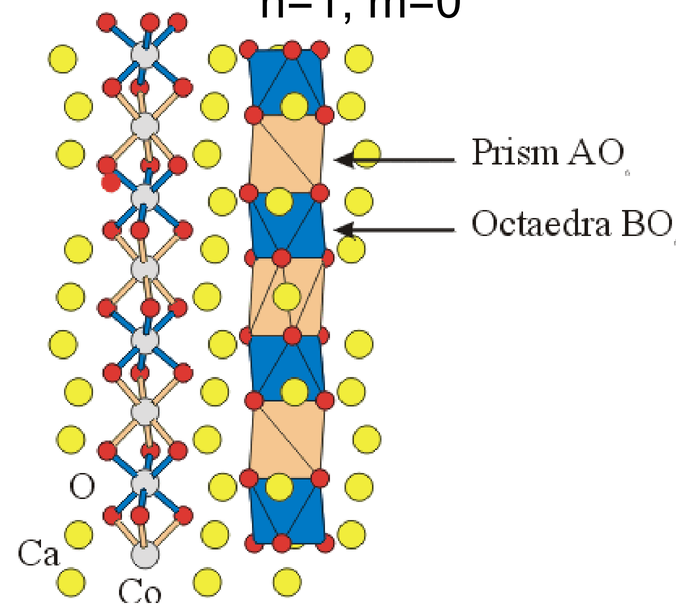

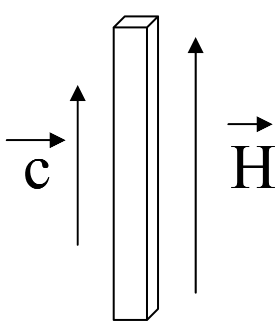

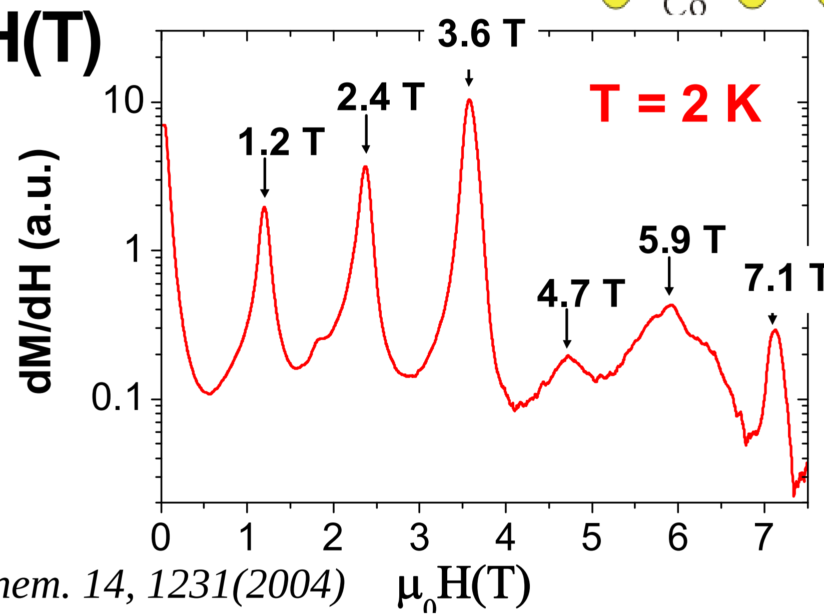

QTM

A. Maignan et al, J. of Mater. Chem. 14, 1231(2004)

$Ca_3Co_2O_6$ – magnetization steps

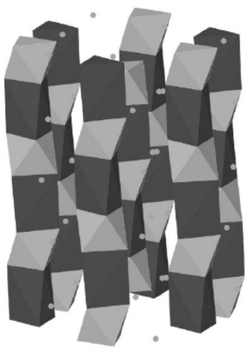

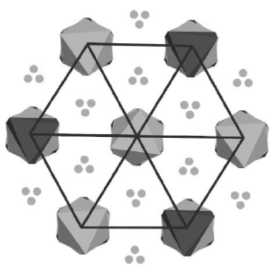

Ising triangular T_N=24K

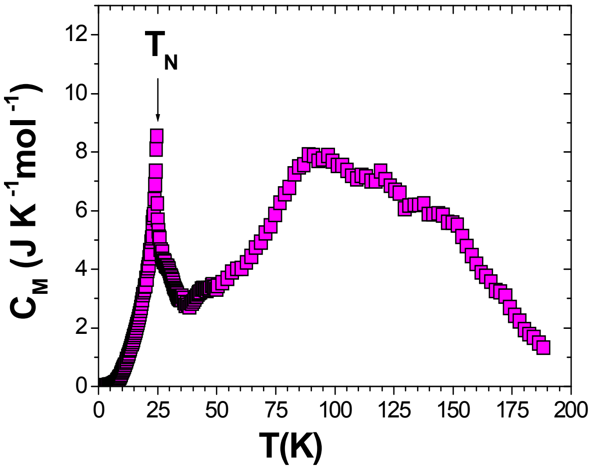

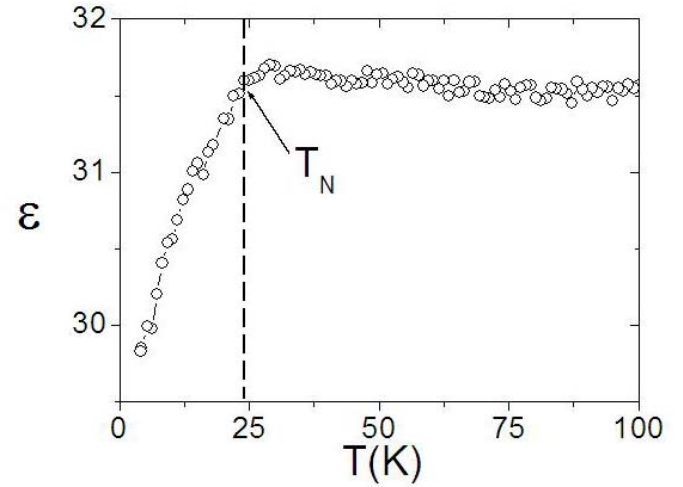

FI → FO

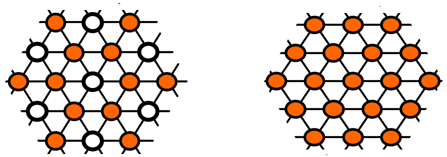

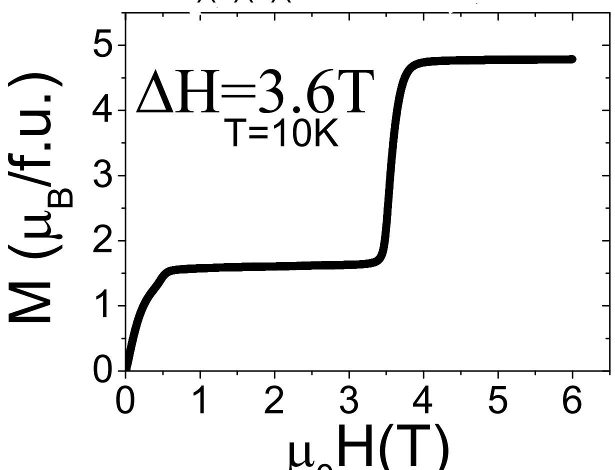

ΔH=1.2T

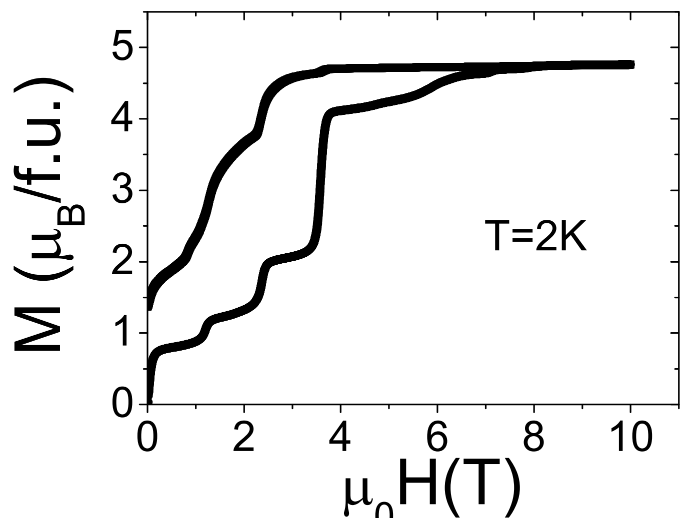

$Ca_3Co_2O_6$ –magnetodielectric coupling

T=10K

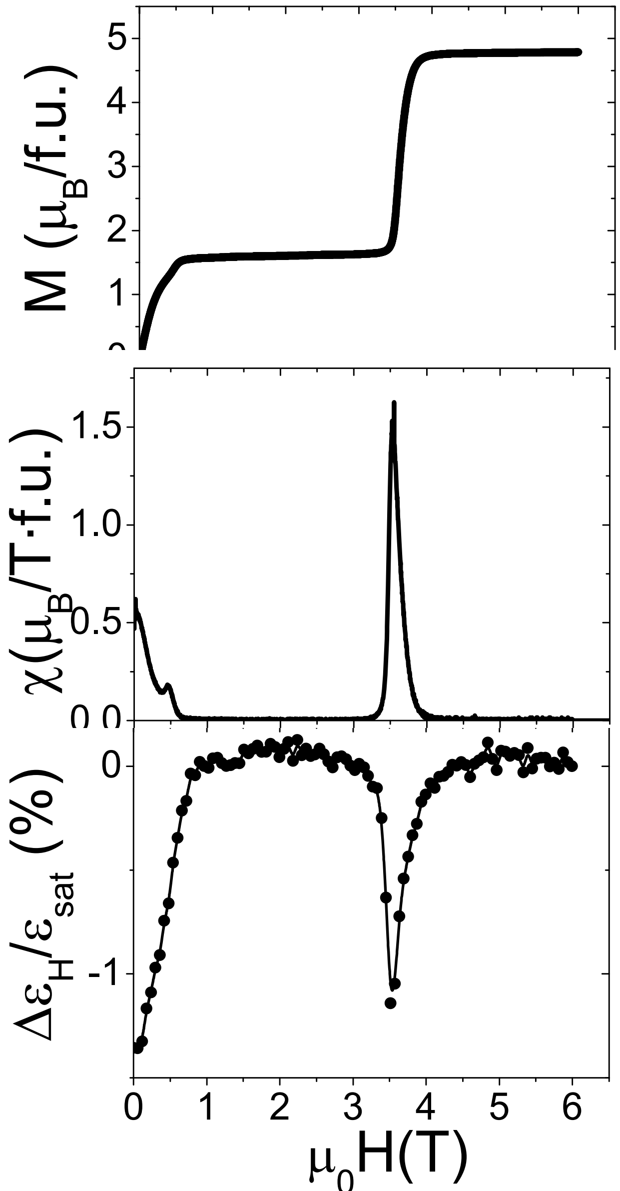

T=4K

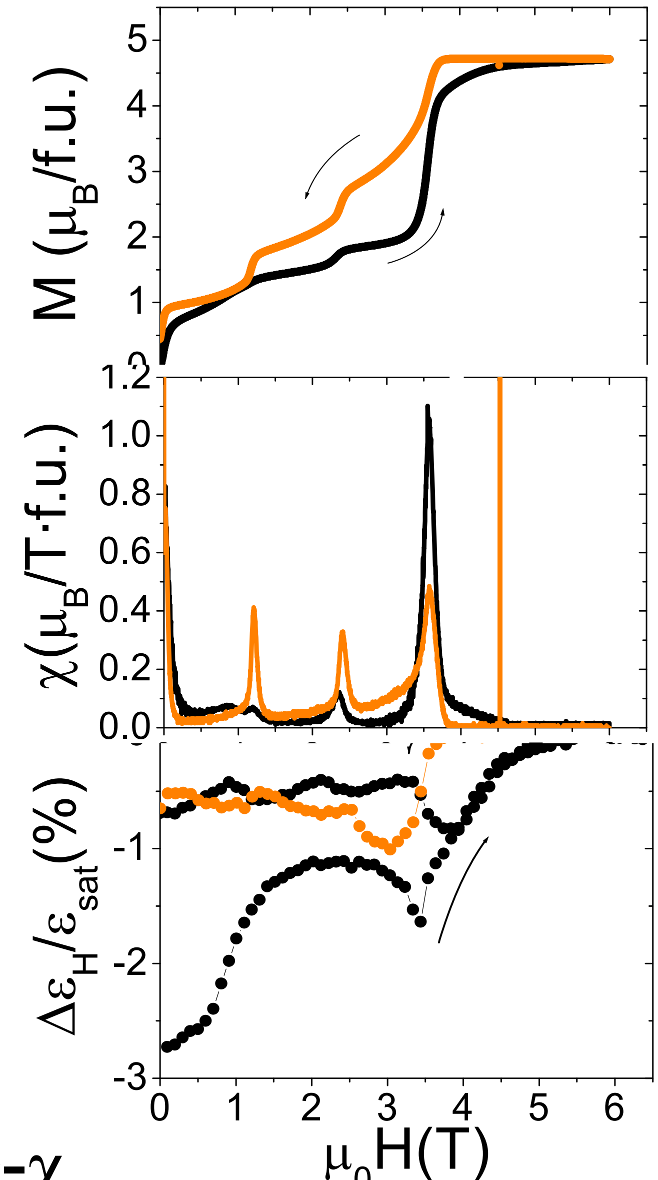

$\Delta\varepsilon \sim -\chi$

Bellido N, Simon C, Maignan A. , Phys. Rev. B 77, 054430 (2008)

Plan:

3D magnetic networks:

CMR in perovskite manganites

MIT in cobaltites

Frustrated lattices of the « 114 » type

1D and 2D TM-O-TM networks: hexagonal perovskites

and CdI_2 type structures

n-type ***vs*** **p-type** conductivity in oxides

How a TE Generator Works ?

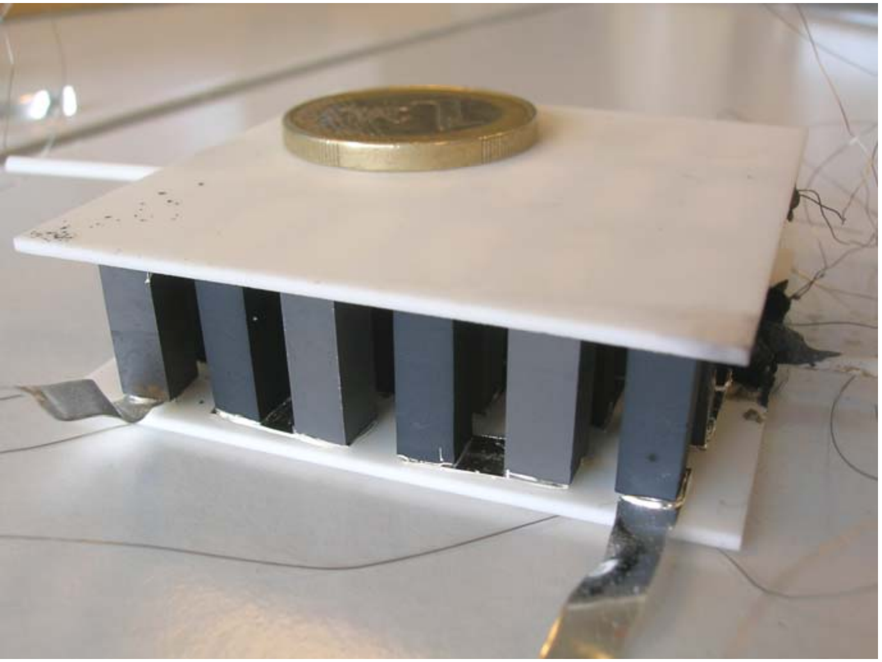

2 ceramic substrates that serve as thermal link and electrical insulation of p-type and n-type dice

Dices connected electrically in series and
thermally in parallel

Solder at the connection joints to ensure the electrical
connections and hold the module together

Thermoelectric Generators (TEG)

$$\Delta V \Leftrightarrow \Delta T$$

Seebeck effect ($\Delta T \Rightarrow \Delta V$) : thermogenerators

Peltier effect ($\Delta V \Rightarrow \Delta T$) : cooling systems

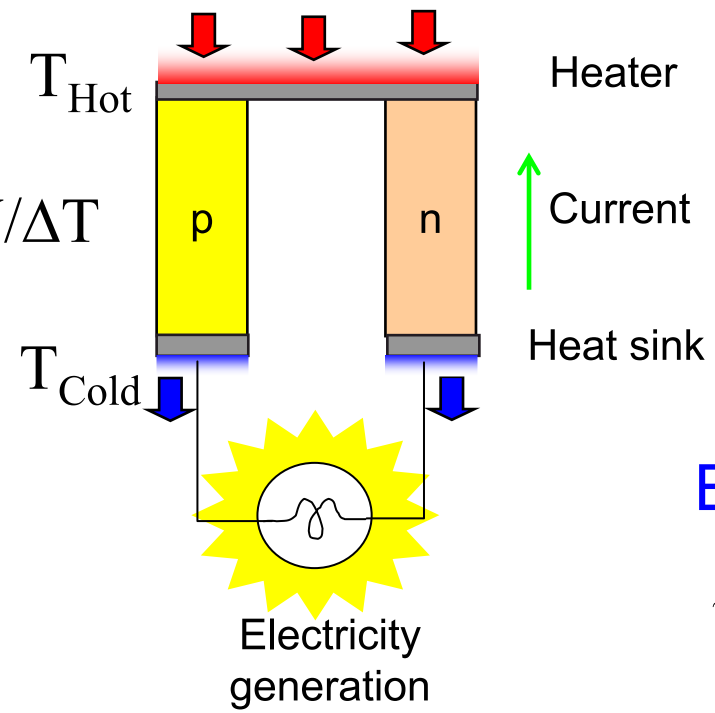

Figure of merit $Z = \frac{S^2}{\rho\kappa}$

Power factor $PF = \frac{S^2}{\rho}$

Efficiency of a thermogenerator

$$\eta_{max} = \frac{T_h - T_c}{T_h} \frac{\sqrt{1+ZT_m} - 1}{\sqrt{1+ZT_m} + \frac{T_h}{T_c}} = \eta_{Carnot} \frac{\sqrt{1+ZT_m} - 1}{\sqrt{1+ZT_m} + \frac{T_h}{T_c}}$$

For applications : n and p type materials with

ZT > 1

Module under test

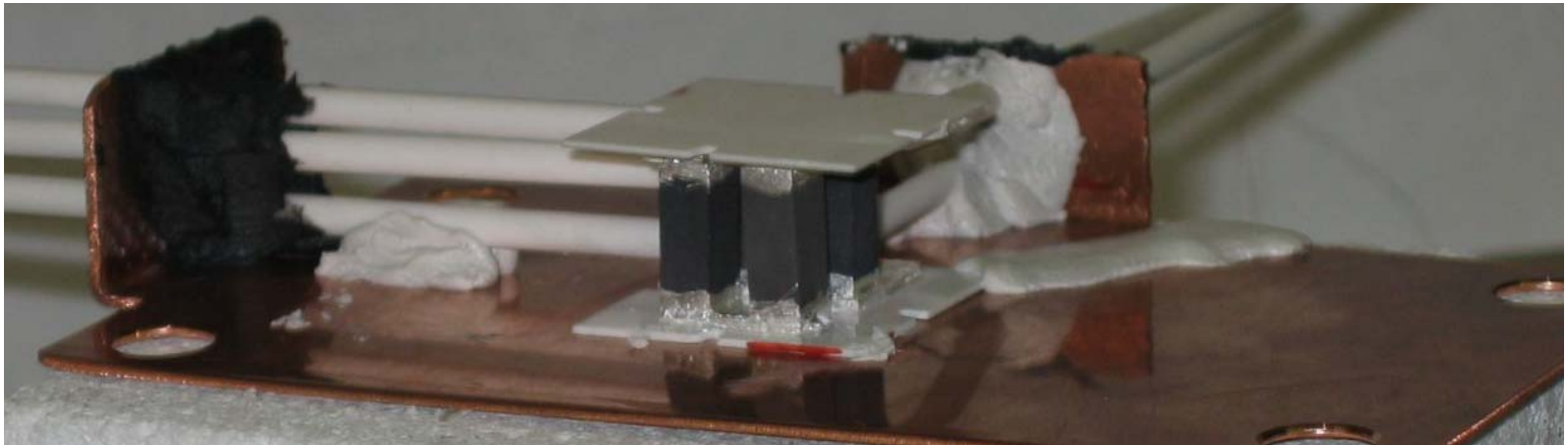

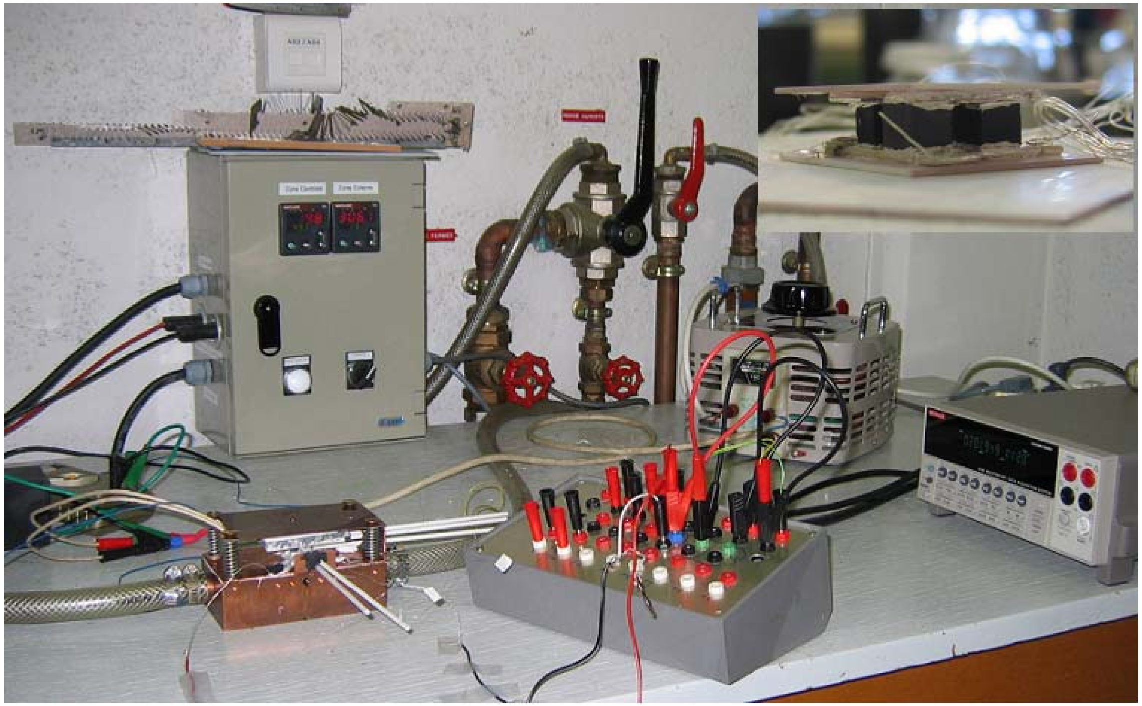

p type

Na_xCoO_2 I. Terasaki
Misfit cobaltites

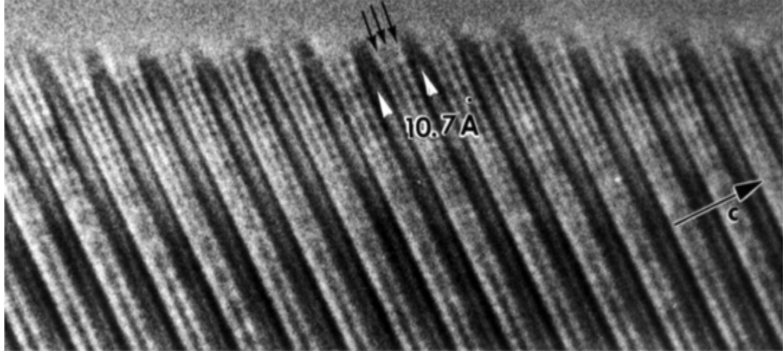

Narrow band systems with strong interactions : the Hubbard model

$$S = \frac{-S^{(2)}/S^{(1)} + \mu/|e|}{T} \rightarrow \frac{\mu/|e|}{T} \quad \text{for } T \rightarrow \infty$$

Limit T →∝ : S ~ entropy / carrier

$$S = \frac{-k_B}{|e|} \ln\left(\frac{1-x}{x}\right)$$

T-independent
Not expected for metal

+ Spin and/or orbital degeneracy β

$$S = -\frac{k_B}{|e|} \ln\left(\beta \frac{1-x}{x}\right)$$

N = 4

$(Bi_{0.87}SrO_2)_2(CoO_2)_{1.82}$ oxide

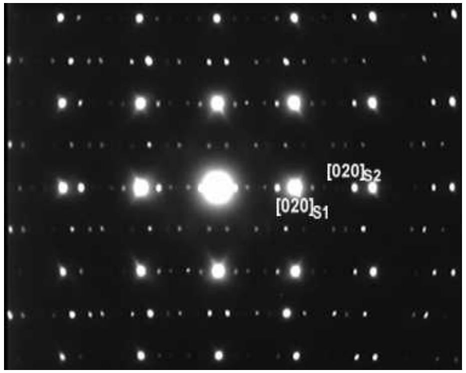

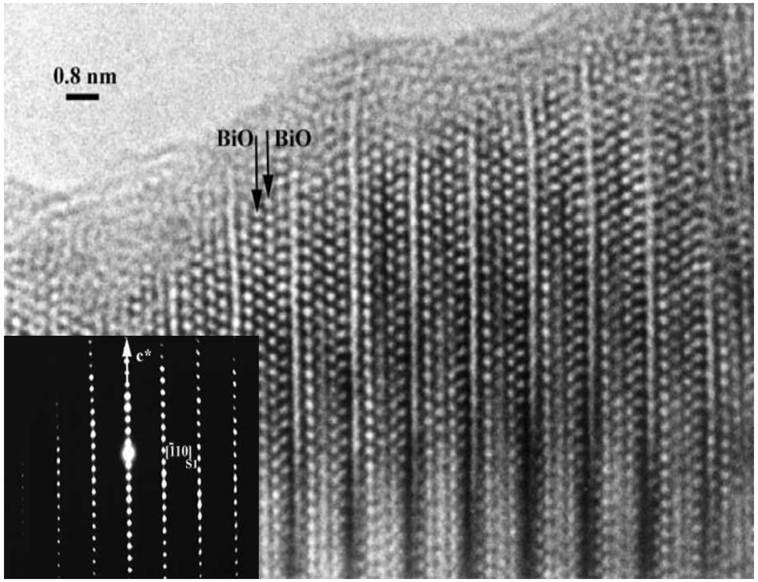

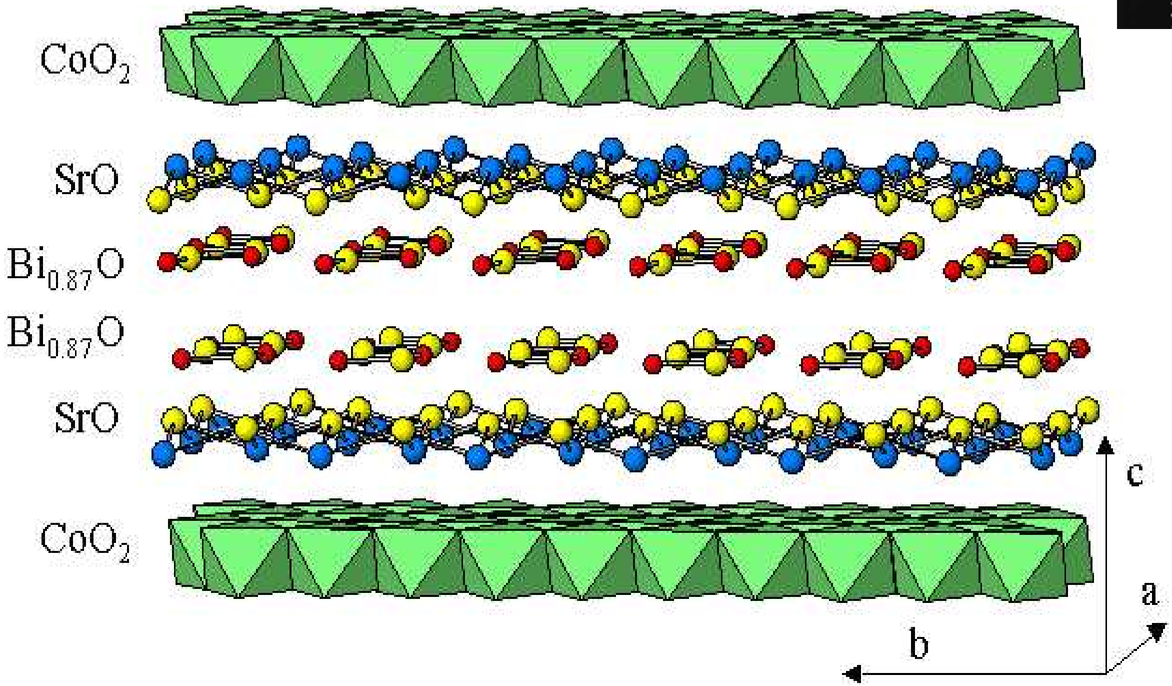

Co network: triangles

H. Leligny et al, C.R. Acad. Sci. Paris, t.2 Série IIc, 409 (1999)

Sous réseau 1 $[(Bi_{0.87}SrO_2)_2]$: a = 4.90 Å, ***b1* = 5.11 Å**, c = 29.86Å, β = 93.4°

Sous réseau 2 $[CoO_2]$: a = 4.90 Å, ***b2* = 2.81 Å**, c = 29.86Å, β = 93.4°

$b_1 / b_2 = 1.82 \approx 11/6$

Origin of large S?

Localized picture : the generalized Heikes formula

Spin and Orbital Degeneracy
Co^{3+} ($3d^6$)/Co^{4+} ($3d^5$)

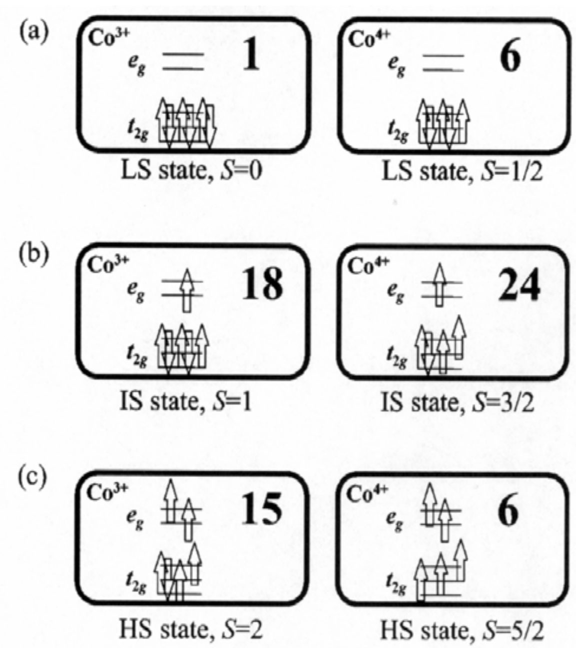

LS states due to CdI_2 layers

At high T : $S = -\frac{k_B}{e}\ln\left(\frac{g_3}{g_4}\frac{x}{1-x}\right)$

Maekawa and cowork. Phys. Rev. B 62, 6869 (2000)

Band structure calculations :

Lifting of the t_{2g} levels degeneracy due to rhombohedral crystalline field of CdI_2 layers

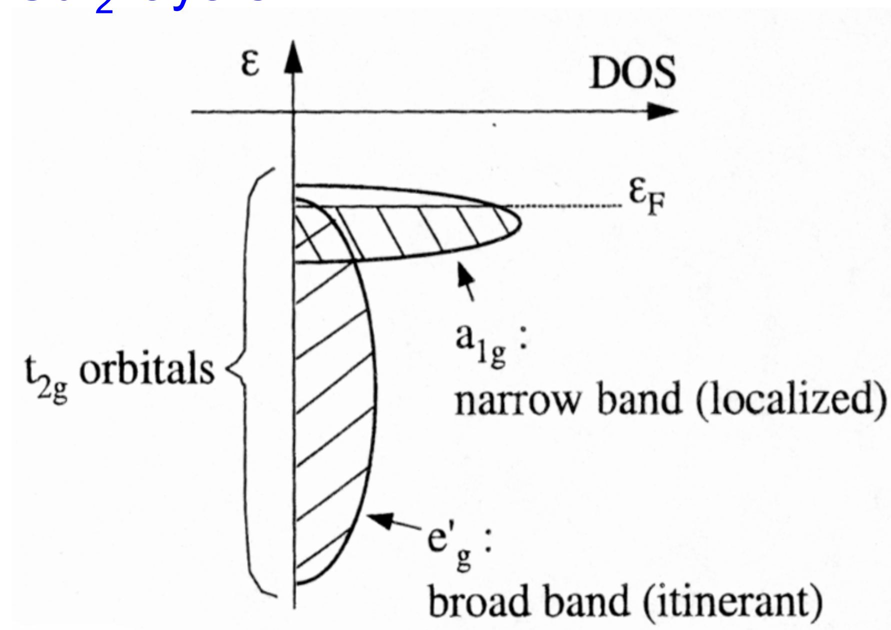

$$\frac{S}{T} = \frac{\pi^2 k^2}{3e}\left(\frac{d\ln(\sigma)}{dE}\right)_{E=E_F}$$

Peak in DOS : large S
+ Metallicity

D. J. Singh, Phys. Rev. B 61, 13397 (2000)
T. Yamamoto et al., Phys. Rev. B 65, 184434 (2002)

Magnetothermopower

NMR

Misfit BiCaCoO

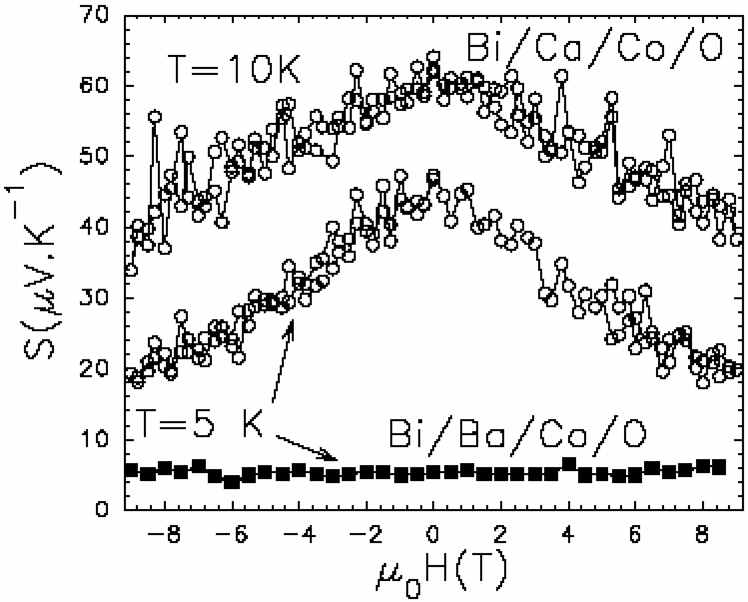

Decrease of S in field at low T

Due to the alignement of paramagnetic spins

J. Bobroff et al, PRB (LPS Orsay)

Peak of susceptibility

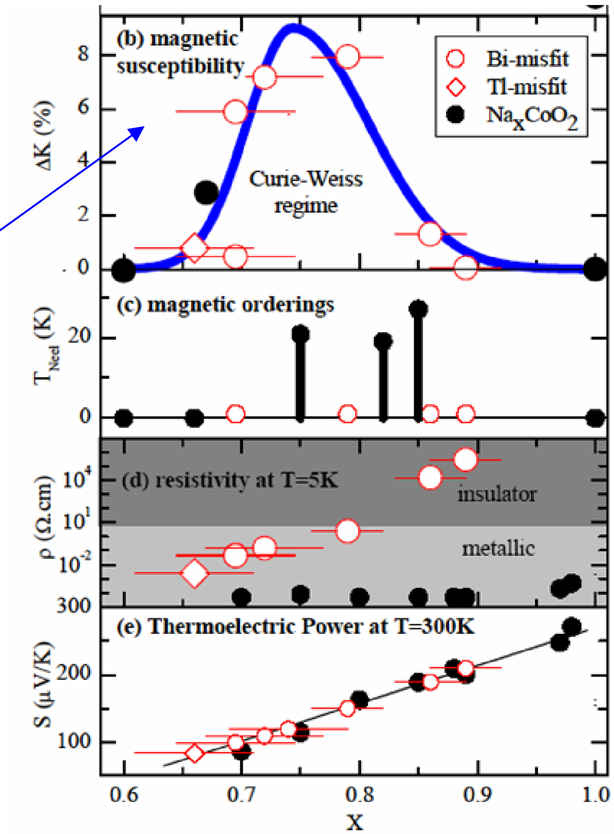

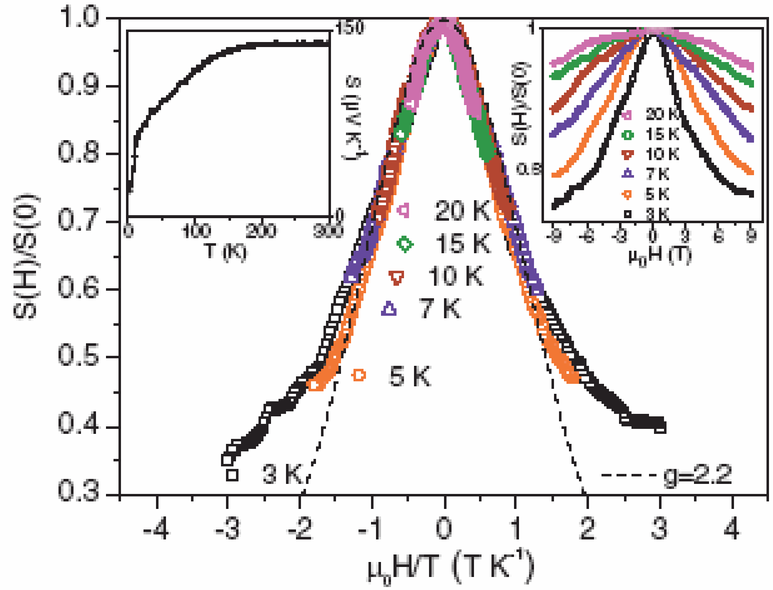

Scaling law for S(H) : paramagnetic spins S=1/2

Brillouin function

$$S(x)/S(0) = (\ln[2\cosh(x)] - x\tanh[x])/\ln(2).$$

Similar to $Na_{0.7}CoO_2$

P. Limelette et al., PRL97, 046601 (2006)

Y. Wang et al., Nature423, 425 (2003)

$[Bi_{1.95}Ba_{1.95}Rh_{0.1}O_4][RhO_2]_{1.8}$

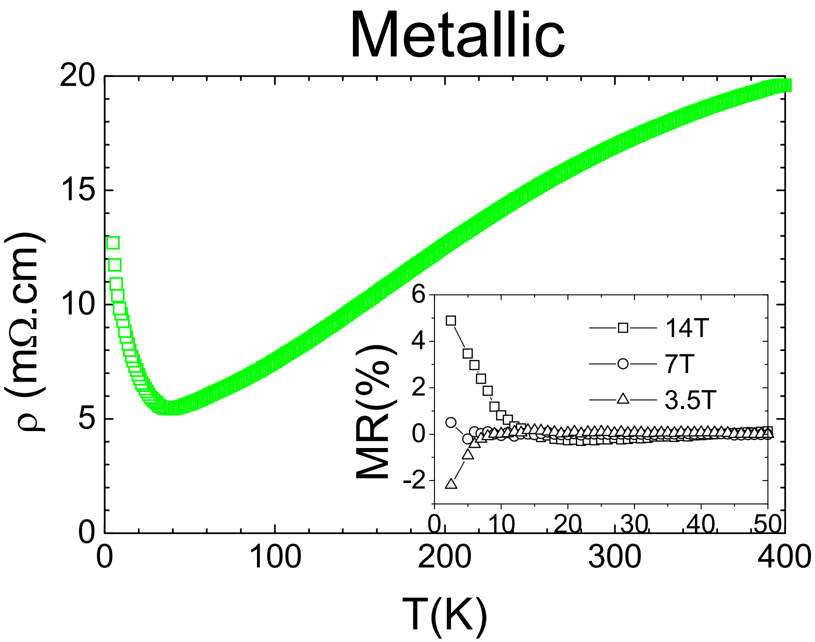

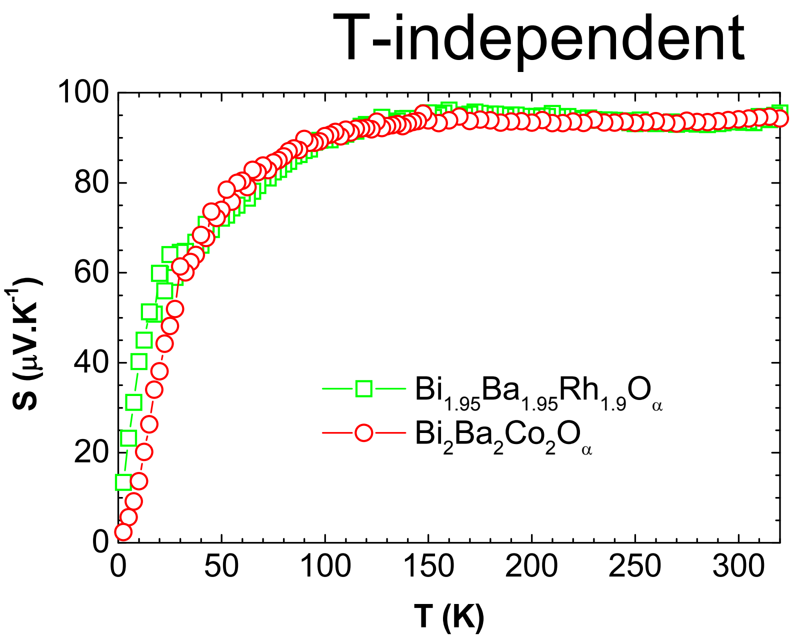

Metallic down to 50K

Large S : spin degeneracy $\beta = 1/6$

Small and positive magneto-resistance

Y. Klein, Phys. Rev. B 73, (2006) 165121

$SrRuO_3$

Chemical formula	Calculated Ru oxidation state
$SrRuO_3$	4
$SrRu_{0.97}O_{2.94}$	4
$SrRu_{0.92}O_3$	4.35
$SrRu_{0.975}Cr_{0.025}O_3$	4 (for Cr^{4+})
$SrRu_{0.9}Mn_{0.1}O_3$	4.11 (for Mn^{3+})
$Sr_{0.8}La_{0.2}RuO_3$	3.80

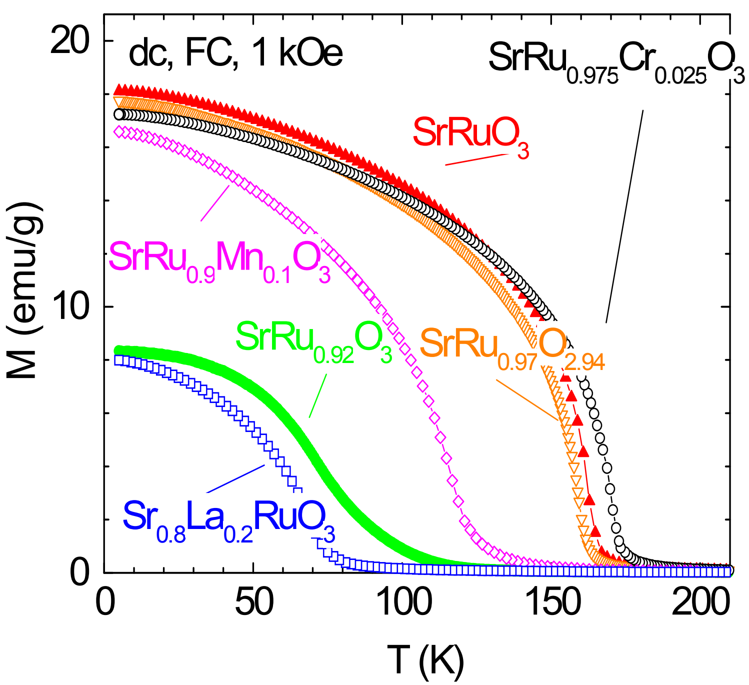

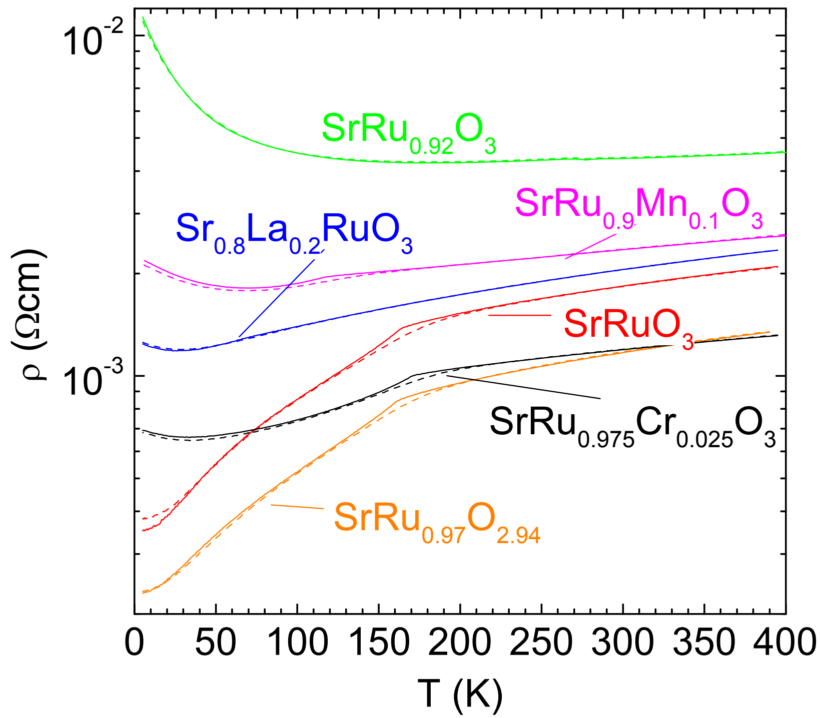

Ruthenates: same behavior for S(T)

Ru^{3+}/Ru^{4+}

$$\beta = \frac{2\times(1/2)+1}{2\times1+1}$$

$S_{spin} = 35\mu V/K$

Ru^{4+}/Ru^{5+}

$S_{spin} = 25\mu V/K$

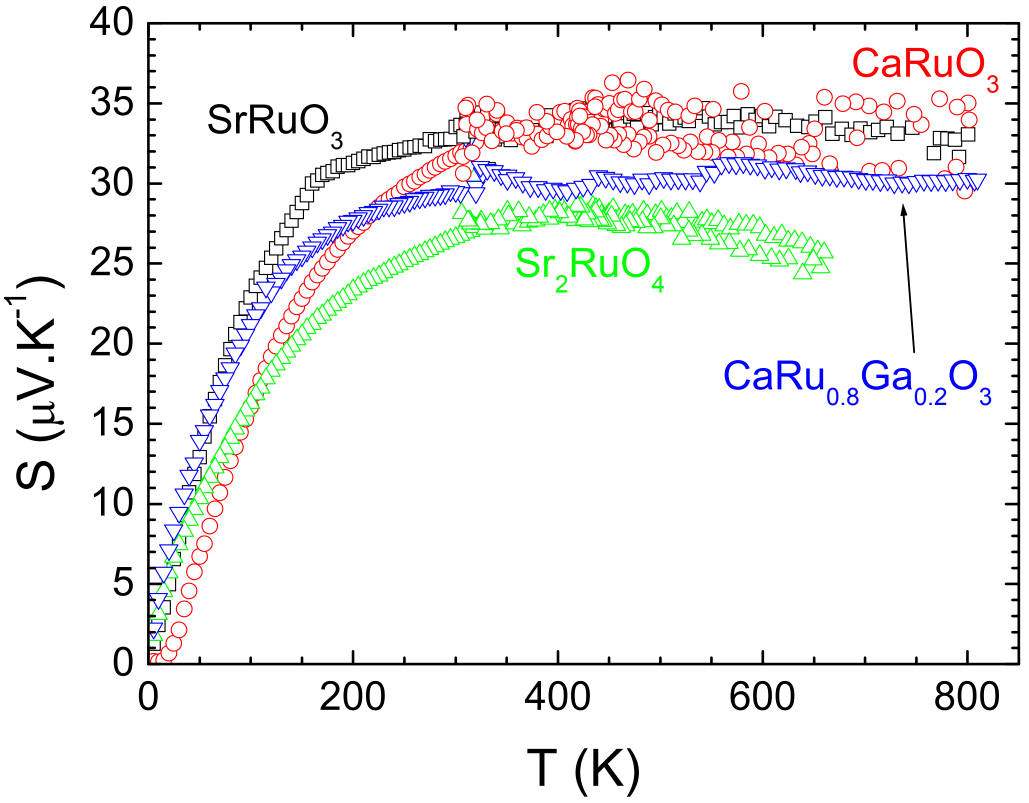

Spin only contribution, works in a metallic compound

$ACu_3Ru_4O_{12}$

Large mass enhancement
(γ=135mJ/fu.mol.K^2 for A=La)
ex: RuO_2 γ=6mJ/fu.mol.K^2

S. Tanaka et al, cond-mat 28 june 2009

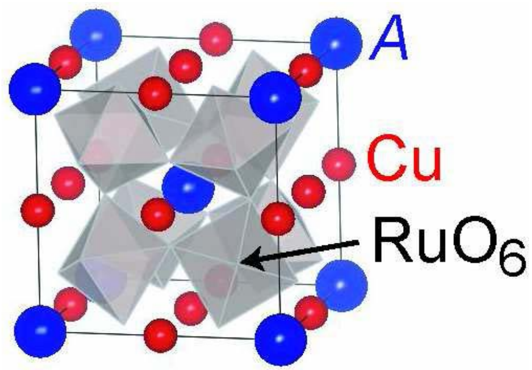

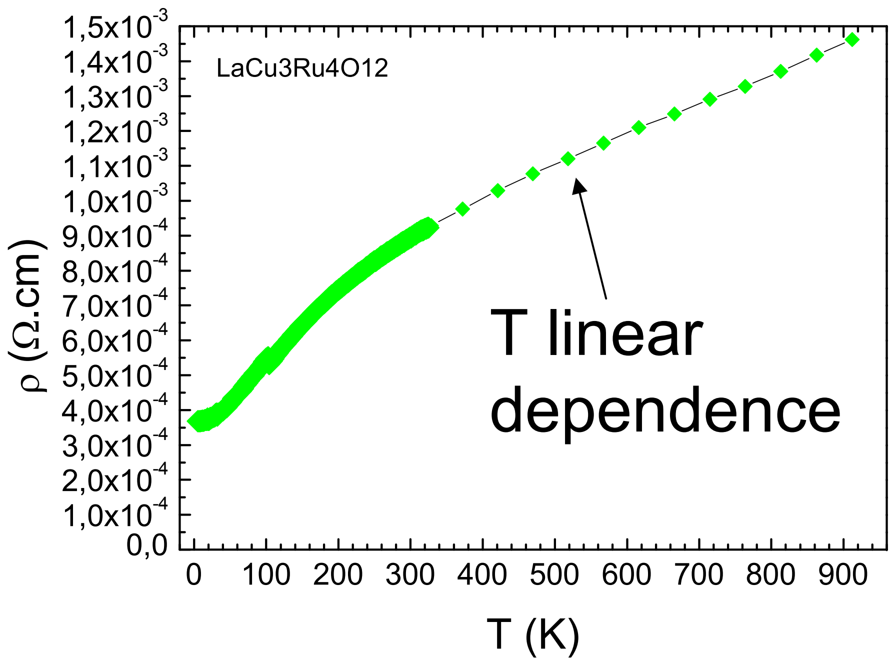

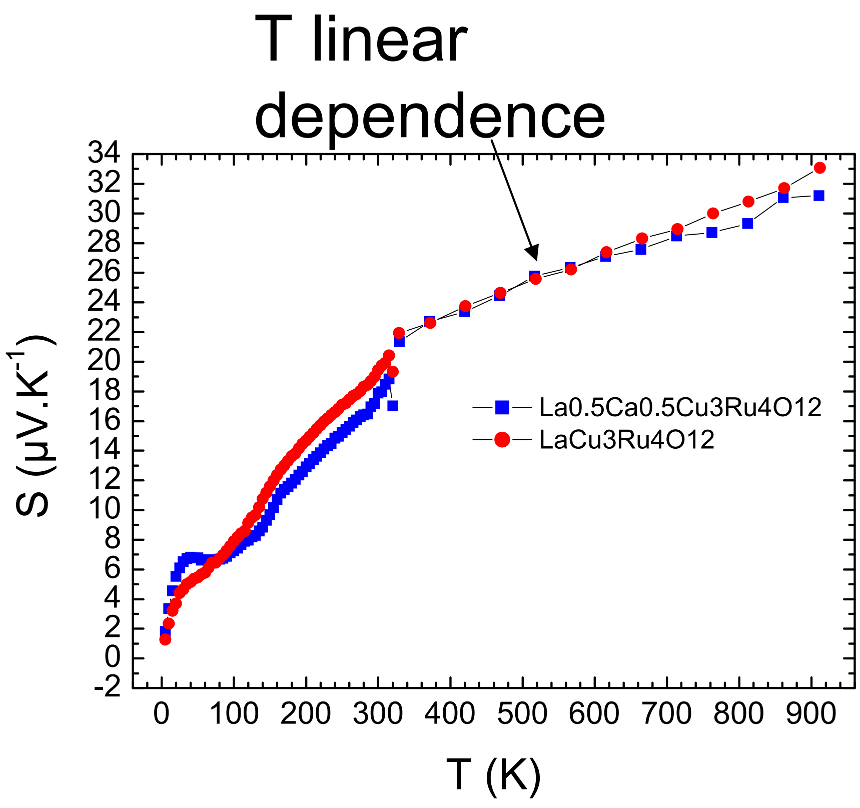

A. Maignan et al (to be published)

Plan:

3D magnetic networks:

CMR in perovskite manganites

MIT in cobaltites

Frustrated lattices of the « 114 » type

1D and 2D TM-O-TM networks: hexagonal perovskites

and CdI_2 type structures

n-type ***vs*** **p-type** conductivity in oxides

Delafossite: layer compound with CdI_2 type layer

AMO_2

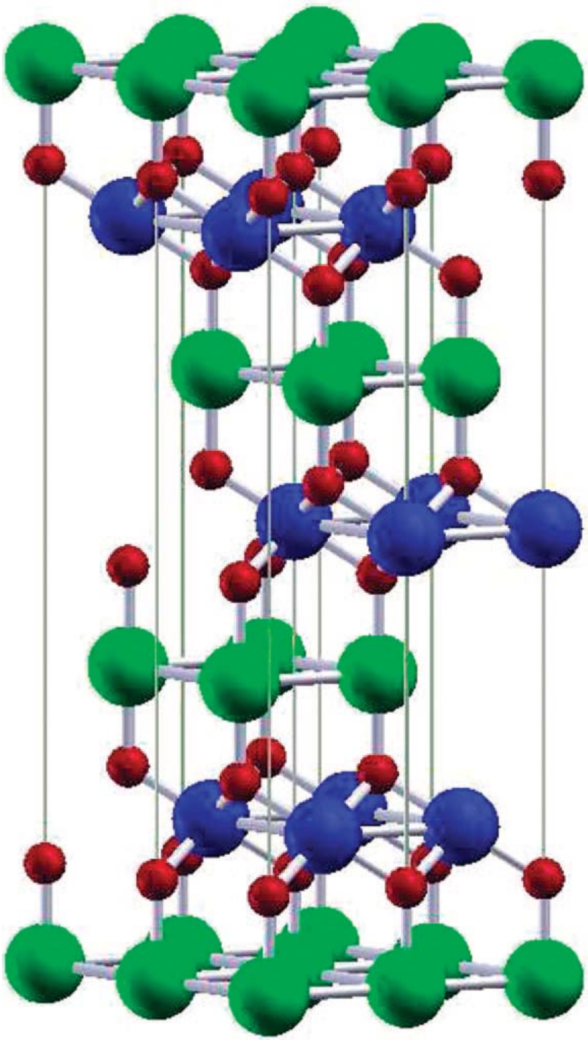

A (dumbell)

MO_2

2H or 3R depending on oxygen packing

$PdCoO_2$: metal, like Pd
DJ Singh

Doped $CuCrO_2$: bad metal with large S

Du Pont 1970

M network: triangles

$CuCr_{1-x}Mg_xO_2$

Triangular AF S=3/2

$CuRh_{1-x}Mg_xO_2$

Pauli paramagnet

S=0

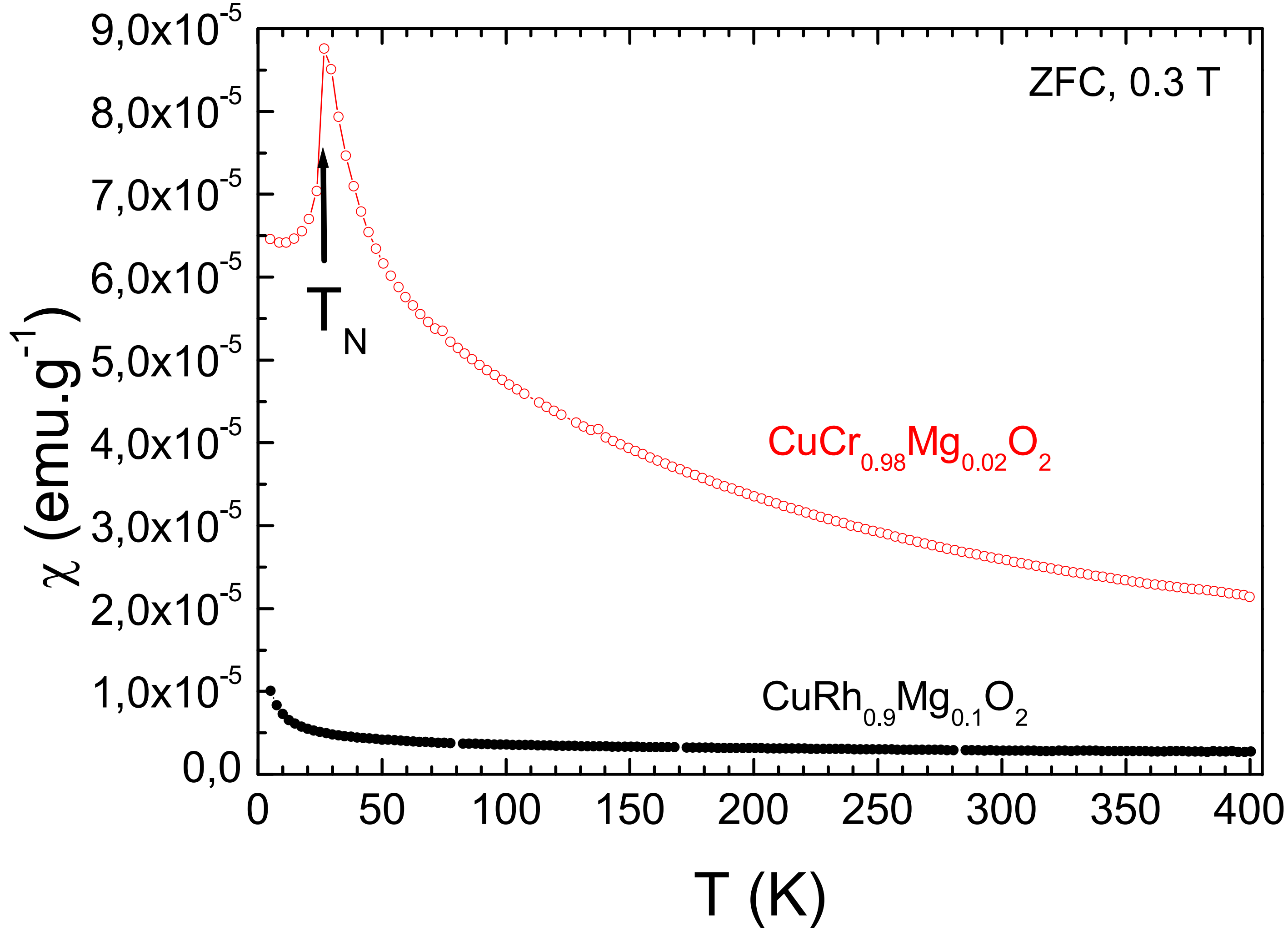

$CuRh_{1-x}Mg_xO_2$

For large enough hole content metal-like behavior as cobaltites

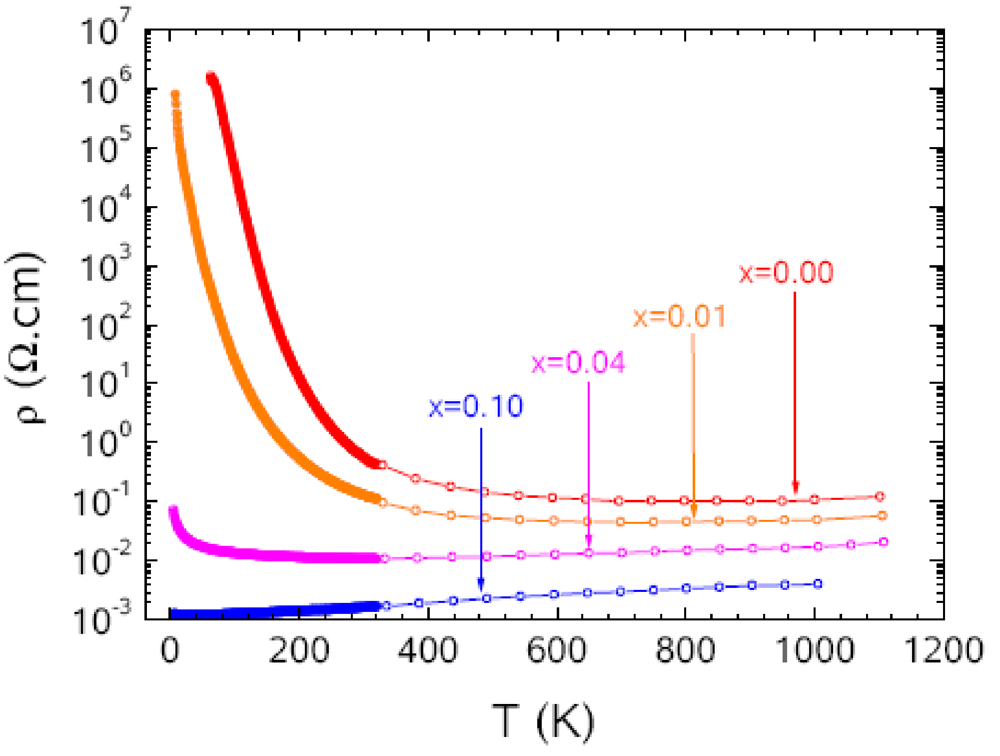

Experiment

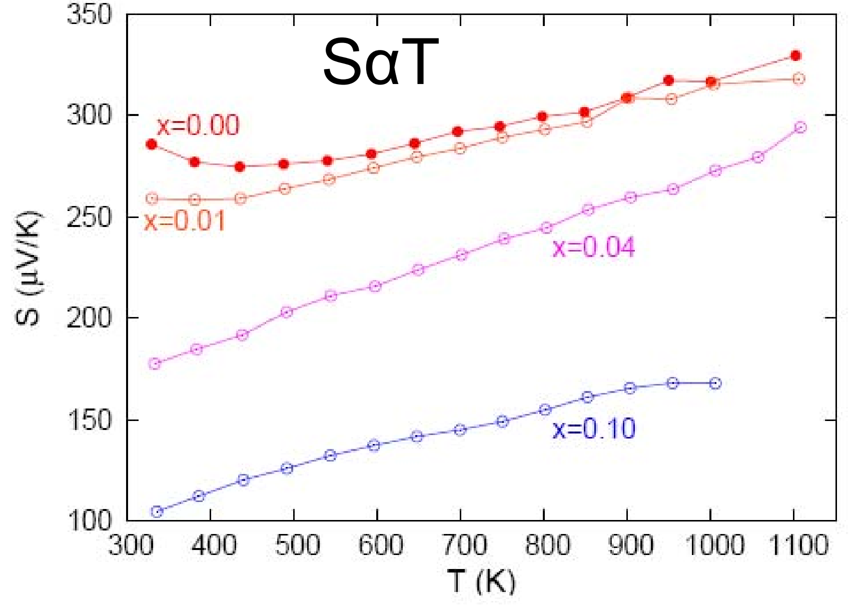

Calculated

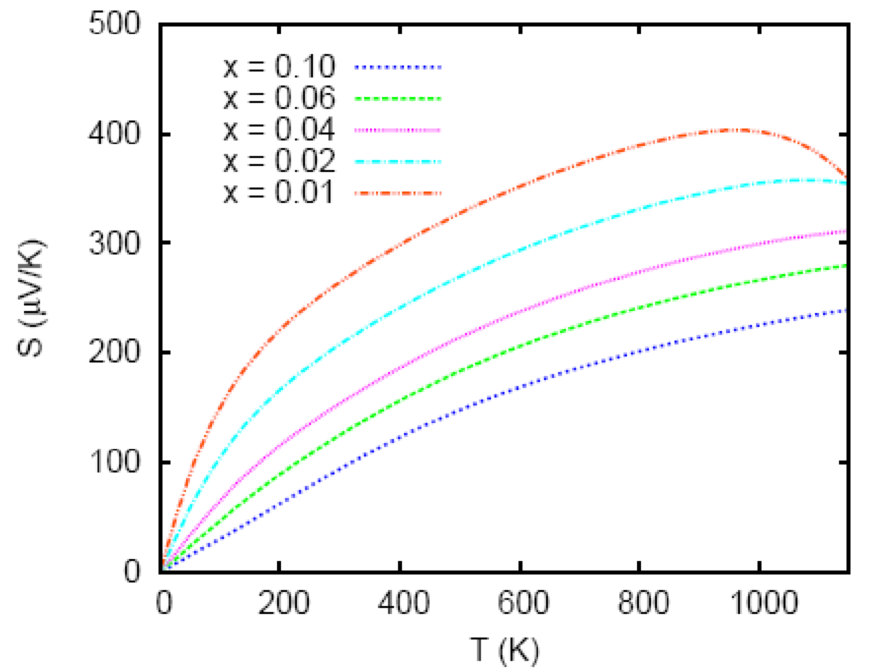

$CuRh_{1-x}Mg_xO_2$

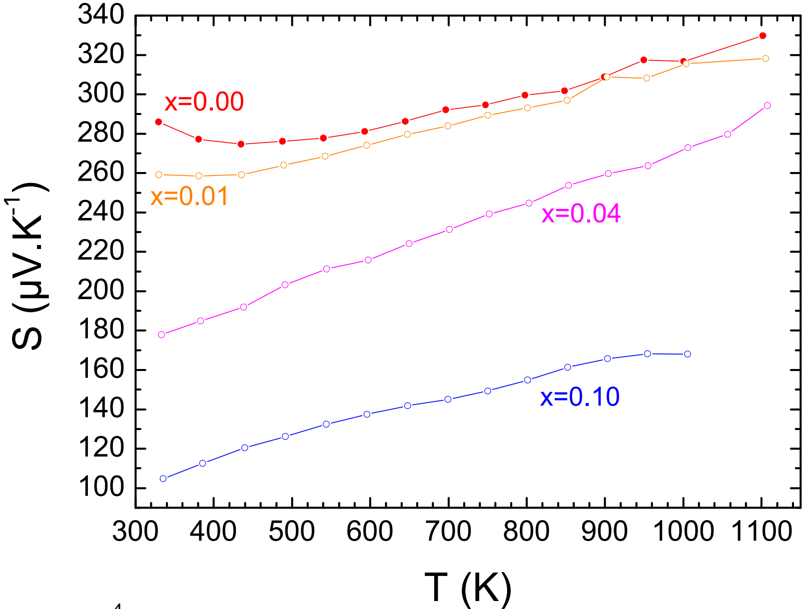

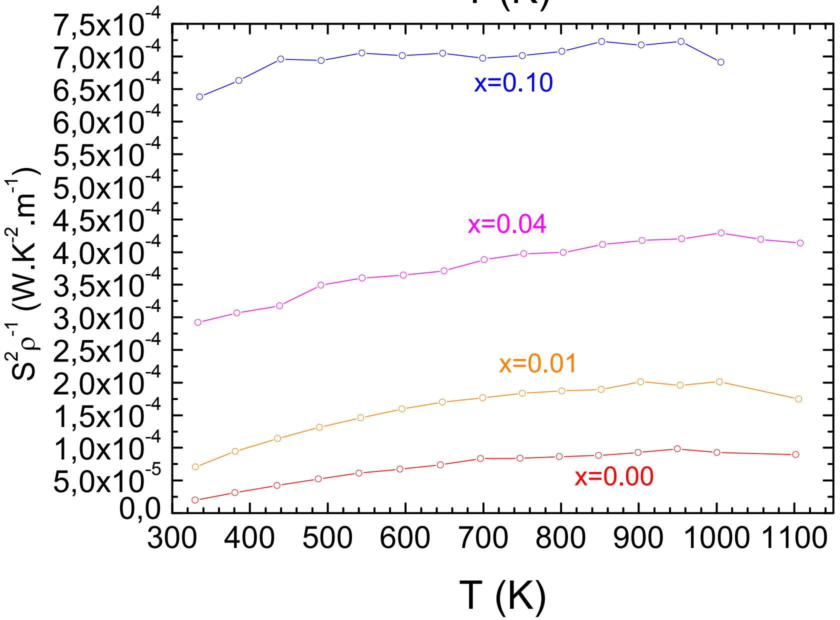

PF is rather T independent

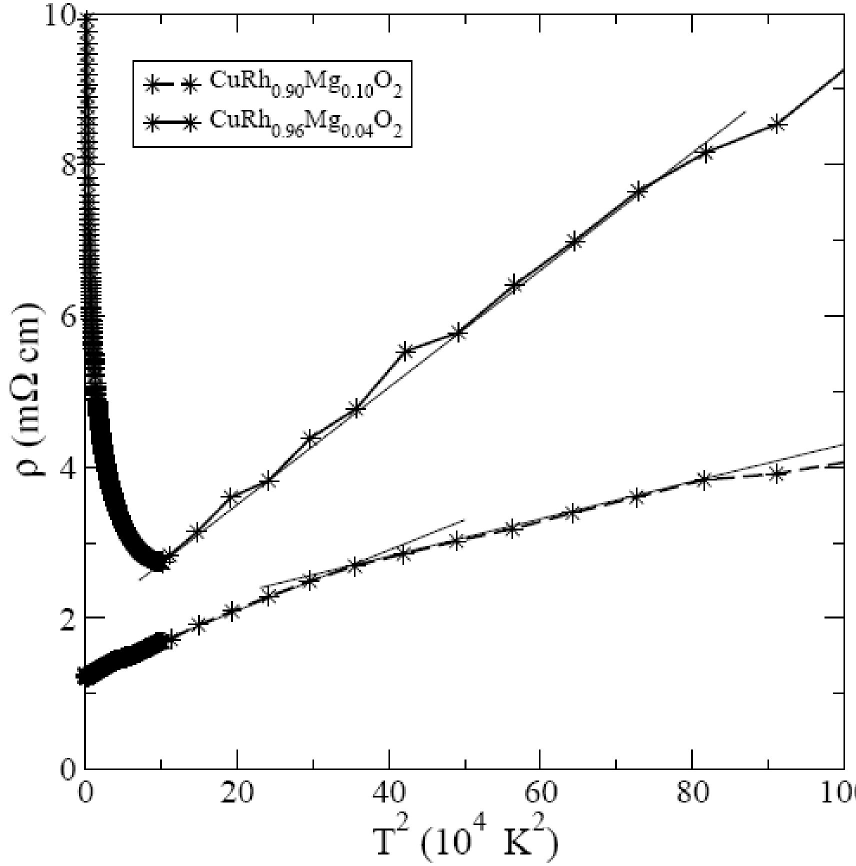

Large T range for Fermi liquid-like behavior

Spiral magnets

Spiral magnets breaking inversion symmetry, in an insulator, induces a polarization.

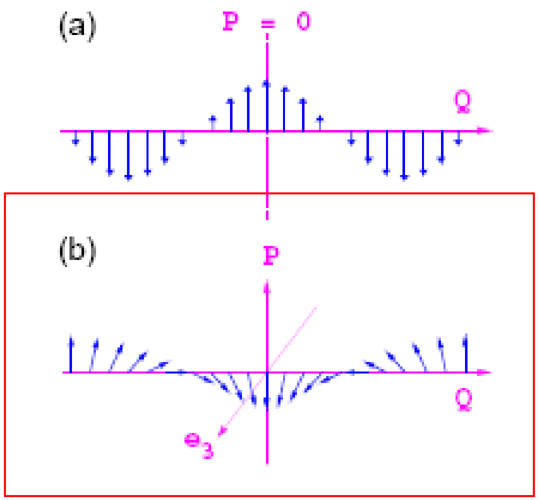

$$\vec{P} \approx [\vec{e} \times \vec{Q}]$$

Spin rotation axis $\neq$ Wave vector of the spiral

$$T_{FE} = T_C$$ ➡ Ferroelectricity is induced by magnetic order

⬇

Peak in dielectric constant

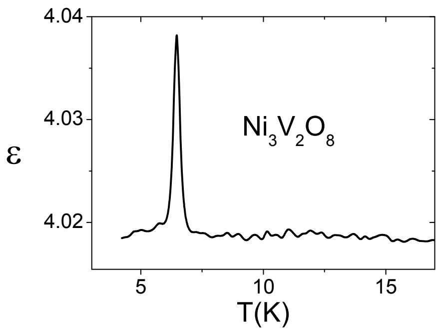

Mostovoy Phys.Rev.Lett.96 067601 (2006)

M. Kenzelmann Phys. Rev. Lett. 95, 087206 (2005)

Modulated antiferromagnetic structures found in *geometrically frustrated insulating materials*

Spin current model

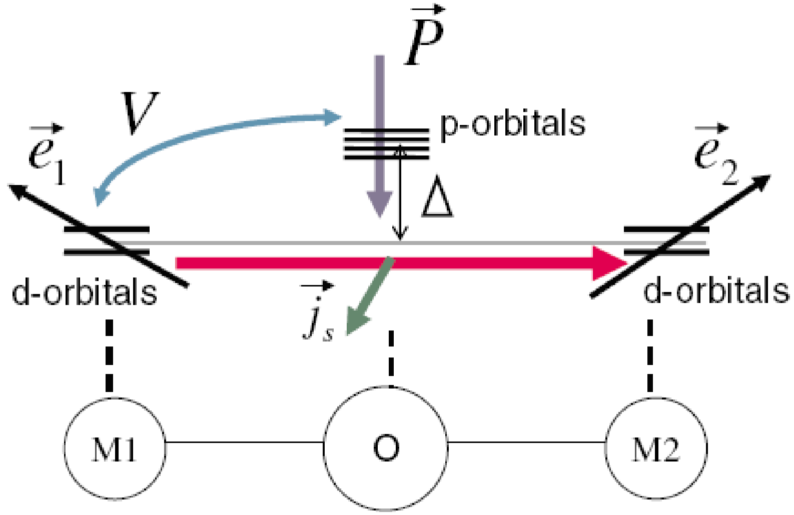

FIG. 1 (color online). The cluster model with two transition metal ions M1, M2 with the oxygen atom O between them. With the noncollinear spin directions $\vec{e}_1$ and $\vec{e}_2$, there arises the spin current $\vec{j}_s \propto \vec{e}_1 \times \vec{e}_2$ between M1 and M2. Here the direction of the vector $\vec{j}_s$ (denoted by the short arrow near the middle of the diagram) is that of the spin polarization carried by the spin current. The direction of the electric polarization $\vec{P}$ is given by $\vec{P} \propto \vec{e}_{12} \times \vec{j}_s$ where $\vec{e}_{12}$ is the unit vector connecting M1 and M2.

Antiferromagnetically stacked proper helical structure (q,q,3/2), q=0.21

Spin current model

$$\vec{P} \approx [\vec{e} \times \vec{Q}]$$

BUT

e//Q (on average) , P=0

~~Spin current model~~

New explanation is required in doped $CuFeO_2$

Crystals to test for the chirality

c is the spin chirality vector

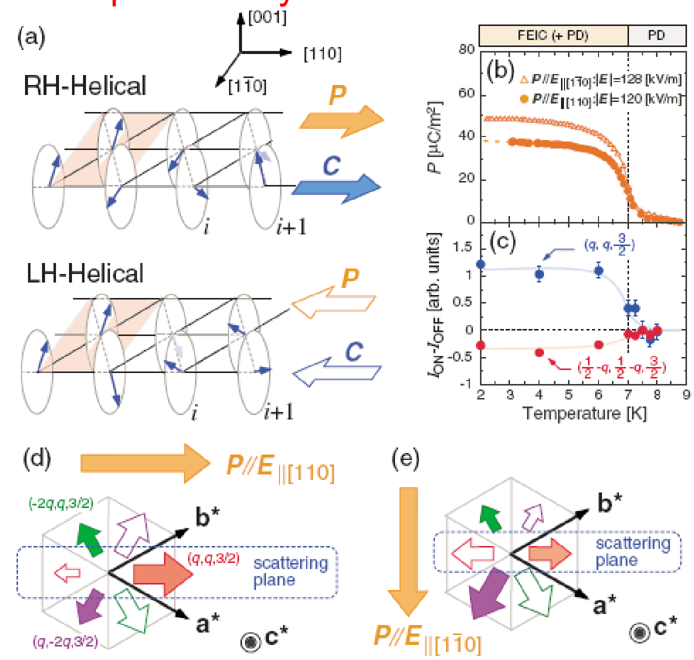

FIG. 3. (Color online) (a) The relationship between the vector spin chirality and the direction of the electric polarization. (b) The temperature variations of the electric polarization along the [110] and [1$\bar{1}$0] axes measured after cooling with a poling electric field parallel to the [110] and [1$\bar{1}$0] directions, respectively. (c) The temperature dependence of $I_{on}-I_{off}$ measured on heating after cooling with a poling electric field (120 kV/m) parallel to the [110] axis. [(d) and (e)] The schematic drawings of the distributions of the RH- (filled arrows) and LH- (open arrows) helical orderings among magnetic domains with three equivalent propagation wave vectors, $(q,q,\frac{3}{2})$, $(-2q,q,\frac{3}{2})$, and $(q,-2q,\frac{3}{2})$, when the macroscopic electric polarization emerges along (d) the [110] axis and (e) the [1$\bar{1}$0] axis. The directions of the arrows denote the (001) projection of the three modulation wave vectors. The size of the arrows shows the fractions of the RH- or LH-helical orderings.

Transport properties of $CuCr_{1-x}Mg_xO_2$

Maekawa

Trivalent Cr S=3/2

Large resistivity drop up to x=0.02

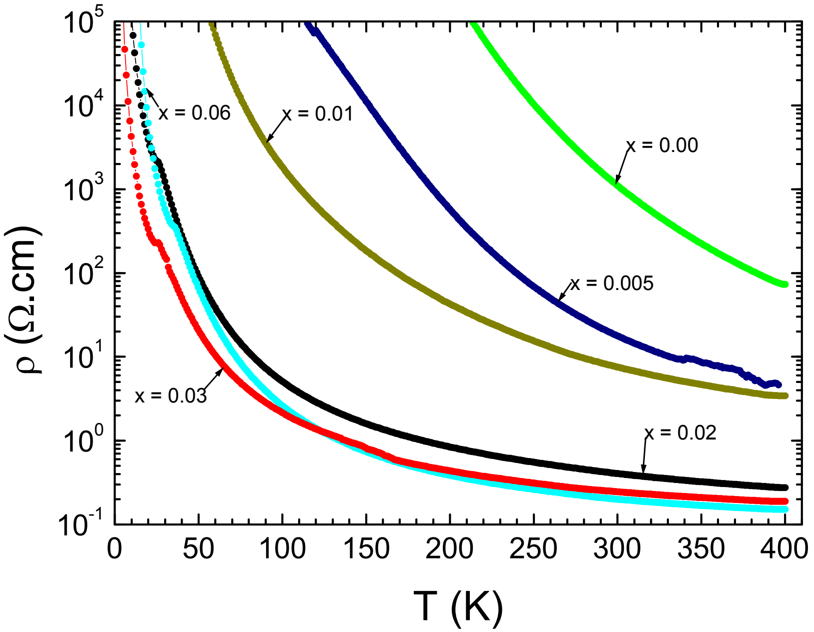

Large S drop up to x=0.02

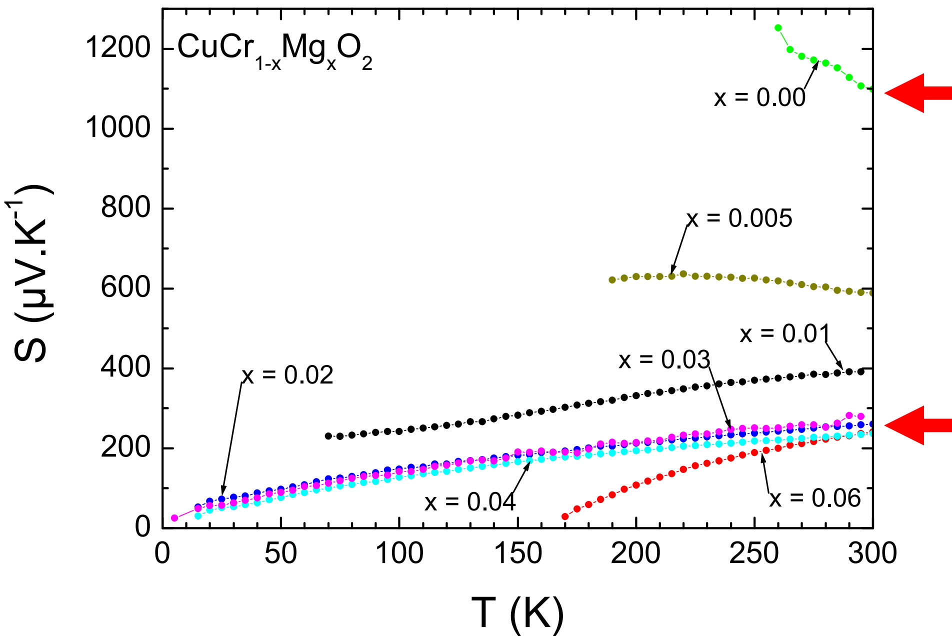

Activated (x=0.00) to small polaron (x>0.01)

TEM/ED/EDX/XRD: x_{max} =0.01

Holes : Cr^{4+}

Undoped: insulator

$CuCrO_2$

Trivalent Cr S=3/2

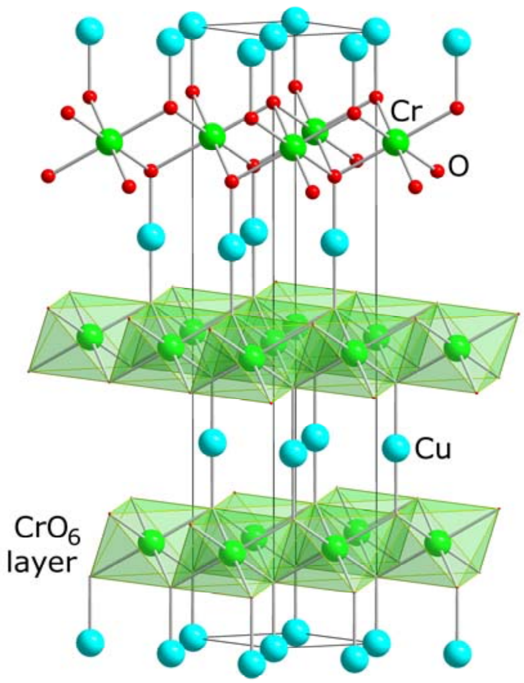

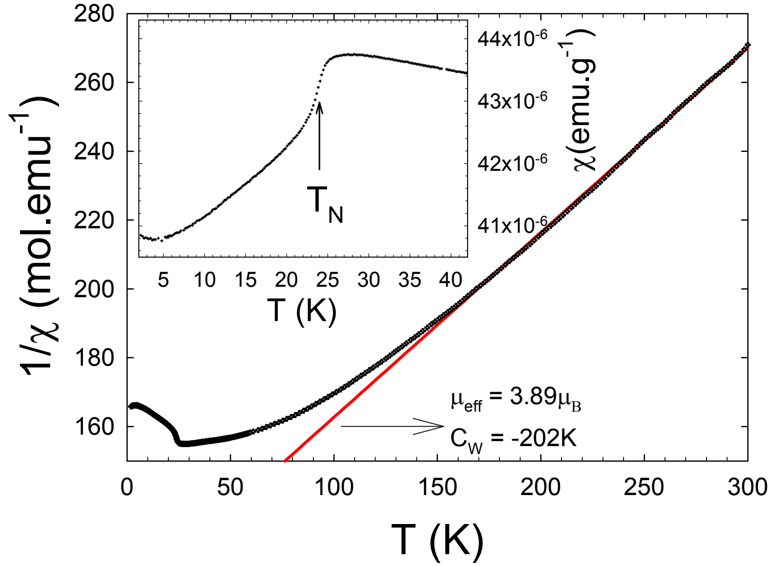

SG: R-3m

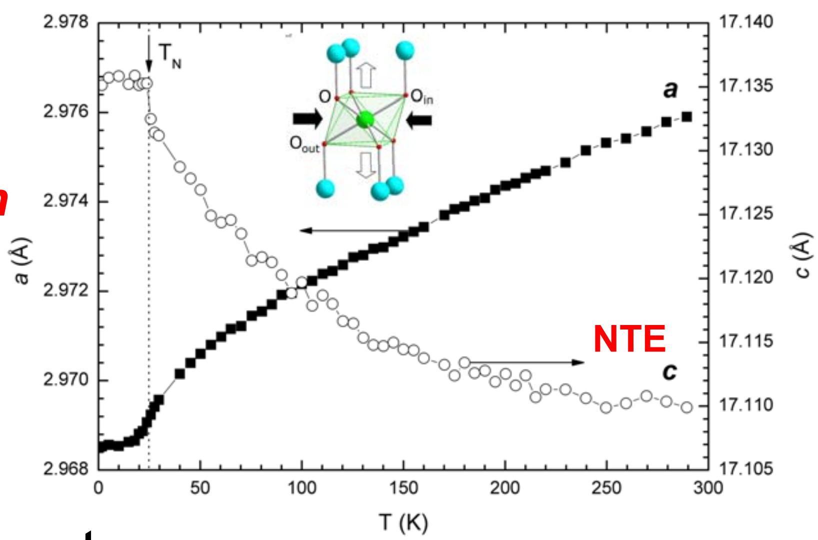

No structural transition

Keeps a centrosymmetric structure

$CuCrO_2$

K. Kimura et al, Phys. Rev. B 78, 140401R 2008
exp: in-plane polarization

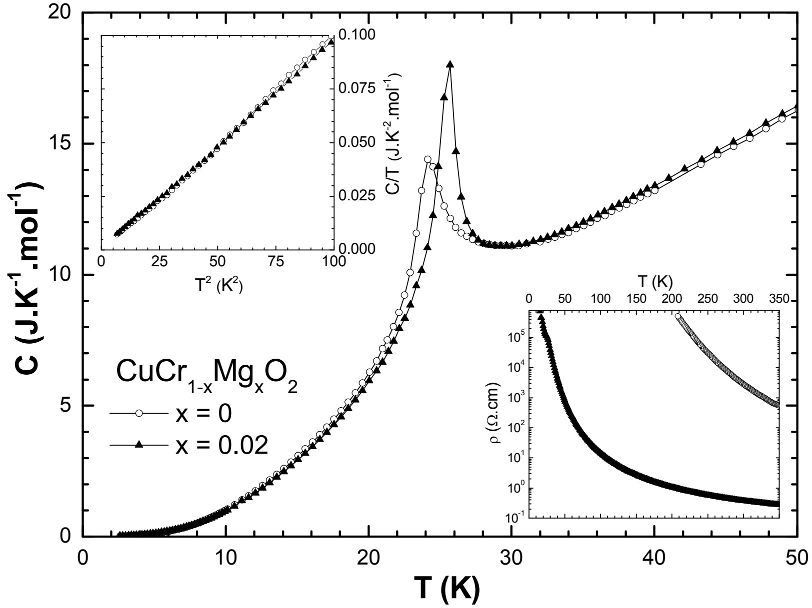

AF, incommensurate propagation vector
k = (*q*, *q*, 0) with *q* ≅ 0.329(1)

Helicoidal AF

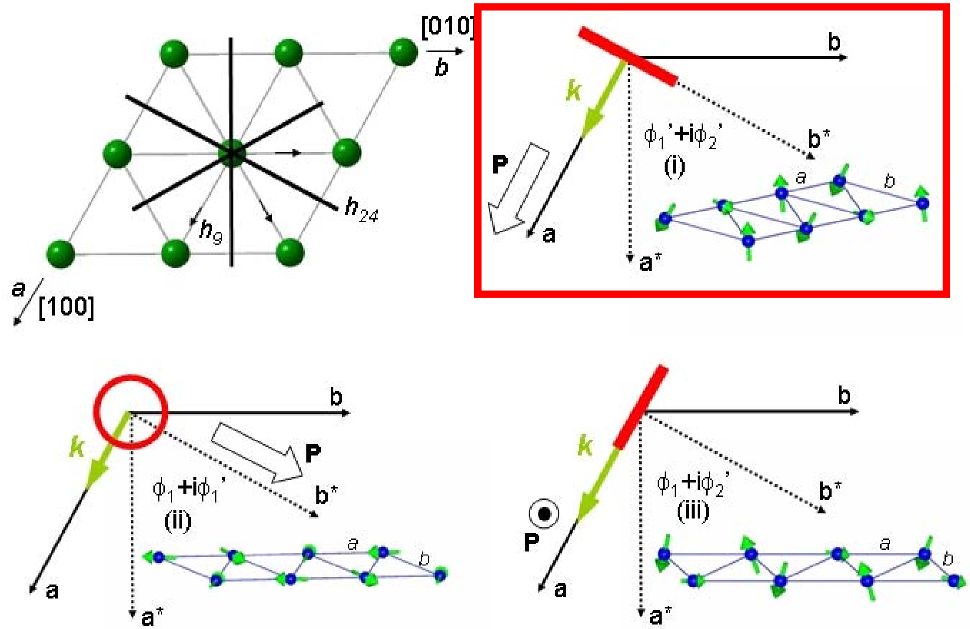

FIG. 5. (Color online) (a) Projection in the (a,b) plane of the symmetry elements in the little corepresentation group $[R\bar{3}m,\ k=(2q,-q,0)]$ and corresponding schematic drawings of the three possible magnetic structures (i), (ii), and (iii) derived from corepresentation analysis (see text). For each case, the magnetic propagation vector (k) is given, the spin rotation plane is shown as a thick bar (red online) in (i) and (iii), or as a circle in (ii), and the large arrow indicates the expected direction of the polarization (**P**). (b)

M. Poienar et al, Phys. Rev. B 79, 014412 (2009)

$CuCrO_2$

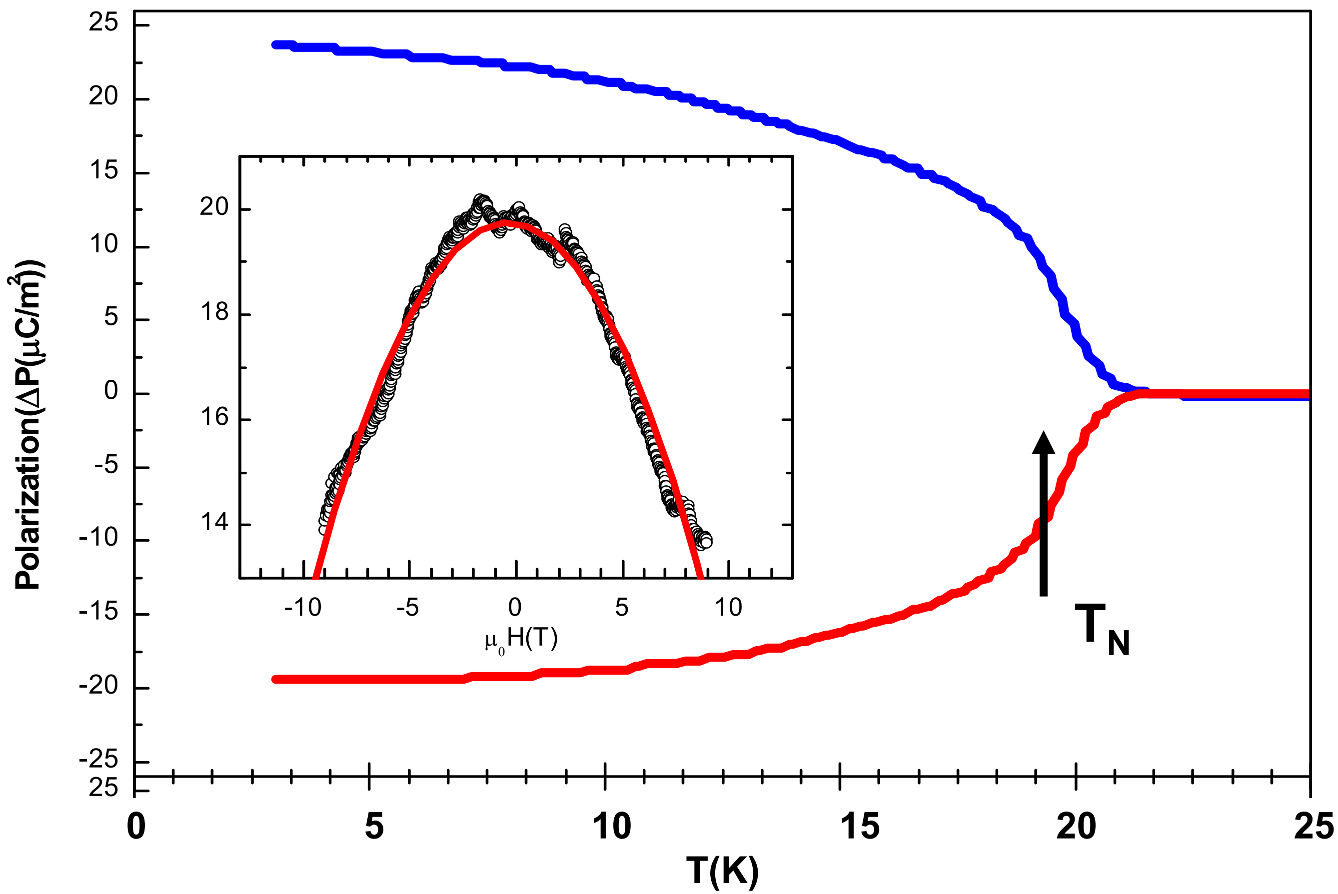

Related to structural changes

S → O $AgCrS_2$

acentric *R3m* rhombohedral

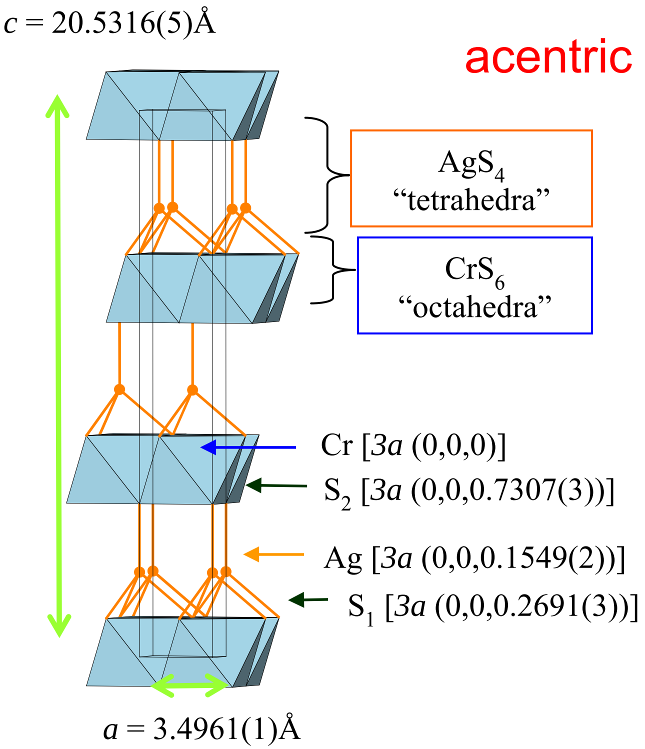

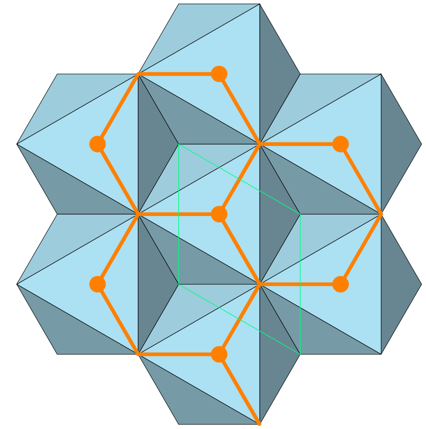

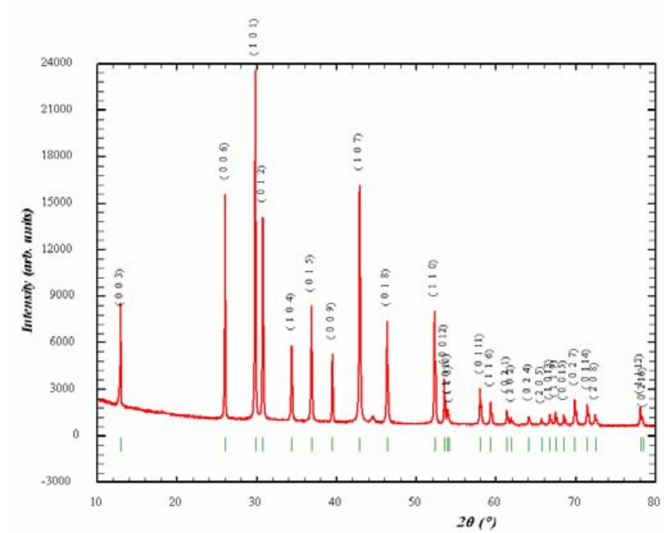

Two sets of three Cr-S interatomic distances (about 2.386 Å and 2.447 Å)
Different from the 6 equivalent Cr-O distances of delafossites

$AgCrS_2$

AF insulator

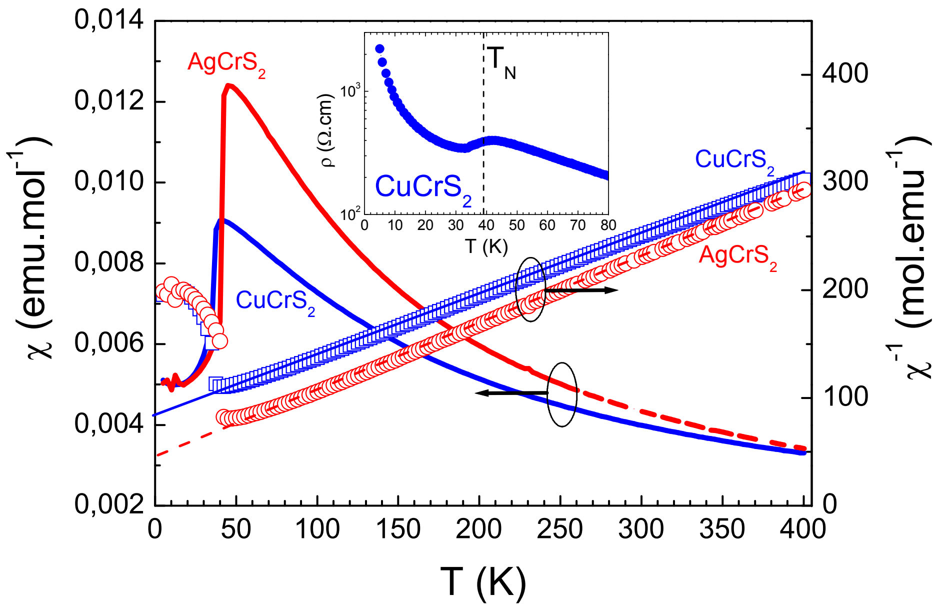

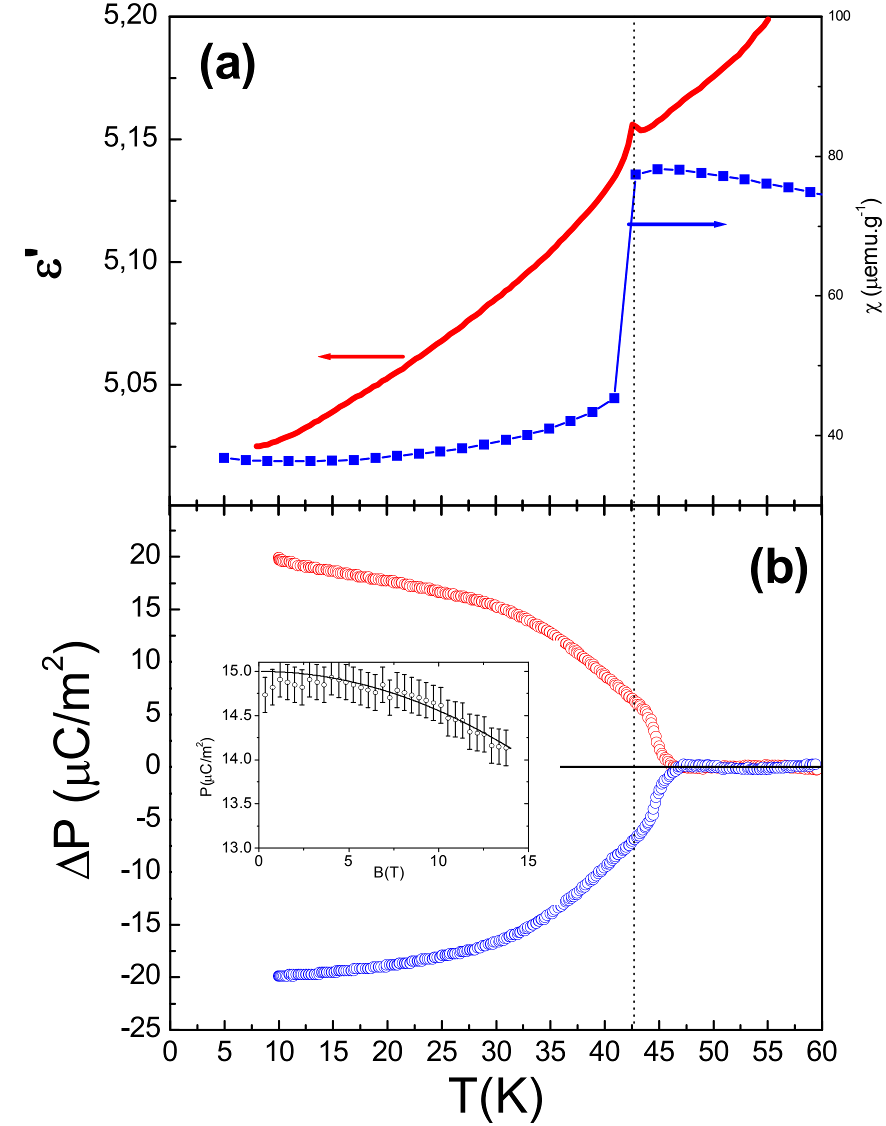

K. Singh et al, Chem. Mater. 2009, 21 (21), pp 5007–5009

S=2

$NaMnO_2$

M. Jansen and R. Hoppe, Zeitschrift Fur Anorganische Und Allgemeine Chemie 399, 163 (1973)

JT-cation: $CuMnO_2$

crednerite C2/*m*

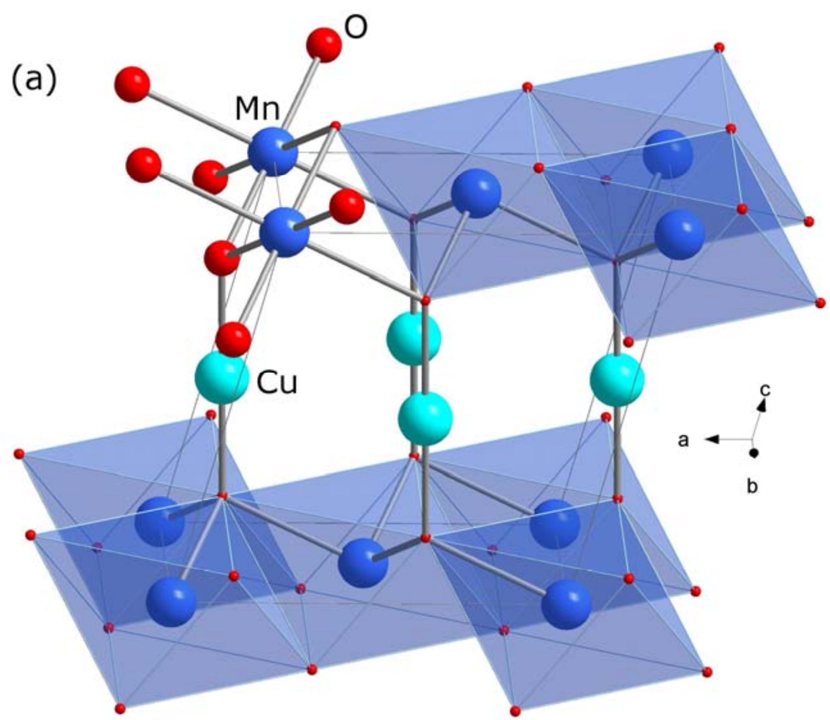

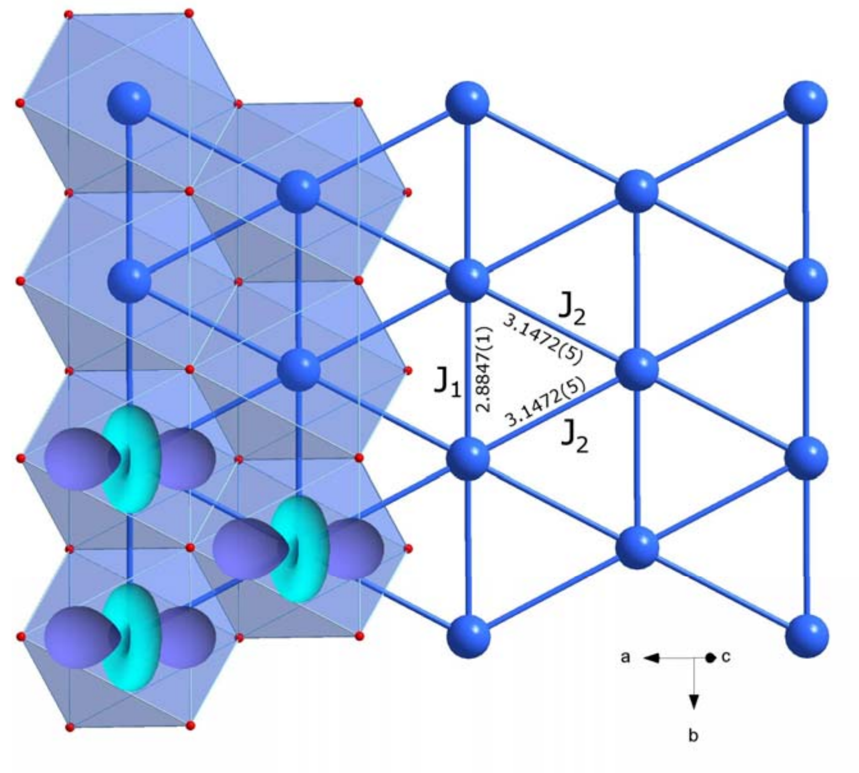

a **= 5.5945(2)Å,** ***b*** **= 2.8847(1)Å,** ***c*** **= 5.8935(2)Å and** ***b*** **= 103.97(2)°**

JT distortion lifts the e_g orbital degeneracy

Orbital ordering

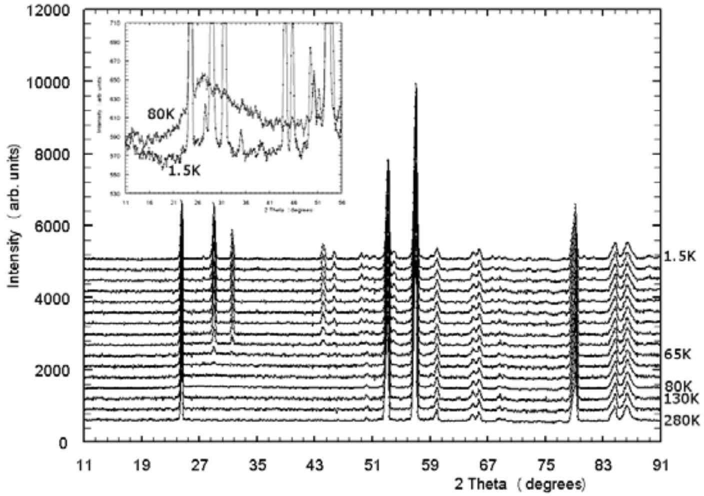

monoclinic (C2/*m*) to strained triclinic C $\bar{1}$

T_N=65K

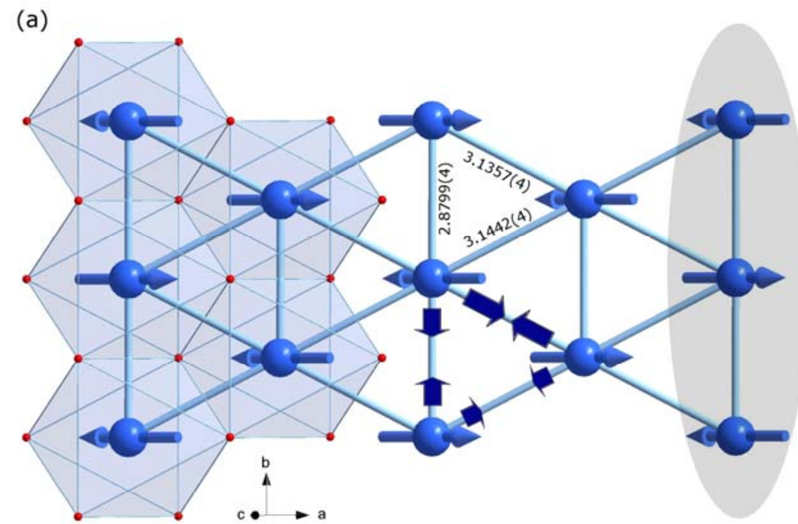

propagation vector k1 = (-½ ½ ½)

Anisotropic magnetic in-plane interactions

No magnetoelectric properties

F. Damay et al , Phys. Rev. B 80, 094410 (2009)

Plan:

3D magnetic networks:

CMR in perovskite manganites

MIT in cobaltites

Frustrated lattices of the « 114 » type

1D and 2D TM-O-TM networks: hexagonal perovskites and CdI_2 type structures

n-type ***vs*** **p-type** conductivity in oxides

n type

$$ZT = \frac{S^2}{\rho\kappa} T = \frac{S^2}{\rho(\kappa_e + \kappa_1)} T$$

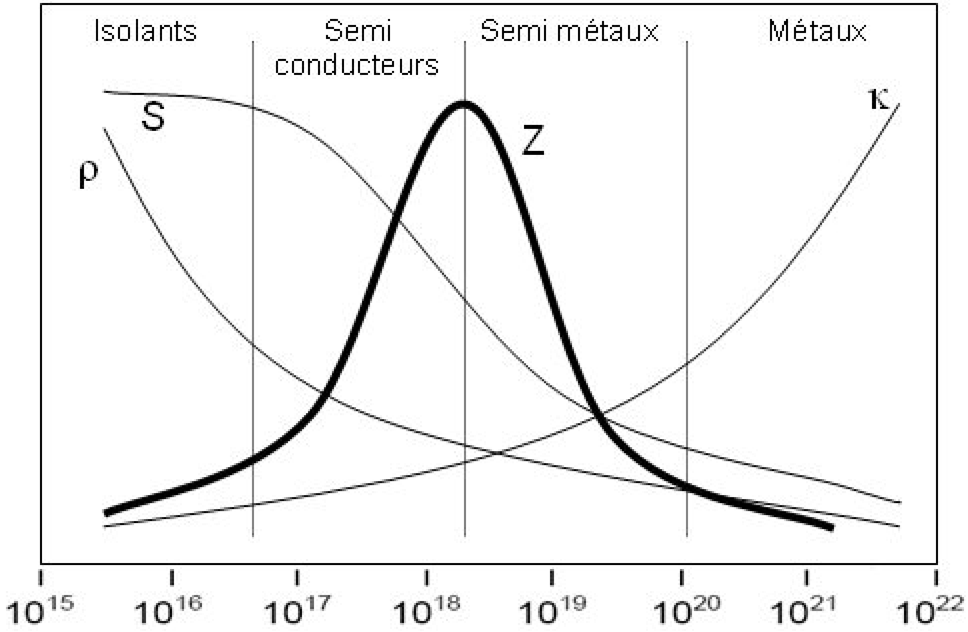

Degenerate semiconductors , best TE

TCO physics:

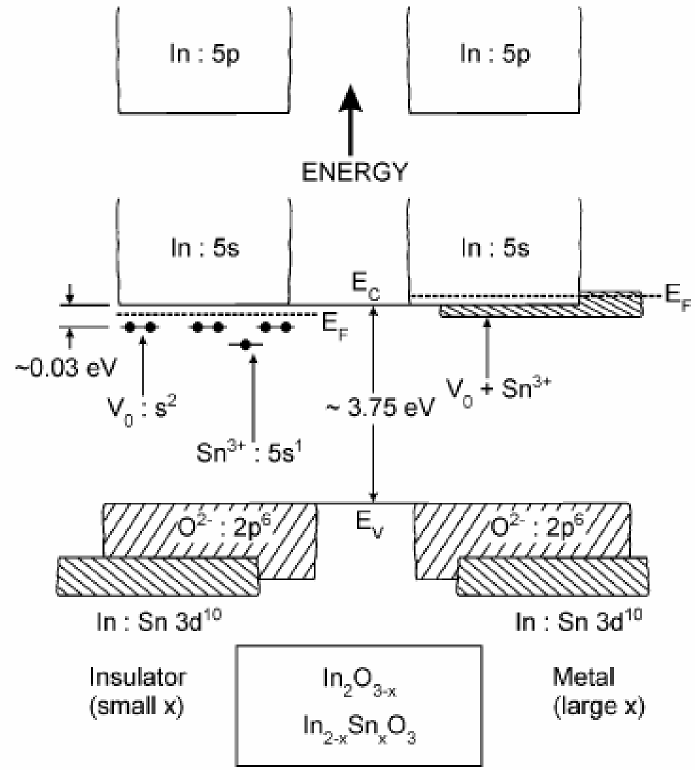

Fig. 2 Schematic energy-band model for tin doped In_2O_3 for small x (insulating) and large x (metallic) modified from Fan and Goodenough.[13] The issue as to whether the 'impurity band' (for large x) is separate from, or placed inside the In 5s (host) conduction band is not resolved at this time.

$Zn_{1-x}Al_xO$ (x = 0 – 0.1)

ZT = 0.6

M. Ohtaki et al

$Zn_{1-x}Al_xO$

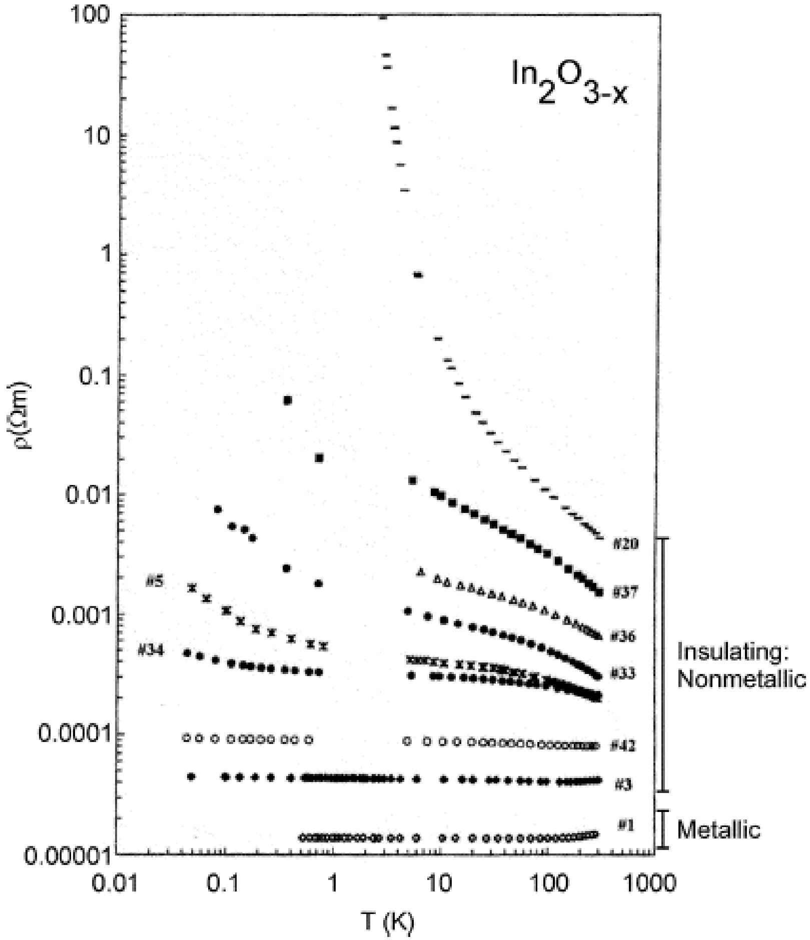

Fig. 4 Electrical resistivity *vs.* temperature dependence for a number of amorphous indium oxide samples. A clear metal–nonmetal transition is observed.[19] Sample #1 is metallic, all the others are shown to be nonmetallic by careful analysis of their temperature-dependent resistivity behaviour.

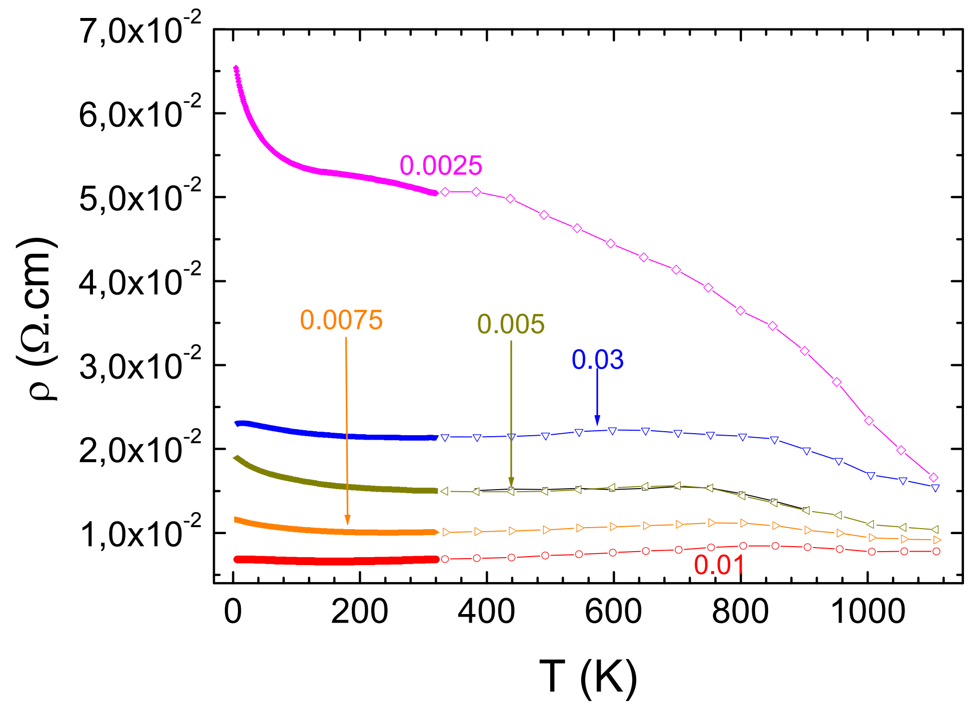

ρ minimum for x=0.01

Proceedings ICT 2008

$Zn_{1-x}Al_xO$

$$S = \frac{\pi^2 k_B^2}{3e} T \left(\frac{\partial \ln \sigma(E)}{\partial E}\right)_{E=E_F}$$

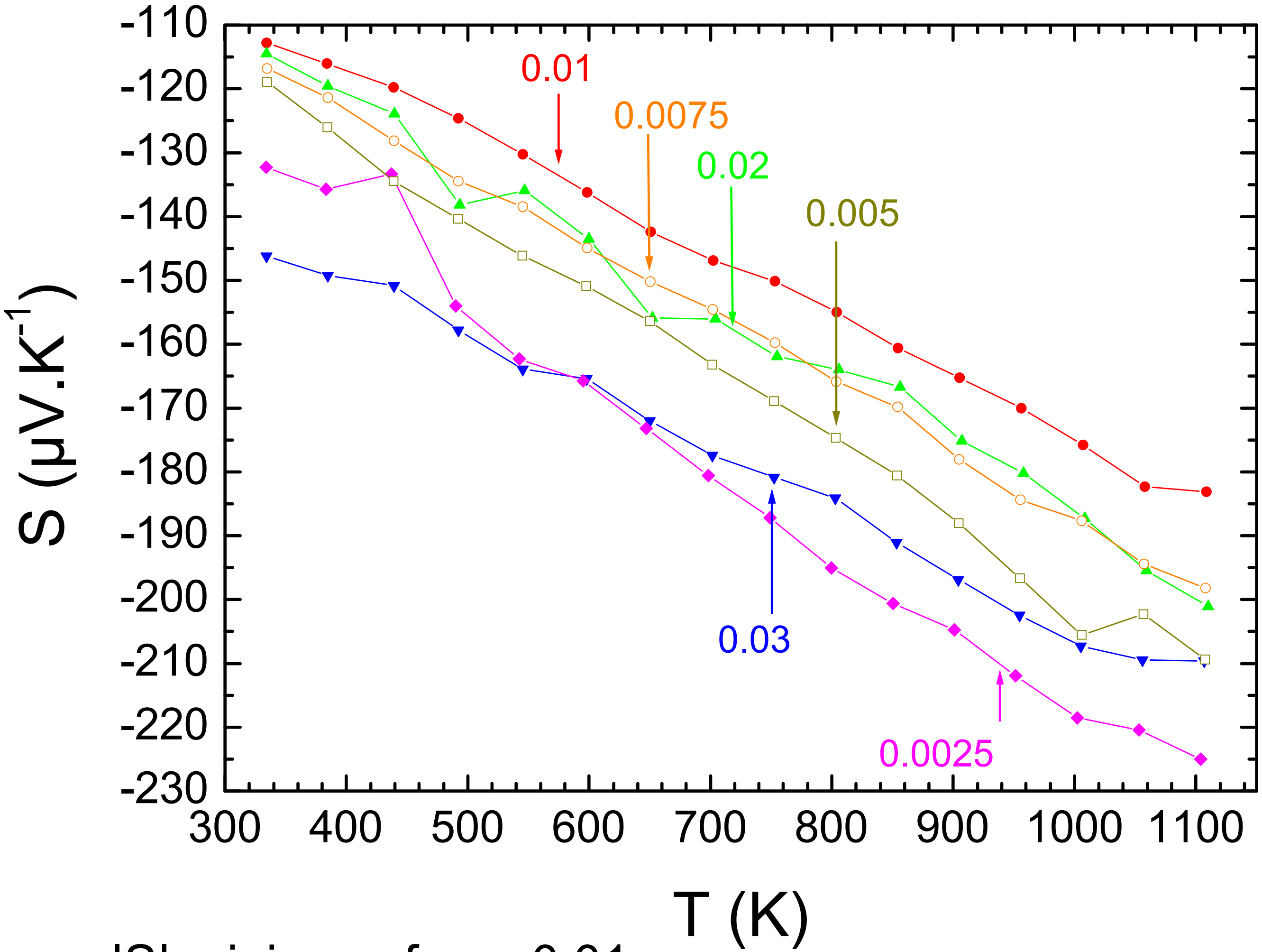

|S| minimum for x=0.01

Not able to reproduce

$Pb_{1.6}V_8O_{16}$

Hollandite

1D structure

1.4e$^-$ in the V empty t_{2g} orbitals

n type?

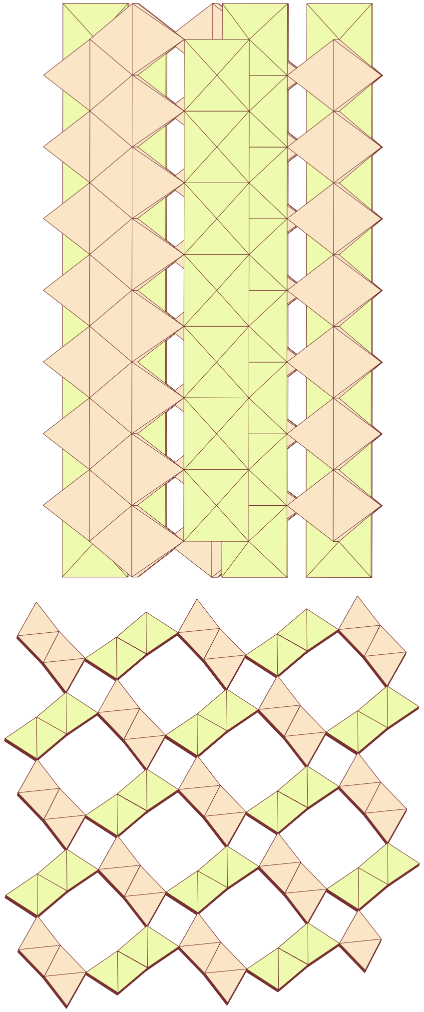

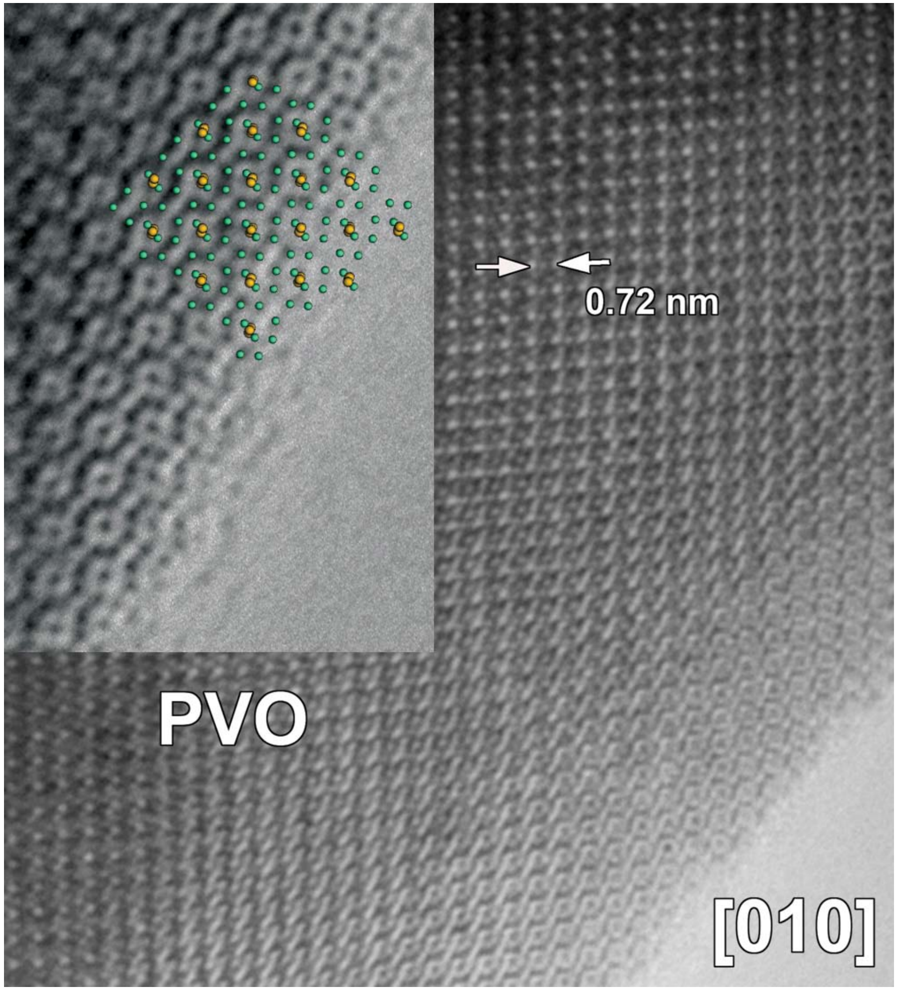

I12/m1 space group with a=10.125Å, b=2.902Å and c=9.880Å

$Pb_{1.6}V_8O_{16}$

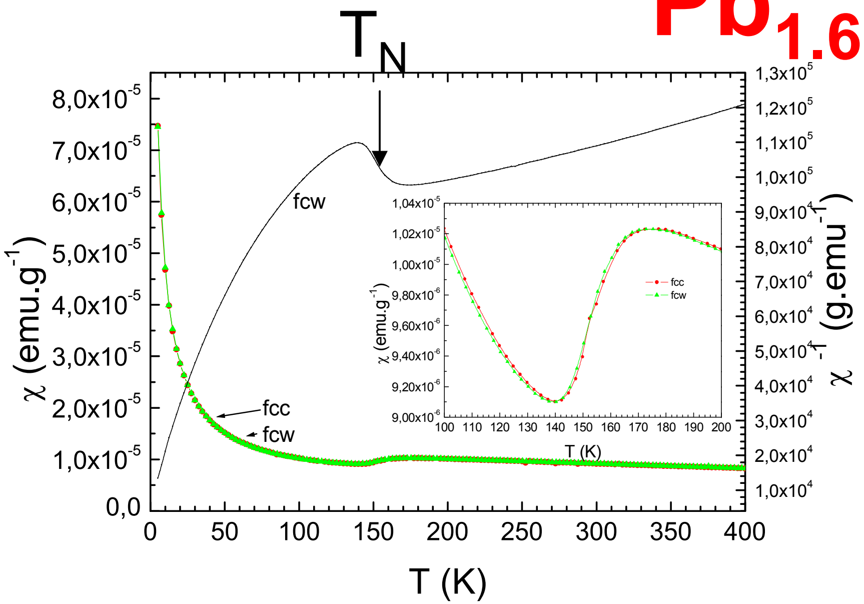

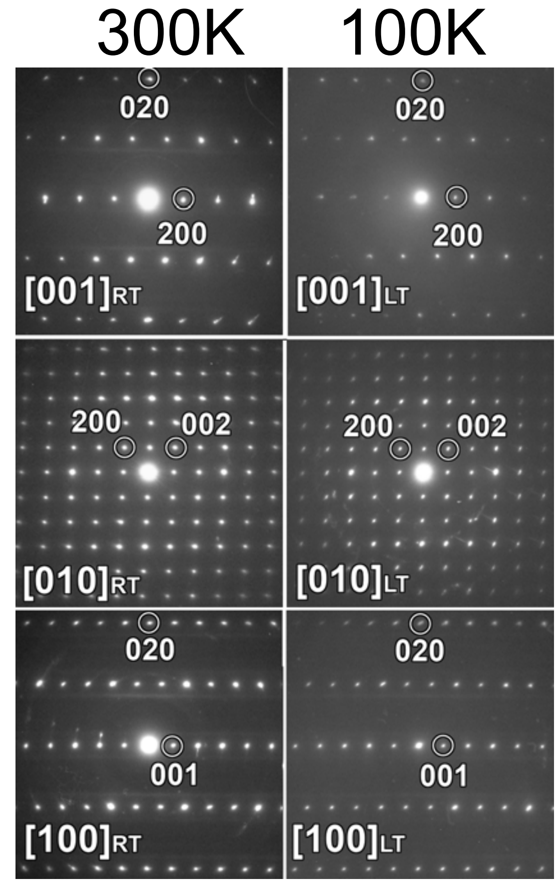

From ED: no struct. transition

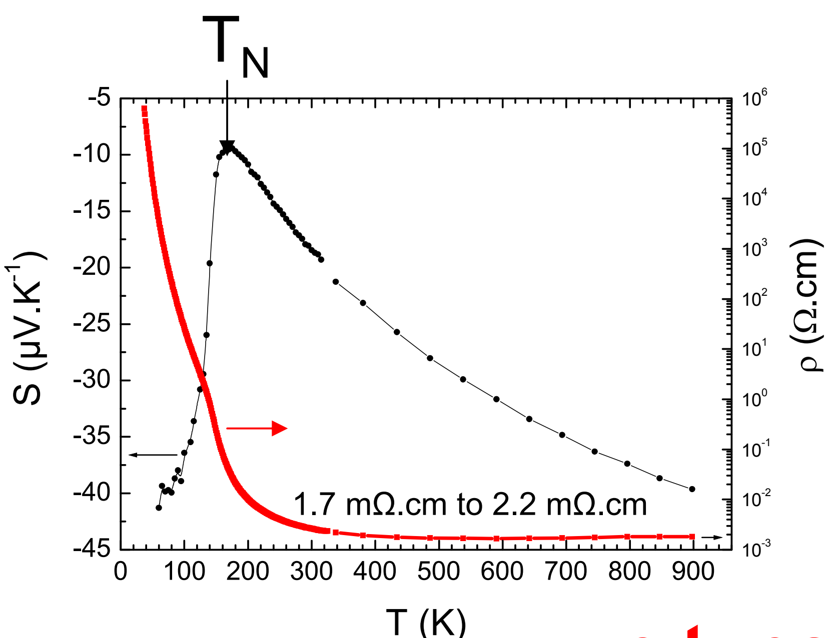

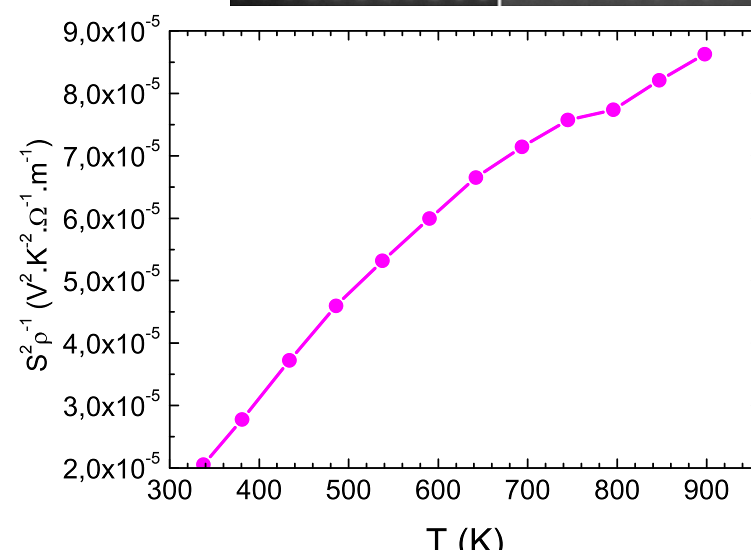

n type!

PbV_6O_{11}

5/3 e^- in the V empty t_{2g} orbitals

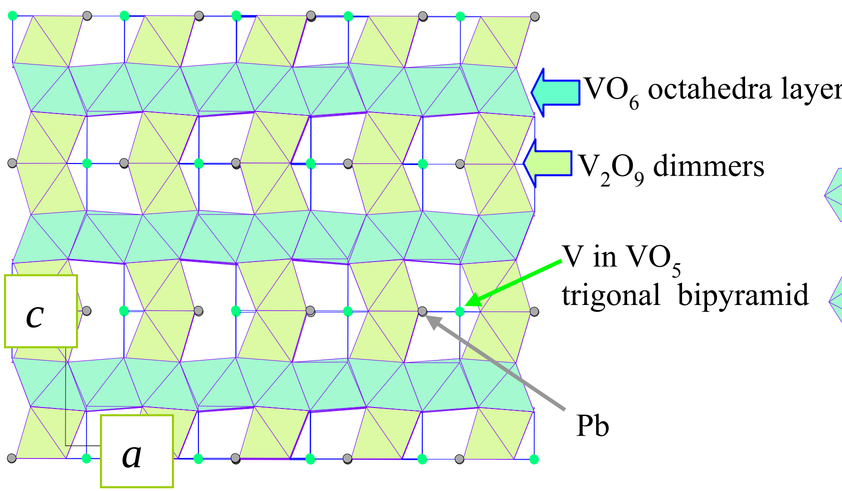

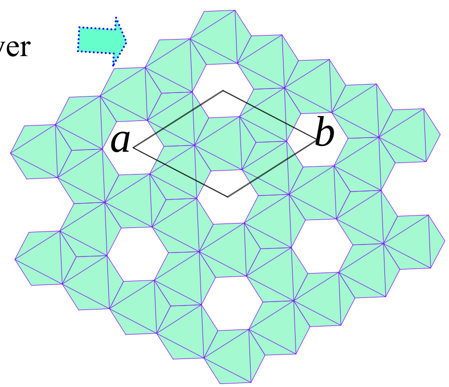

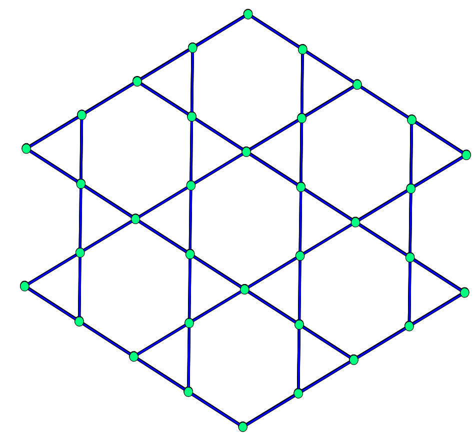

kagome

RT : 5.7567(1) Å and 13.2662(2) Å

$P6_3mc$

PbV_6O_{11}

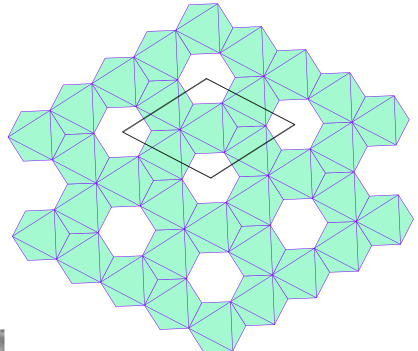

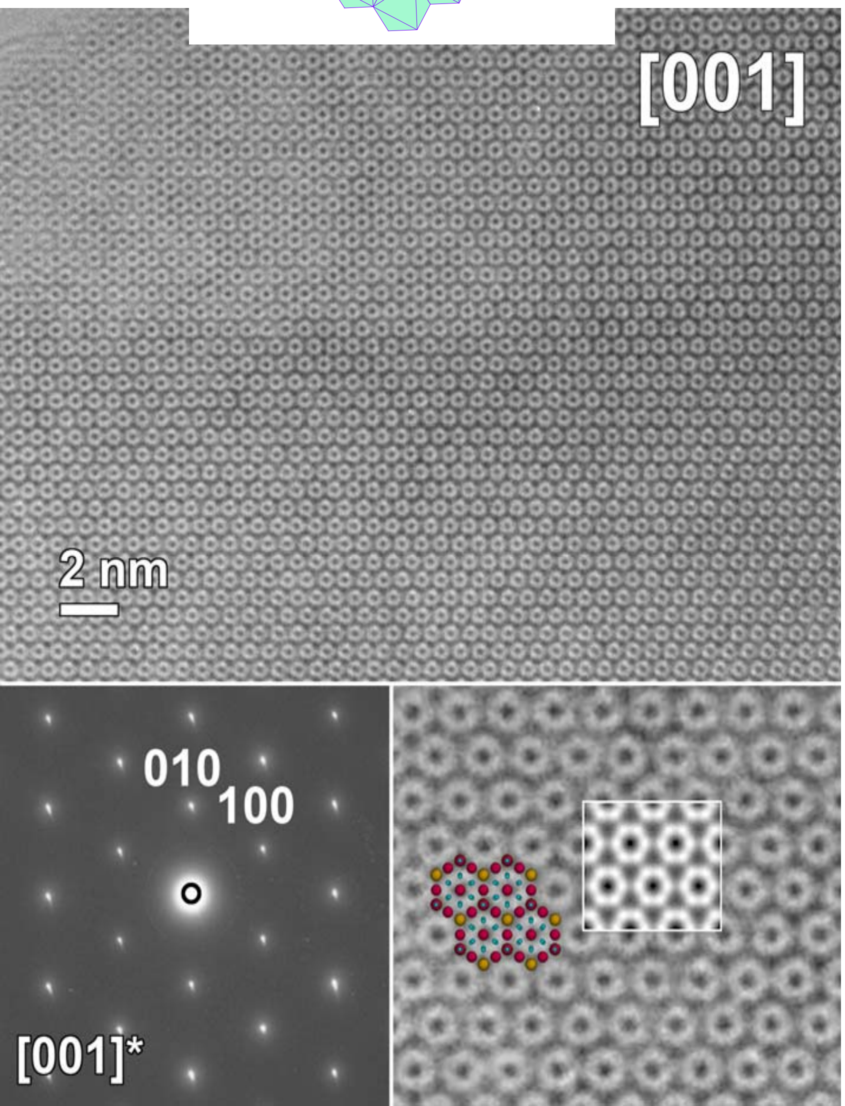

Ferro. Like component

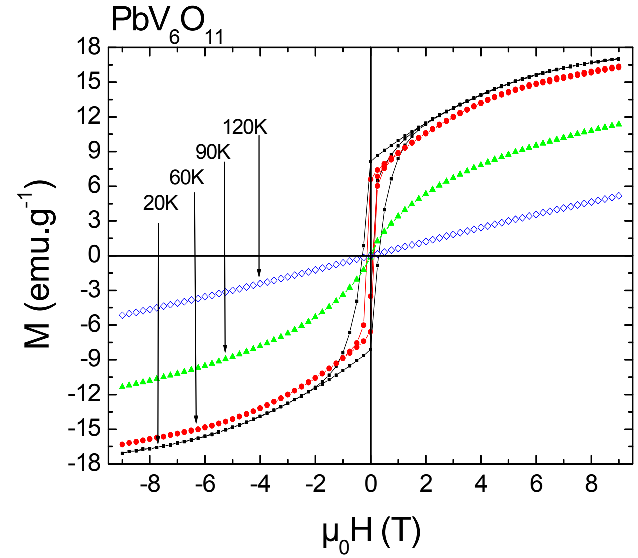

SPINTRONIC

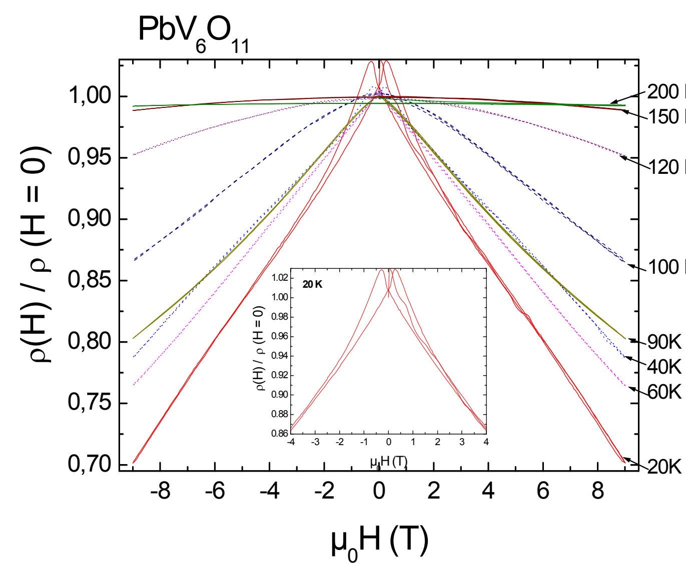

A.Maignan et al, APL (in press)

PbV_6O_{11}

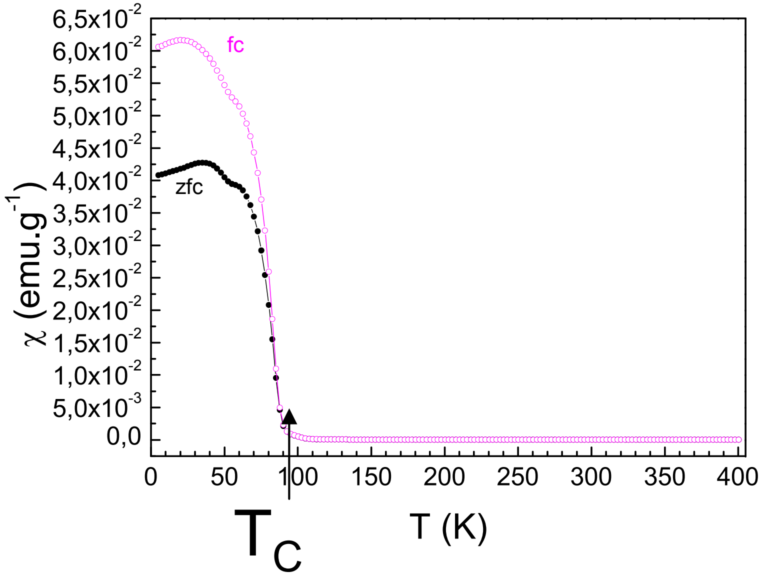

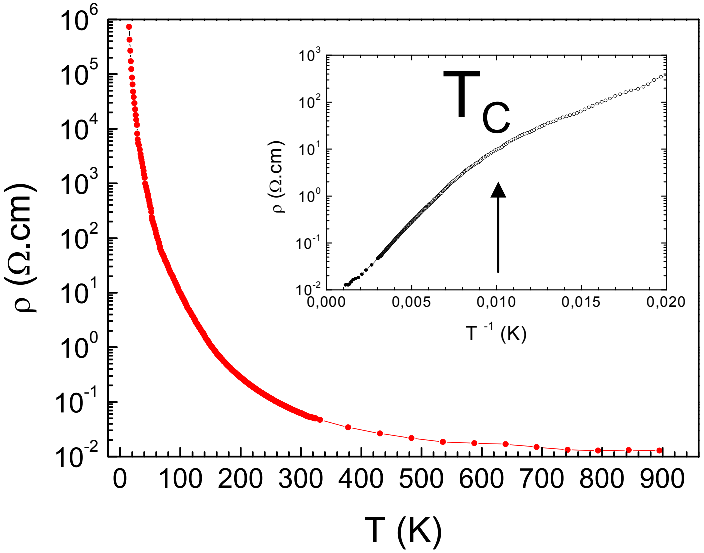

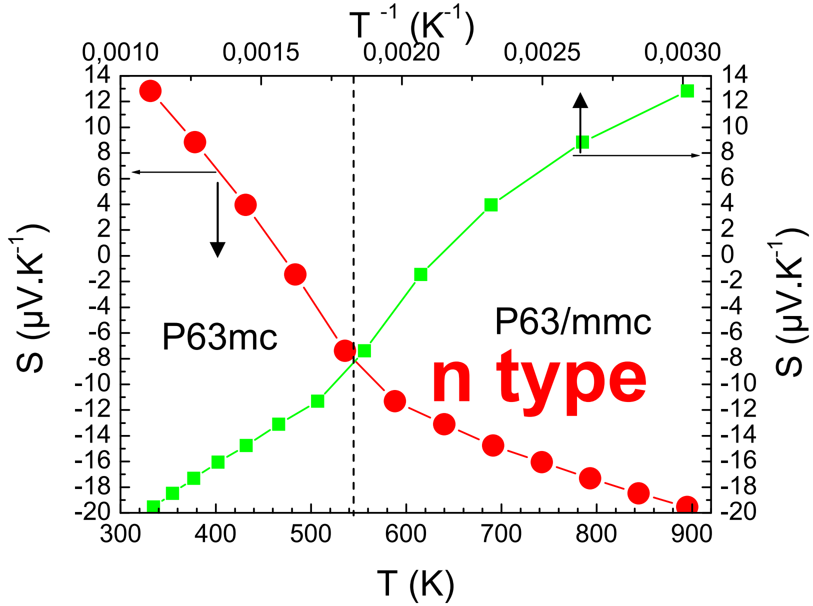

Structural transition
Frustration is lifted

Conclusions :

Many things still to be discovered in oxides !!!!!!!!!!!

Decreasing the thermal conductivity :
polyanions ?

Electronic correlations,
spin/charge/orbital coupling

Thanks to my Colleagues

Christine Martin, Denis Pelloquin, Sylvie Hébert
Raymond Frésard, Oleg Lebedev, Charles Simon,
Vincent Caignaert, Valérie Pralong, Bernard Raveau

and
LPS, UJF, IPCMS, ICMCB
LLB, ILL, ISIS,
MPI Dresden, Koeln and Augsburg Univ. ,
NIU

and

Post-docs, PhDs